UNIVERSIDAD COMPLUTENSE DE MADRID

FACULTAD DE CIENCIAS QUÍMICAS

TESIS DOCTORAL

Design of tailor-made resins for 3D printing by vat photopolymerization.
Preparation of thermosensitive hydrogels for cell manipulation

Diseño de resinas a medida para impresión 3D por fotopolimerización en cuba.
Preparación de hidrogeles termosensibles para manipulación celular

MEMORIA PARA OPTAR AL GRADO DE DOCTOR

PRESENTADA POR

Pedro Liz Basteiro

DIRIGIDA POR

Alberto Gallardo Ruíz
Juan Rodríguez Hernández
Enrique Martínez Campos

Dedicado a mi padre, mi madre, mi hermana y mis abuelos

Agradecimientos. Acknowledgments

Siempre es difícil agradecer a la gente que te ha apoyado, ayudado o simplemente sacado una sonrisa en algún momento, pero en este caso tengo bastante claro por dónde debo empezar. Empiezo por la persona que me dio la oportunidad de poder cambiar la visión que tenía sobre la ciencia, pero sobre todo por ser el "jefe" que todo el mundo querría tener. Muchísimas gracias Alberto por ser mi mayor guía durante estos 4+1 años, gracias por ser mi director de tesis, pero sobre todo gracias por ser mi amigo, compañero y rival de pádel!

Muchísimas gracias también en especial a Juan y Kike por aceptar ser mis directores de tesis, por vuestros consejos y por enseñarme todo lo que sabéis del mundo de la impresión 3D y de las células. Continuando con FUPOL, me gustaría agradecer a Pine, Helmut y Felipe por haberme permitido disfrutar de tantos años en el grupo con risas, cafés y sobre todo con esas bonitas "discusiones" Atleti – Real Madrid.

Gracias a este mismo grupo, tuve la oportunidad de compartir grandes momentos, sobre todo desayunos tomando nuestras queridas "barritas con tomate" con Marina, Raúl, Lara, Anselmo, Naroa, Ana, Lucía, Rubén…, o incluso disfrutando de las siempre divertidas "Fiestas de Navidad", congresos, ¡y mucho más! También me gustaría agradecer a todos los estudiantes de prácticas, TFG y TFM por haberme ayudado a completar parte de las innumerables horas de laboratorio.

Por otro lado, me gustaría agradecer a la Dra. Silvia Marchesan y todo su grupo de trabajo por permitirme hacer y ayudarme en lo posible en mi estancia en Trieste. Pero sobre todo a Gore, Arturo, Marc, Yoel, Laura y Bea por conformar ese grupo de "Actividades Triestinas" que me hizo conocer Europa y gente encantadora como vosotros.

Cerrando un poco el círculo de trabajo, me gustaría agradecer a Lola por sus infinitas conversaciones arreglando nuestras vidas, a Luisito y Jorge por todas las risas en congresos o únicamente cuando nos cruzábamos en los pasillos, a Jose por esos "saludos" a las 9 de la mañana tan "tuyos", y aprovechando esto… Gracias por esas "reuniones" de los jueves a las 13 h a Alberto, Helmut, Jose, Raúl y Gary.

Se podría considerar también trabajo, o hobbie, o incluso pasión, y no me refiero a la ciencia… me refiero a mi parte como entrenador de fútbol, esa parte de mí que me ha permitido conocer durante estos años a una enorme cantidad de pequeñas personitas, conocidos por todos como “mis niños”. Muchísimas gracias a todos y cada uno de “mis niños” que he tenido la suerte de entrenar durante estos 4 años, habéis sido mi alegría, mi desconexión y con vuestros encantadores padres y madres, mi pequeña gran familia madrileña. Con mención especial a Jose y Juanjo por los innumerables favores, horas de pádel, cervezas,…

Una mención especial se merecen por supuesto mis amigos, los cuales sin ellos todo esto habría sido imposible. Empezando por los que tuvieron la suerte, o mala suerte, de poder convivir conmigo durante estos 4 años, Dani, Óscar, Fran y Juli, gracias por hacer más amena esta aventura, pero, sobre todo, mucho más divertida. A Víctor, que aunque no hemos vivido juntos es como si lo hubiésemos hecho por la cantidad de tiempo que hemos pasado y disfrutado juntos! A Gonza, Cede y Santi por ser Galicia pero en Madrid, permitiéndome disfrutar de tanto fútbol, pádel, cenas, fiesta,… A Guille por nuestras infinitas risas de cosas sin sentido. Por último pero no menos importantes, la vuelta a casa, tener esos amigos que cuando vuelves a casa es como si no hubiese pasado el tiempo vale oro, gracias, por absolutamente todo, David, Pablo V, Fari, Mati, Kinder, Juanillo,... GRACIAS A TODOS!

Ahora sí, llega el momento más complicado, y posiblemente el más emotivo para mí, el de agradecer a toda mi familia por haber estado apoyándome en todo momento. Muchísimas gracias a mi hermanita Sofía, mis primos Luis y Manu, mi tía Casilda, y sobre todo a mis queridísimos abuelos Manolo y Elvira, por el cariño, y amor incondicional que transmitís. Mención especial para mi Hipi, que aunque ya no estés con nosotros, esos recibimientos tan cariñosos también fueron parte fundamental de recargar energía.

A mitad de la tesis, me fui a mi primer congreso, nervioso, pero sin esperarme que me iba a cambiar la vida completamente, ya que tuve la suerte de coincidir con Goretti. Gracias por hacerme sonreír tanto estos años y por permitirme disfrutar de ti y de Wiski, sois especiales. Gracias también a mi familia política por acogerme tan bien siempre, gracias Nini, Julio, Julito e Isa.

A mi madre y a mi padre, por ser como sois, por querer siempre lo mejor para mí, por apoyarme en este largo viaje y en cada decisión que tomo. Mamá, gracias por las infinitas llamadas ayudándome y queriéndome tanto, eres la mejor. Aitatxo, no podía tener un referente mejor, como científico, como padre y como persona, gracias por la ayuda y paciencia infinita. Gracias de corazón a los dos.

Abstract

Polymeric networks are three-dimensional structures formed by crosslinked polymers whose mechanical and chemical properties make them versatile for a wide range of applications. Hydrogels are polymeric networks with a high water retention capacity, which has made them very attractive components for various biomedical applications, among others, the one addressed in this thesis focused on the use of hydrogels as supports for non-aggressive detachment of cell monolayers by temperature change. The objective of this thesis is to develop resins that allow the formation of networks and hydrogels in both 2D and 3D models, using photopolymerization techniques. These techniques include photopolymerization in a UV curing chamber and, most importantly, 3D printing using vat photopolymerization, the latter being one of the main additive manufacturing technologies. Photopolymerization has significant advantages in terms of the control of the reaction rate and the homogeneity of the resulting polymer network.

In the context of Industry 4.0, additive manufacturing is a core technology that allows the production of complex and lightweight structures, optimizing weight and material expenditure. It also allows a reduction in the number of parts in stock and the decentralization of activities, as this technology makes it possible to manufacture where and when you want, reducing logistics costs and promoting the economic development of areas with low population density.

In this work, firstly, resins have been developed that allow the printing of both sacrificial parts and readjustable networks through the hydrolysis of hydrolysable crosslinkers synthesized and used as polymerizable components in the resins. This hydrolysis is pH-dependent.

In addition to resins that allow the printing of pH-sensitive parts, resins that allow obtaining temperature-sensitive hydrogels have been developed during this thesis; both types of hydrogels are promising candidates for specific biomedical applications, such as cavity fillers for regenerative medicine, implantable systems, controlled drug release systems, or as supports for cell culture and non-aggressive detachment as mentioned above. Temperature sensitivity was achieved by incorporating vinyl-lactams such as *N*-vinylcaprolactam into the resin

formulation, allowing reversible changes in the hydrogel structure in response to temperature variations in the medium. Finally, the properties of the vinyl-lactam-based hydrogels were modulated by loading them with functionalized carbon nanotubes, thus improving their mechanical and conductive properties without compromising their ability to be printed by vat photopolymerization.

In conclusion, temperature- and pH-sensitive 2D and 3D hydrogels prepared by photopolymerization represent a versatile and promising platform for a wide range of applications, such as biomedical applications.

Resumen

Las redes poliméricas son estructuras tridimensionales formadas por polímeros entrecruzados, cuyas propiedades mecánicas y químicas las hacen versátiles para diversas aplicaciones. Los hidrogeles son aquellas redes poliméricas con una alta capacidad de retención de agua, lo que los ha convertido en componentes muy atractivos para diversas aplicaciones biomédicas, entre otras, la abordada en esta tesis centrada en el uso de hidrogeles como soportes para despegado no agresivo de monocapas celulares por cambio de temperatura. El objetivo de esta tesis es desarrollar resinas que permitan la formación de redes e hidrogeles tanto en modelos 2D como 3D, utilizando técnicas de fotopolimerización. Entre estas técnicas, se incluyen la fotopolimerización en cámara de curado UV y sobre todo la impresión 3D mediante fotopolimerización en cuba, siendo esta última una de las tecnologías principales de la fabricación aditiva. La fotopolimerización presenta ventajas significativas en términos de control de la velocidad de reacción y la homogeneidad de la red polimérica resultante.

La fabricación aditiva, en el contexto de la Industria 4.0, es una tecnología principal que permite la fabricación de estructuras complejas y ligeras, optimizando el peso y gasto de material. Además, permite reducir el número de piezas almacenadas y la descentralización de las actividades, ya que, con esta tecnología, es posible fabricar dónde y cuándo se quiera, reduciendo los costes logísticos, lo que fomenta el desarrollo económico de zonas con baja densidad poblacional.

En este trabajo, en primer lugar, se han diseñado resinas que permiten imprimir tanto redes sacrificables como redes reajustables mediante la hidrólisis de entrecruzantes hidrolizables sintetizados y utilizados como componente polimerizable en las resinas. Esta hidrólisis es dependiente del pH.

Además de resinas que permiten imprimir piezas sensibles al pH, se desarrollaron durante esta tesis resinas que permiten obtener hidrogeles sensibles a la temperatura; ambos tipos de hidrogeles son candidatos prometedores en aplicaciones biomédicas específicas, tales como rellenos de cavidades para medicina regenerativa, sistemas implantables, sistemas de

liberación controlada de fármacos, o como soportes para cultivo y despegado celular de manera no agresiva, mencionada antes. La sensibilidad a la temperatura se obtuvo al incorporar vinil-lactamas como la *N*-vinilcaprolactama en la formulación de las resinas, permitiendo cambios reversibles en la estructura del hidrogel en respuesta a variaciones de temperatura en el medio. Finalmente, se modularon las propiedades de los hidrogeles basados en vinil-lactamas cargándolos con nanotubos de carbono funcionalizados, mejorando así las propiedades mecánicas y conductivas, sin comprometer su capacidad de ser impresos mediante fotopolimerización en cuba.

En conclusión, los hidrogeles 2D y 3D sensibles a la temperatura o al pH preparados por fotopolimerización representan una plataforma versátil y prometedora para una amplia gama de aplicaciones, como pueden ser las de uso biomédico.

Contents

List of abbreviations

2D: Two-dimensional

3D: Three-dimensional

3D CAD: Three-dimensional computer-aided design

AIBN: Azo-bis-isobutirenitrile

AM: Additive manufacturing

ATR-FTIR: Attenuated total reflectance-infrared spectroscopy

BAPO: Phenylbis(2,4,6-trimethyl benzoyl) phosphine oxide

BJ: Binder jetting

CAD: Computer-aided design

C_d: Cure Depth

CEA: 2-Carboxyethylacrylate

CNTs: Multi-walled carbon nanotubes

DED: Directed energy deposition

Di-Me: Dimethacrylates

Di-V: Divinylurea

DLP: Digital light processing

DMAc: Dimethylacetamide

DMD: Digital micromirror device

DMEM: Dulbecco's Modified Eagle Medium

DMF: *N, N*-Dimethylformamide

D_p: Penetration depth

DVI: 1,3-divylimidazolidin-2-one

E_c: Critical energy for polymerization

ECM: Extracellular matrix

EGDMA: Ethylene glycol dimethacrlylate

E_{max}: Irradiated light energy on the surface

FBS: Fetal bovine serum

FDM: Fused deposition modeling

FEP: Fluorinated ethylene propylene

FT-IR: Fourier transmision infrarred spectroscopy

FUPOL: Polymer functionalization group

G: Gage length

G’: Storage/elastic modulus

G’’: Loss/viscous modulus

GFP: Green fluorescent protein

GMM: Glycerol monomethacrylate

HCL: Hydrolysable crosslinker

HCL(jef): Hydrolysable crosslinker based on jeffamine

HCL(pip): Hydrolysable crosslinker based on piperazine

HCPK: 1-hydroxyl cyclohexyl phenyl ketone

HEA: 2-Hydroxy ethyl acrylate

HF-CNT: High functionalization

HIPS: High impact polystyrene

I*: Primary active center

IAM: Isoamyl nitrite

ICA: Icariin

IPN: Interpenetrating network

IR: Near-infrared

L: Length of narrow section

LCD: Liquid crystal display

LCST: Lower critical solution temperature

LEDs: Light-emitting diodes

LF-CNT: Low functionalization

LVR: Linear viscoelastic region

M: Monomers

MAA: Methacrylic acid

MAPTAC: Methacrylamidopropyltrimethyl-ammonium chloride

Me: Methacrylates

MeCN: Acetonitrile

MEX: Material extrusion

MF-CNT: Medium functionalization

MJ: Material jetting

MTT: (4,5- dimethylthiazol-2-yl)-2,5-diphenyltetrazolium bromide

NaOH: Sodium hydroxide

NIPAm: *N*-isopropyl acrylamide

NMP: *N*-methyl-2-pyrrolidone

NMR: Nuclear magnetic resonance

NP: Non postcured

P: Postcured

P/S: Penicillin, streptomycin

PBS: Phosphate-buffered saline

PBF: Powder bed fusion

PCL: Poly (*ε*-caprolactone)

PEG: Poly (ethylene glycol)

PEGDMA: Poly (ethylene glycol) dimethacrylate

PEGMEA: Poly (ethylene glycol) methyl ether acrylate

Pn: “Dead” polymer chain

Pn*: Active growing center

pNIPAM: Poly *N*-isopropyl acrylamide

PVA: Poly (vinyl alcohol)

pVCL: Poly *N*-vinyl caprolactam

R: Radius of fillet

RM: Regenerative medicine

RT: Room temperature

S: Swelling

SCL: Stable crosslinker

SEM: Scanning electron microscopy

SL: Sheet lamination

SLA: Stereolithography

SP: Spheres

STL: Standard template library

Sudan I: 1- (Phenyldiazenyl)naphthalen-2-ol

T: Transfer agent

T*: Active moiety after the transfer step

TE: Tissue engineering

TEM: Transmission electron microscopy

TERM: Tissue Engineering and Regenerative Medicine

Tg: Glass transition temperature

TGA: Thermogravimetric analyzer

TPO: Diphenyl(2,4,6-trimethyl benzoyl) phosphine oxide

Tu: Tubes

UCST: Upper critical solution temperature

UV: Ultraviolet

VA: 4-Vinylaniline

VCL: *N*-Vinylcaprolactam

VP: 1-Vinyl-2-pyrrolidone

VPP: Vat photopolymerization 3D printing

VPTT: Volume phase transition temperature

VTL: Video time-lapse

W: Width of narrow section

Z: Layer thickness

List of Figures

List of Tables

Chapter 1. Introduction

1.1. Conventional free radical (photo)polymerization: general principles

Conventional free radical chain polymerization is the most extensively employed method for the industrial production of commercial synthetic polymers because, among others, this polymerization technique does not require stringent reaction conditions (for instance, it is tolerant to environmental humidity) and can be broadly applied to a wide myriad of monomers bearing different functional groups[1]. Other advantages include high reaction rates, energy efficiency, and mass polymerization that avoids the use of solvents. As a result, free radical polymerization has been employed for applications in numerous engineering fields such as the elaboration of polymer coatings, dental restoration, and 3D printing[2–5], just to mention few of them.

Free-radical polymerization occurs following the steps schematically depicted in **Figure 1.1.** The first step is the initiation, where radicals (I*) are formed by the dissociation of the initiator. After this, I* react with the double bond of a monomer (M) to start a chain reaction. These primary radicals can give rise to a chain reaction, usually very rapid, in which tens, hundreds, or thousands of monomer molecules are successively incorporated to the chain, in the stage known as propagation to produce chain growth. This chain reaction is the defining stage of polymerization and continues until the active chain end is deactivated for some reason, forming a "dead" or a deactivated chain that is part of the final material. Deactivation occurs when two radicals meet each other in what is called the termination stage[6]. In this termination step, the involved macroradicals are deactivated and no other event affecting the reaction takes place[7]. Alternatively, another mechanistically very different type of deactivation, is the chain transfer. In this case, a growing chain is deactivated by a reaction with a compound T (transfer agent), but in this case, a new T-derived radical (T*) is formed capable of initiating a new chain reaction process. The transfer process is very common in conventional radical polymerization, and any species present in the medium, such as the solvent or the monomer itself, can act as a transfer agent[7,8].

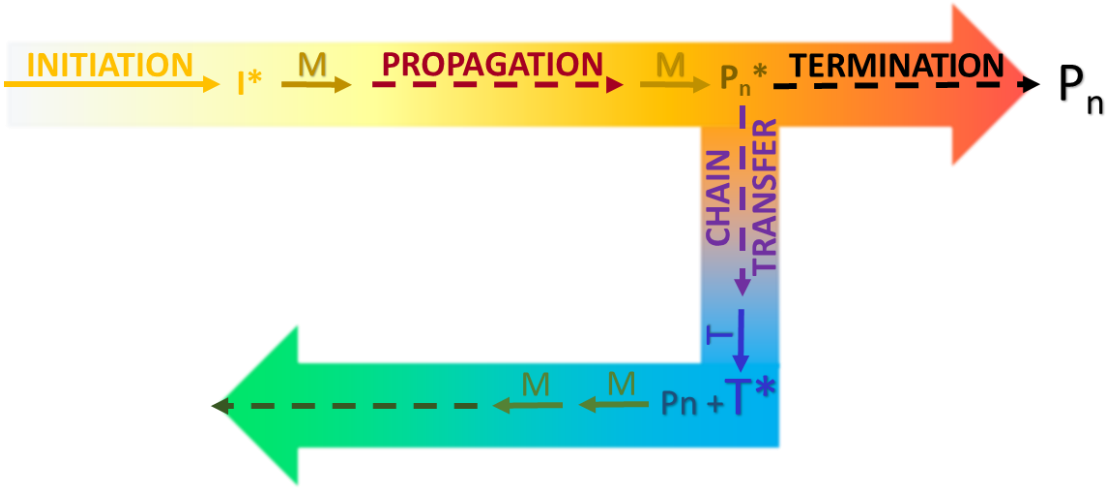

Figure 1.1. Scheme of a free-radical polymerization process. I* = primary active center, M = monomer, Pn* = active growing center, Pn = "dead" polymer chain, T = transference agent, T* = active moiety after the transfer step, capable of reinitiating.

In the context of this thesis, when the monomer is di- or multifunctional, the polymerization yields polymeric networks. Moreover, again to focus this introduction on the thesis work, developed in the framework of photocuring and 3D printing by vat photopolymerization, it should be noted that in these processes the initiation is always photoinitiation, *i.e.*, the fragmentation of the initiator takes place after the appropriate initiator is irradiated with a suitable wavelength.

The term photopolymerization, or photocuring reaction, therefore refers to radical polymerizations in which initiation of the chain polymerization is triggered by light, usually UV light. However, in a broader context, photopolymerization involves the light-induced increase in polymer molecular weight and may also encompasses the photocrosslinking of multifunctional macromolecules comprised within the formulation. These processes rely on light absorption by the photoinitiator to produce active species, which are then utilized to react and incorporate the monomers and crosslinking agents into the growing chain. Vinyl polymerization can be initiated both by photosensitive ionic species as well as by free radicals photoinitiators. However, the majority of photopolymerization examples occur via free-radical[9].

Free radicals capable of initiating polymerization of vinyl monomers can be photochemically generated from a diverse range of chemical compounds. However, not all free radicals can initiate polymerization reactions. A radical must

meet certain energetic criteria to initiate the polymerization of a vinyl monomer. The chain radical formed must be stable enough compared to the primary radical, thus requiring consideration of the bond energies and resonance stabilization of the species involved. It is also worth mentioning that, in some instances, photolytic decomposition of the monomer can also generate free radicals. This, of course, requires that the absorption spectrum of the monomer falls within the spectral range of the incident radiation and can also lead to a polymerization reaction[4].

During the curing reaction, the glass transition temperature (Tg) of the material rises due to the increase in molecular weight and crosslinking density of the polymer[10]. Typically, higher conversion is expected to increase molecular weight and crosslinking, thereby reducing free chain ends and restricting polymer chain mobility[10]. The kinetics of the curing process are markedly influenced by factors such as light intensity, temperature, type of monomer/crosslinking agent, and resin composition (e.g., initiator concentration, use of solvents,…)[11]. As a result, the combination of all these factors will play an important role in the fabrication of both 2D and 3D crosslinked materials. In general, higher light intensity, temperature, or initiator concentration typically result in faster photopolymerization rates, leading to higher conversions[10]. Nevertheless, it is imperative to consider that too much UV exposure time and intensity, or the presence of an excessive amount of photoinitiator can lead to over-curing of the liquid resin, a phenomenon also referred to as bleeding. This can result in deterioration in the details of the cured pieces. In addition, in the case of 3D parts overcuring can also produce a loss of sharp edges and poorly defined objects. Besides, if the Tg of the final polymer is higher than the reaction temperature, vitrification takes place. Vitrification refers to the formation of a glassy solid material caused by an increase either in the crosslinking density and/or the molecular weight of the polymer being formed during the polymerization. After vitrification, the reaction rate significantly decreases as it becomes controlled by the diffusion of the reactive species[7].

1.1.1. A particular type of monomers for radical polymerization: methacrylates with hydrolysable side chains

Commercial resins for vat radical photopolymerization contain mainly di- or multifunctional acrylics that after photopolymerization give rise to rigid and highly crosslinked final parts. However, as will be indicated below, this thesis pioneers the evaluation of novel monomers with labile side groups as precursors for the formation of 3D printed parts that can be either solubilized by complete degradation of the network or partially degraded to produce highly swellable parts.

This approach is based on the group's extensive experience in the preparation of new methacrylates by selective Michael addition on asymmetric divinyl compounds[12,13]. Using acrylate/methacrylate-type divinyl compounds, Michael addition of amines occurs selectively on the acrylate functional group (see **Figure 1.2.** Michael selective addition scheme for amines.), leaving the polymerizable methacrylate intact. Furthermore, in the process, a β-amino ester is formed which is known to be activated for hydrolysis[13–15].

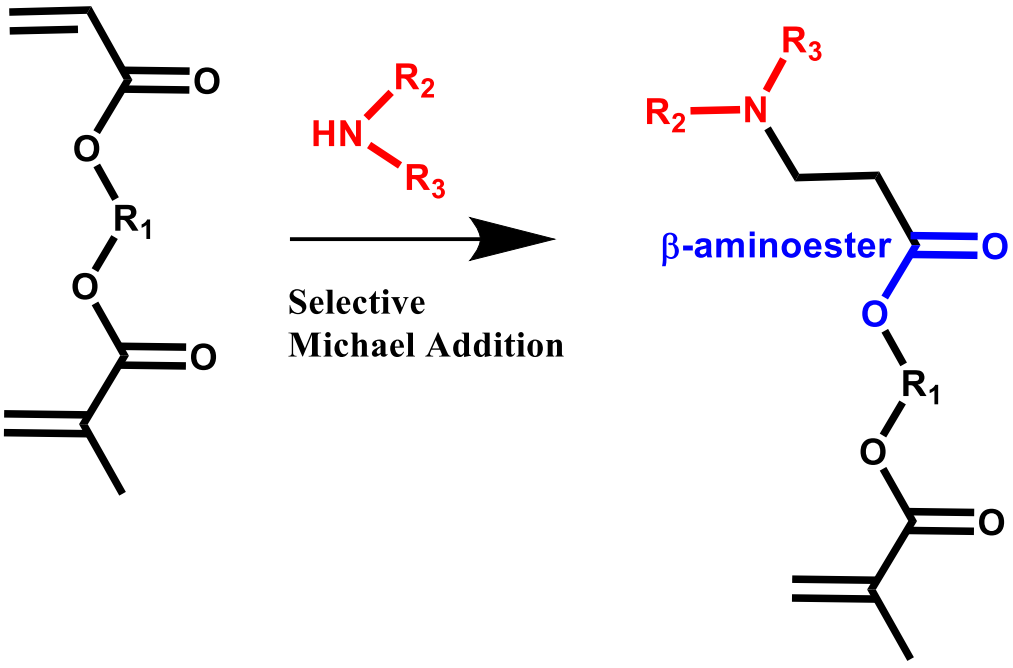

Figure 1.2. Michael selective addition scheme for amines.

Since commercial resins are limited to the use di- or multi-functional stable precursors, in this thesis work the preparation of dimethacrylates with a hydrolysable spacer based on the chemistry mentioned in the previous paragraph

has been designed for the first time. These dimethacrylates will be incorporated into the resins evaluated in 3D printing by vat photopolymerization.

1.1.2. Compositional and crosslinking density heterogeneities related to reactivity issues. Vinyl-lactams vs methacrylate's

Along this thesis, vinylcaprolactam (VCL)-based systems prepared by radical photo polymerization will be extensively investigated for the preparation of thermoresponsive materials. VCL is a vinyl-lactam (like vinylpyrrolidone, VP) and belongs to the family of precursors with low activation for radical polymerization. This means that if VCL is simultaneously copolymerized (via radical reaction) in a closed reactor with other more activated monomers, such as methacrylates (Me), compositional heterogeneity associated with the difference in reactivity will occur. Taking as an example an equimolar copolymerization of VCL and Me, in the early stages of the reaction very Me-rich chains are formed because Me is more reactive. When Me is consumed, very VCL-rich chains are formed in the medium. While this heterogeneity can be "a priori" seen as a drawback, it is also an opportunity to prepare self-ordered systems in a single step. A more detailed description of this process can be found in the literature[16,17].

If difunctional, crosslinker monomers are used, this compositional heterogeneity is transferred to the crosslink density. Thus, if VCL is radically polymerized (in a closed vessel) with a small amount of dimethacrylate (di-Me), the di-Me is preferentially incorporated at the beginning of the reaction because it is more reactive and the result is that a first di-Me rich network will be obtained in the first stages, and a very poorly crosslinked network (or simply non-crosslinked pVCL chains) will be obtained in the final stages of the reaction.

If in addition to di-Me another crosslinker with low activated groups such as a divinylurea (di-V) is added to the medium, the resulting structure is somewhat more complex (see **Figure 1.3**). A first di-Me rich network is still formed, and when di-Me is mostly consumed, a second di-V cross-linked network started to be formed. As a result, even though it is all a VCL network, it is a pseudo-ordered structure with a tendency toward an interpenetrated network type structure, IPN. The di-Me/di-V ratio can define the characteristics of the two networks and the asymmetry in crosslink density between both of them. It is worth mentioning at

this point that this latter structure is the basis of the iFABCell technology hydrogels described in detail in the literature[18]. Part of this thesis will be focused on the preparation and evaluation of 3D hydrogels belonging to the iFABCell technology, which is described in Section 1.3.2 of this Introduction. These hydrogels, which are being sought to be transferred to society, offer advanced cell manipulation capabilities.

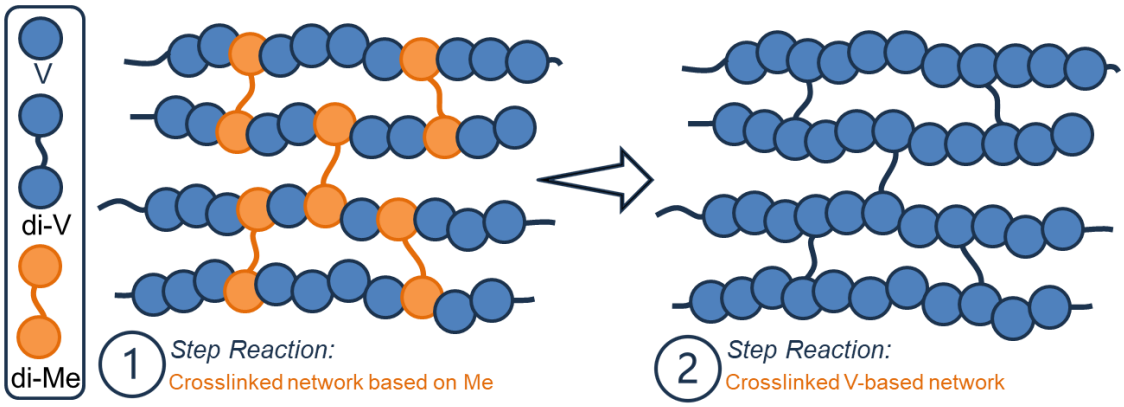

Figure 1.3. Scheme of the crosslinking process of VCL-based iFABCell hydrogels.

1.2. Hydrogels: crosslinked networks with high water affinity

As mentioned in the previous section, if the precursors used in radical polymerization contain crosslinkers, *i.e.*, monomers possessing two or more functional groups, referred to as di- or multifunctional monomers, such polymerization yields are capable of forming polymeric networks. Polymeric networks, in any case, can be prepared by other methods and can have very different architectures. When hydrophylic monomers are employed, those networks are capable of absorbing water and are the so-called hydrogels. Part of this thesis is focused on the preparation and evaluation of hydrogels. In this section, a global vision of this type of structure will be attempted to be given.

A polymer network is, therefore, a three-dimensional structure in which polymer chains are interconnected via covalent or non-covalent/supramolecular interactions, creating a macroscopic material that, unlike conventional isolated macromolecules, polymeric networks are no longer soluble, but rather only capable of swelling in certain solvents[19,20]. These networks are formed through a process called crosslinking, where the functional groups of the difunctional monomers (crosslinking agents) react with each other, resulting in a vast network

of interconnected chains. Crosslinkers are the key feature of polymer networks that differentiate them from other types of polymeric structures[20,21]. Polymeric networks play a critical role in various applications, including the development of hydrogels.

Hydrogels constitute a class of materials capable of retaining a significant amount of water due to their structure, formed by hydrophilic crosslinked polymeric chains[22]. These crosslinked hydrophilic matrices facilitate the flow of oxygen and nutrients, possess mechanical properties similar to many soft tissues, and are capable of supporting cell adhesion and protein sequestration[23]. These materials were the first polymeric biomaterials crafted for implementation within the human body[24,25]. Upon swelling, the high water content of hydrogels, their elastic nature, and the smoothness of the polymer networks are responsible for their excellent biocompatibility, minimal inflammatory response reactions, reduced adverse effects, working with specific compositions, and made them particularly suitable for bio-related applications[26]. Hydrogels can be crosslinked through chemical (such as click chemistry, radical polymerization reactions, Michael additions, etc.) or physical mechanisms (including entangled chains, crystallization, stereocomplex formation, hydrogen bonding, hydrophobic interactions, ionic interactions, etc.)[27,28]. The structure of hydrogels becomes highly influenced by the synthetic procedures employed, the solvent utilized, the types and ratios of monomers/crosslinking agents, and even the history of the polymer (degradation and mechanical stress suffered, among others)[29]. Furthermore, hydrogels can be chemically modified with precise functional groups to exhibit specific stiffness, porosity, biodegradability, and cell compatibility[27].

Hydrogels can be classified as physical or chemical based on the chemical nature of the crosslinking[28,30]. On the one hand, physical crosslinks result in reversible hydrogels. Although these physical crosslinks may not be permanent, they are still capable to render hydrogels insoluble in aqueous media[31]. Chemical or permanent hydrogels, focus of this thesis, are, on the other hand, formed through the covalent crosslinking of polymer chains[28]. Chemical hydrogels can be synthesized in numerous different strategies[28,32], being the most extended the polymerization from monomeric precursors that include crosslinkers (employed in this PhD thesis). Usually, these types of polymerizations to obtain hydrogels

are by radical chain polymerization, initiated either thermally or using a photoinitiator[33–37]. Thermal polymerization occurs when monomers are converted into polymers solely through thermal energy[38]. In contrast to the hydrogels obtained by thermal polymerization, in the case of the hydrogels prepared by photopolymerization, as mentioned before, the initiation of the chain polymerization process is triggered by using light.

Hydrogels have numerous biomedical applications including, for instance, as cell encapsulation matrix or for drug delivery. These applications focused on implantable systems are based on their high biocompatibility, high permeability to oxygen and nutrients, manufacturing flexibility, adaptable composition, and favorable physical properties resembling physiological conditions, independently or in conjunction with cells[31,39]. Therefore, these materials can be used as 3D supporting structures, scaffolds for tissue engineering, carriers for cell encapsulation[40] or drug and gene delivery[41], as well as adhesives or barriers between tissue and material surfaces[42,43]. They can also act as temporary carriers for the formation of cell sheets controlling the cell attachment in a reversible manner[29,44]. In addition to biomedical applications, polymer hydrogels have been explored for domestic uses such as diapers or watering beads for plants, agriculture industry, molds, contact lenses, food packaging industry, enhanced oil recovery, separation technology, plastic surgery, and environmental applications such as treatment of water source[45–47].

In addition to the variety of crosslinking method and the type of monomers employed, hydrogels can exhibit diverse final shapes and morphologies. They may exist, for instance, as amorphous, semicrystalline, supramolecular, or colloidally aggregated structures[48,49].

Hydrogels can be also categorized based on their polymeric origin as natural, synthetic, or hybrid (semi-synthetic). Natural hydrogels are derived from biological sources, encompassing polysaccharides (such as chitosan, dextran, etc.), proteins/peptides (including gelatin, elastin, collagen, alginate, fibroin, etc.), and decellularized extracellular matrix-based polymeric networks[50,51]. Comparing to synthetic biomaterials, natural biomaterials have good biocompatibility and bioactivity[51]. In general, natural hydrogels exhibit biocompatibility (low toxicity), bioactivity (promoting cell activity), and high availability. They mimic the

microstructure, biochemical, and biophysical characteristics of native tissue, facilitating growth and tissue reconstruction[52]. However, their extraction and purification can be costly, and as natural products they exhibit high batch-to-batch variability, thus significantly limiting their reproducibility[53]. Alternatively, the category of synthetic hydrogels comprises polymers prepared from fossil source chemicals. This is, for instance, the case of hydrogels based on vinyl lactams as *N*-vinyl caprolactam (VCL) or *N*-vinyl pyrrolidone (VP) (both monomers employed along this doctoral thesis), or based on poly (ethylene glycol) (PEG) or poly(2-hydroxyethyl methacrylate), among others[50]. Finally, hybrid materials resulting from the combination of synthetic and natural polymers represent a third option[54]. These hydrogels combine the properties of both polymer types and can be engineered, among others, to emulate the biophysical and biochemical characteristics of the natural extracellular matrix[55].

1.3. From the use of thermoresponsive polymers to the fabrication of smart hydrogels: iFABCell Technology.

As mentioned in the previous section, VCL-based responsive hydrogels, which are prepared by radical photopolymerization to obtain smart supports, will be extensively explored throughout this doctoral thesis. These polymeric networks are thermo-responsive hydrogels that undergo structural and mechanical changes in response to slight fluctuations in temperature. In this part, an overview of these smart hydrogels will be provided from a global perspective, with a final focus on those based on VCL.

The thermal response of a particular polymeric material typically arises from the presence of polymer chains that, depending on the external temperature, are able to form either intramolecular interactions (low solubility) or intermolecular interactions (within the environmental water – high solubility)[56]. These materials have attracted considerable interest for their use in biomedical applications since they can be designed to present the thermal response close to the physiological temperature of 37 °C and, therefore, they can act or present a particular response within this range. In aqueous medium, there are typically two basic types of thermoresponsive behaviors exhibited by linear polymers: those with an upper critical solution temperature (UCST) dissolve upon heating[57], while those with a lower critical solution temperature (LCST) precipitate upon heating. However,

there are only a few known polymers that display a controllable UCST in an aqueous medium. This behavior is more commonly observed in organic solvents or water/organic solvent mixtures[58].

On the other hand, LCST polymers have been extensively studied. Their behavior in aqueous solutions is peculiar but useful, as heat does not favor dissolution but rather phase separation. Despite its counterintuitive nature, LCST behavior is quite common, with virtually uncharged water-soluble macromolecules exhibiting a LCST in water. This behavior occurs because polymers dissolve in water due to favorable interactions with the solvent, primarily hydrogen bonds. At elevated temperatures, these weak polymer−solvent interactions are easily disrupted, leading to phase separation.

Nevertheless, it is necessary to highlight that, for the case of thermosensitive polymeric networks (crosslinked systems), by modulating a change in the absorption volume (swell or not swell happened) according to the temperature of the environment, the most appropriate term to define the transition range is not LCST, but volume phase transition temperature (VPTT)[48,59].

The expansion or collapse associated with the critical shift in aqueous solubility produced by changing the environmental temperature has been exploited as a mechanism for drug delivery[60], membrane separation/cleaning, microfluidics[61], sensors, and more recently, *in situ* gelling scaffolds for tissue regeneration[62].

In this doctoral thesis, the thermosensitive systems investigated are polymeric networks based on VCL. pVCL is a thermosensitive monomer that allows for drastic and reversible modulation of the network structure depending on the environmental temperature, causing variations in terms of swelling that also has associated modifications in their mechanical properties, the materials transmittance, or permeability levels[63]. For polymeric networks based on VCL, it is necessary to understand that they are in a hydrophilic state when the temperature is lower than their VPTT (in the range of 32-34 °C for pVCL), as hydrogen bond formation occurs between the hydrophilic segments of the polymer chain and the water molecules in the medium, thus, resulting in swelling of the hydrogel, as mentioned. Conversely, when the temperature is raised above the VPTT value, the hydrophobic segments of the chain fold together, resulting in partial expulsion of the absorbed volume[64].

Most of the literature reported so far focuses on the use of the polymer poly *N*-isopropyl acrylamide (pNIPAm) due to its low cost, reversibility, and physiological temperature response range[65]. In spite of this, in the case of this doctoral thesis, as previously mentioned the selected thermosensitive polymer is pVCL. Both temperature-responsive polymers, *i.e.*, pNIPAm and pVCL present very similar properties, such as being water soluble, non-ionizable, and exhibiting a LCST value (in the range between 32 and 34 ºC[66]) similar and close to the physiological temperature (37 ºC), which makes them very attractive in the biomedical field. However, there are some important differences between the two polymers. First of all related to their biocompatibility[67]. According to the scientific literature pNIPAm is still today a questioned polymer for use in biomedicine[64,67]. Whereas for pVCL, although less studied, it has been described so far as non-toxic[68] and no studies are questioning its biocompatibility. Another difference between the two polymers may be that in the case of pNIPAm, in a possible hydrolysis process under acidic conditions, low molecular weight amine-type residues would be produced, which are potentially neurotoxic[69], while in the case of pVCL the residue would remain anchored to the polymeric chain. These differences have made pVCL as a great option in the field of biotechnology as a thermosensitive polymer, thanks to its cytocompatibility, versatility in terms of LCST value modification, and its solubility in polar and apolar solvents[70]. While pVCL has been employed for a wide range of biomedical applications, this thesis will explore this material for its potential in tissue engineering[71,72]. Therefore, the next part of the introduction will focus on tissue engineering and its role in regenerative medicine.

1.3.1. Tissue engineering applied to the fabrication of cell monolayers: design of thermosensitive support surfaces for cell manipulation

One of the early definitions of tissue engineering (TE) was established in 1993 by Langer and Vacanti[73], who described TE as "an interdisciplinary field that applies principles from engineering and life sciences intending to develop biological substitutes to restore, maintain, or enhance the functions of damaged tissue or organs"[73]. Similarly, the field of regenerative medicine (RM) encompasses the definition of TE including the use of self-regeneration techniques, and, as a result, regenerative medicine is focused on the study of

human cells[74]. This refers to studies where the body itself, with or without the assistance of external agents, applies a regeneration mechanism to the damaged tissue or organ. The combination of these two terms, largely interchangeable in current usage, is known as Tissue Engineering and Regenerative Medicine, represented by the acronym TERM.

The development and application of polymers, among others, as scaffolds for tissue engineering have shown significant potential in regenerative medicine as mentioned[75]. However, there are properties of polymeric materials that presented some limitations for the reconstruction of several tissues (such as cardiac tissue), either for specific tissue features or due to their mechanical properties, degradation rate…etc. In these models, a suitable balance between the rate of tissue growth from cells and the rate of biomaterial degradation is required[76]. These limitations reduce their clinical applications, and the search for the ideal support method for tissue regeneration is still under investigation[77]. In this context, engineering cell monolayers on polymeric supports may be a suitable alternative to overcome these limitations[78]. This technique usually relies on the use of temperature-sensitive (or other stimuli-sensitive) surfaces, as those described in section 1.2.1.1, on which cell monolayers are obtained after cell culture and can be transplanted along with their intact extracellular matrix (ECM). The final objective is to reconstruct the damaged tissue, not through an injection of a cell suspension or by using a polymeric support (scaffold), but from a scaffold-free approach, using cell monolayers for the treatment of the damaged tissue, where both cell-cell junctions and focal adhesions between them, as well as cell-ECM interactions, are maintained. Additionally, in contrast to chemical or enzymatic methods to detach cells from polymeric substrates, in this case, ECM molecular components that regulate cell growth and differentiation are also preserved[77]. Therefore, cells can be noninvasively harvested as intact monolayers together with their ECM[79]. This biological construct retains cell activity and architecture, and as the ECM remains present on the basal surface of the cell sheets, they can be transplanted directly or can even overlap, creating three-dimensional tissue-like structures[75,80]. Moreover, automated systems have been designed to manipulate these biological constructs and be applied in clinical practice[81].

In 1990, Okano's group[82] proposed a novel technology that allows efficient and non-aggressive detachment of cultured cell monolayers. For this purpose, conventional culture plates were coated covalently with the thermosensitive pNIPAm polymer. As an indication of the efficiency of the process, the plate with the smart support showed practically 90% difference in terms of cell detachment when the temperature was lowered, compared to a control plate, evidencing the sensitivity of the culture in terms of cell adhesion and morphology to temperature stimuli. Consequently, it was evidenced, for the first time, that thermosensitive smart surfaces can reversibly modulate cell adhesion due to a change in the hydrophilic character of the supporting surface by decreasing temperature, as shown in **Figure 1.4**. As a result of these findings, currently, there is a material on the market called UpCell that shares the capacity to grow cells and allow for mild cell detachment for application in multiwell plates for cell culture[83]. Working with this pNIPAm-based model, a noticeable success has been obtained in several clinical indications[84,85], such as cardiac, corneal, periodontal, lung, or cartilage tissue. In these procedures, an additional carrier (such as a nitrocellulose membrane) has been used to transport cell sheets from the rigid thermosensitive support to the injured tissue.

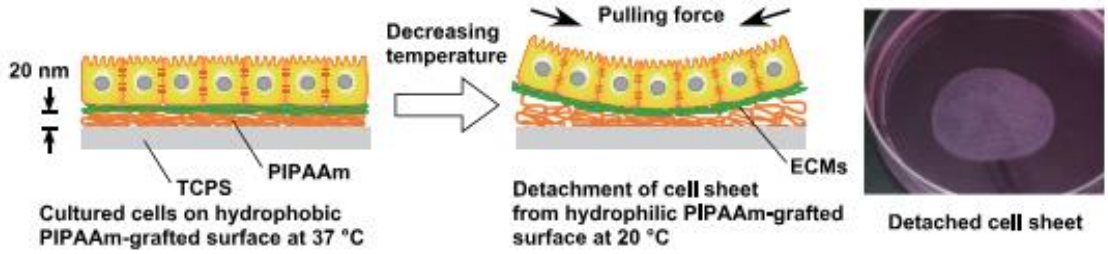

Figure 1.4. Illustrative scheme of a cell sheet monolayer prepared using a temperature-sensitive cell culture surface. The pNIPAm surface allows the cultured cells to detach as a continuous sheet by simply lowering the temperature[76].

In addition to pNIPAm-based supports, other strategies and polymers can be used as a basis for stimuli-dependent cell sheet harvesting. In particular, a notable example is the use of hydrogels, as will be described throughout this thesis. Based on the preparation of pVCL-based supports previously reported by our group[71], in this thesis we describe the preparation of 2D (planar) and 3D (non-planar) hydrogel platforms, using as a main component VCL. Moreover, the optimal conditions for culture of C166-GFP mouse endothelial cells, as well as

for cell sheet formation and detachment will be evaluated. In this context, tissue engineering based on cell monolayer transplantation can be used for the fabrication of various tissues or to be directly applied as a cell therapy for tissue regeneration[86,87].

1.3.2. iFABCell Technology: thermoresponsive polymeric platforms for cell growth and non-aggresive monolayer detachment.

Based on the previous sections, the Polymer Functionalization group (FUPOL) has optimized a technology called iFABCell. This technology (**Figure 1.5**), a key component of this doctoral thesis, involves preparing free-standing hydrogels that allow cell culture and cell detachment upon temperature decrease, and that are ideal for direct transplantation of cell monolayers into the body due to their remarkable mechanical strength and elasticity/flexibility, enabling them to effectively regenerate damaged tissue. Moreover, this approach allows the hydrogel to be placed directly on the target tissue for in situ cell transplantation, eliminating the need for additional carriers (as in the case of pNIPAm surfaces mentioned before). Furthermore, these hydrogels facilitate the culture and detachment of isolated cells, making them useful for maintaining cell cultures or as platforms for the analysis of cell processes such as adhesion, proliferation or differentiation. It is worth mentioning that this technology can be also employed to coat multiwell plates typically utilized in cell culture labs.

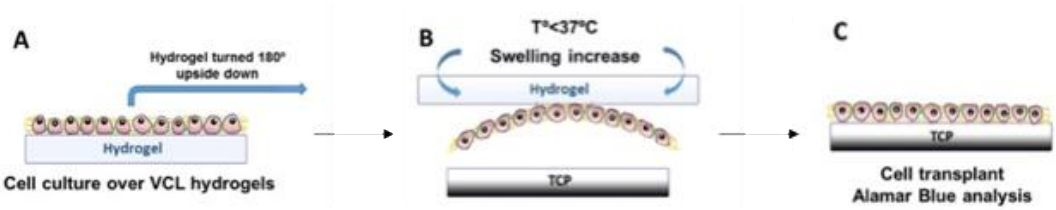

Figure 1.5. Scheme of the procedure of the technology underlying iFABCell to produce and recover cell sheet monolayers.

There are some important differences between UpCell, described before and can be thus considered as the competitor for mild cell detachment, and iFABCell. First of all, both systems are chemically different. While iFABCell is based on pVCL hydrogels, UpCell utilizes another thermosensitive polymer, pNIPAm. In addition to the type of monomer employed, the main difference between iFABCell supports and their competitor UpCell lies in their dimensionality. UpCell consists

of individual thermosensitive pNIPAm macromolecular chains grafted onto the surface of a polystyrene plate, with a thickness of a few nanometers (macromolecular chain length scale). In contrast, iFABCell is based on pVCL polymer crosslinked networks, therefore, with interconnected chains to form a single entity that can exist as a free-standing hydrogel or be anchored as a coating to a support material, such as a multiwell plate. The thickness of these iFABCell coatings is several orders of magnitude greater than the pNIPAm grafts (ranging from 1 to 1000 microns, *i.e.*, macroscopic scale). As a result, the thermosensitive swelling/deswelling effects are more pronounced, thereby facilitating cell culture detachment, whereas UpCell has thickness restrictions causing inefficiency in cell culture detachment[88]. Additionally, the robust properties of the iFABCell technology allow for their chemical customization formulating the hydrogels with other functional monomers, and the encapsulation and controlled release of active compounds. As mentioned before, part of this thesis is devoted to preparing advanced iFABCell hydrogels, including the implementation of their 3D printing.

1.4. Additive manufacturing: as tool to create customized freeform parts: definitions and technologies

Since, on the main objectives of this thesis is to develop and evaluate different resins for 3D printing by vat photopolymerization, in this section it is aimed to provide a general overview about 3D printing or additive manufacturing focusing later on vat photopolymerization.

Additive manufacturing (AM), also known as 3D printing, is one of the critical components of what has been recently named Industry 4.0[89–92]. AM can be defined as a process of joining materials to make objects from 3D digital models, usually created by the addition of material layer by layer, as opposed to subtractive manufacturing methods, where the material is gradually removed to obtain the desired shape[93]. The AM concept was first introduced in the 1980s with the aim of producing in a straightforward manner functional prototypes[94]. With the rapid development of digital technologies[95], AM has become a key technology for fabricating customized products. Equally, AM technologies present additional advantages including the possibility to create sophisticated objects with advanced attributes (new materials, geometries, shapes,

mechanical, thermal, and solubility properties)[90] the possibility to modify the object by directly modifying the computer-aided design (CAD) design or the significant reduction of the material waste just to mention few of them. However, one of the major limitations of AM is still the limited amount of available materials, many of them optimized for other polymer processing technologies, with low availability of high-performance materials with specific properties such as biocompatibility[96].

The main objective of AM is to swiftly produce prototypes or base models (with more and more examples of functional parts), serving as the foundation for the development of optimized models and lastly, in a short period of time obtain the final product[8]. The fundamental principle of this technology lies in the direct manufacturing of a model, initially created using a three-dimensional (3D) CAD software, using a 3D printer that significantly reduces the number of tools required as well as the planning of the process.

The materials currently used in 3D printing include metals, polymers, ceramics, and concrete. Most of these materials have been directly transferred from other fabrication technologies into 3D printing. However, more recently developed sophisticated materials have become available that have been specifically designed for 3D printing. Currently, 3D printing stands as a leading-edge technology with a wide scope in different fields of application, including rapid prototyping, biomedicine, hearing aids[97], dental industry[93], jewelry manufacturing[98], automotive[99], electronics[100], aerospace and robotics[101,102], but also for the preparation of molds[47] and tooling[103] just to mention a few. Ongoing research efforts continue to advance the concepts of 3D printing technology, leading to fast and cost-effective product manufacturing, along with huge improvements in manufacturing resolution and, therefore, the quality of printed objects[102].

1.4.1. AM materials and technologies

Seven types of additive manufacturing technologies are usually recognized, based on the employed methodology, with each having its corresponding type of material. Nowadays, a wide variety of materials are used, ranging from thermoplastics or thermosets to ceramic materials or even metal powders. **Figure**

1.6 shows the different 3D printing technologies currently available in the industry.

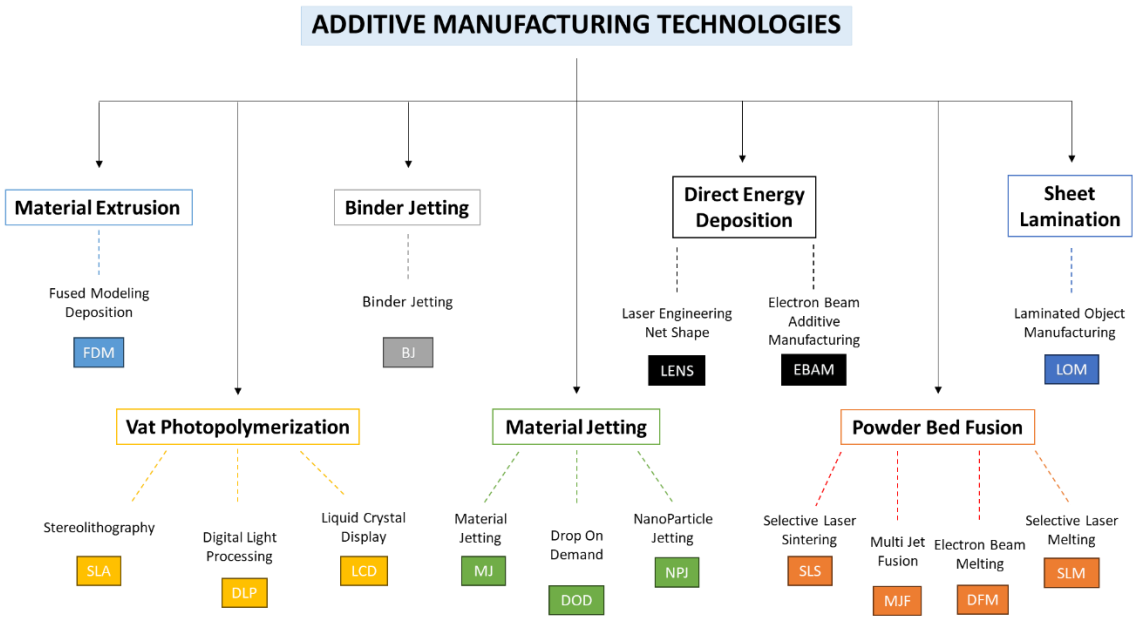

Figure 1.6. Overview of the existing process categories within additive manufacturing using poylmers, ceramics and metals. (According to EN ISO 17296-2).

- Material extrusion (MEX): Typically employed for the fabrication with thermoplastic polymers but also with ceramics dispersions and viscous materials. These materials, in filament or paste format, are melted and selectively dispensed through a nozzle.
- Vat photopolymerization (VPP): A liquid-to-solid conversion process is produced, using photopolymerization to fabricate solid objects from a vat of liquid resins under ultraviolet (UV) light irradiation. The UV source can come in the form of localized lasers or using projectors or LED screens. The materials used in this technology are liquid or paste photoreactive resins with or without fillers.
- Binder jetting (BJ): In this AM process, a liquid bonding agent is precisely deposited to fuse powder materials. Those areas covered with the bonding agent are consolidated through chemical and/or thermal reactions. The materials for this type of technology are polymers, metals, and ceramics.
- Material jetting (MJ): In this type of 3D printing, the materials that can be used are photopolymers, metals, or waxes. The manufacturing material is

selectively deposited in droplets using inkjet-style printheads and solidified by UV light exposure. In contrast to VPP in this case the 3D printer does not require the use of a vat and the material is directly dispensed onto the fabrication area.

- Directed energy deposition (DED): Focused thermal energy is used to fuse materials by melting as they are being deposited. The materials suitable for this technology are polymers, metals, and ceramics.
- Powder bed fusion (PBF): A laser beam scans selected locations of the powder bed at a controlled speed, fusing the powder to the solid material beneath through either full or partial melting. The materials appropriate to be employed in this technology are polymers, metals, and ceramics.
- Sheet lamination (SL): The process of SL involves stacking multiple layers of foil material to fabricate an object. Each foil layer is precisely cut into shape, either manually with a mechanical knife or using a laser, to fit the object's cross-section. The materials used in SL are metallic sheets, ceramics, and hybrid materials.

Among all these AM technologies available, in this doctoral thesis, a technique enabling the photopolymerization of tailor-made resins has been selected in order to produce targeted hydrogels. Our group has extensive experience in the design of photosensitive resins, but their fabrication has so far been restricted to solid highly crosslinked 3D structures. Therefore, VPP enables the transition from obtaining materials through 2D photopolymerization to 3D photopolymerization technology, obtaining three-dimensional materials with a more complex shape. Another important advantage of this technique is the excellent definition and smooth surface finish of the fabricated parts, thus, providing an improvement in comparison to other techniques.

1.4.2. Vat photopolymerization: from the pioneer development to the current alternatives

Vat photopolymerization 3D printing, was the first AM technology reported and commercialized in the early 80s. This technology, emerged as a revolutionary fabrication technique, enabling the manufacture of intricate structures with astonishing precision and accuracy[94,104]. The principle of photocuring layer by

stereolithography (SLA) was first reported by Hideo Kodama[105]. However, this technology was patented by Charles Hull in 1986 in a process known as SLA[94,106]. Since its inception, this technique has continued to advance, leading to the appearance of other more recent alternatives such as digital light processing (DLP) or liquid crystal display (LCD), which are among the most widely used additive manufacturing processes [93,107,108]. The process consists of printing successive layers of materials that are formed on top of each other by the use of UV light by solidification of a liquid photosensitive resin layer-by-layer[91]. As will be discussed in the next paragraph, the differences between SLA, DLP, and LCD are related to the light source and the methodology employed to apply the UV light, as can be observed in **Figure 1.7.**

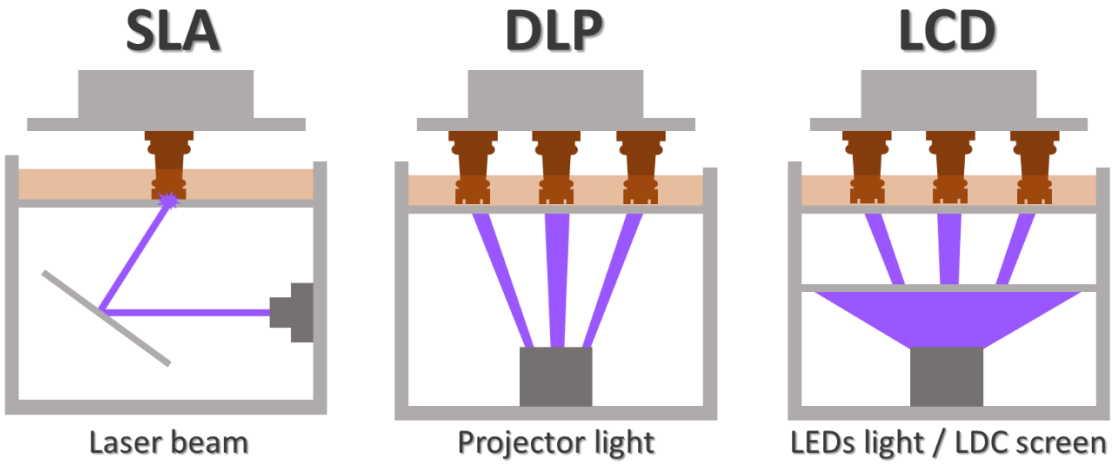

Figure 1.7. Diagram showing the main methodologies employed to apply the UV light of typical vat photopolymerization bottom-up 3D printers: SLA, DLP, and LCD.

In vat printing technologies, the photosensitive resin is placed in a vat or tank placed either above or below the light source depending on the 3D printer configuration[108]. In top-down printing, the build plate remains submerged beneath the resin tank and descends sequentially as each layer is cured. Conversely, in bottom-up printing, the build plate is suspended above the vat, while the light passes through a film or window located at the bottom (**Figure 1.7**). The bottom-up printing is more affordable the top-down printing and has the advantage that the build volume is smaller and less resin is needed, but the printed part is suspended, and more supports are required.

In addition to the set-up of the building plate vs resin tank, considering the type of light and how the light is applied, three different VAT printing techniques are currently commercially available, *i.e.*, SLA, DLP, and innovation based on DLP technology, which is LCD[109]. It is worth noting that all these techniques share the same principle, *i.e.*, are based on the spatially controlled solidification of a liquid formulation upon selective exposure to light.

Vat photopolymerization is known for its exceptional resolution and accuracy in comparison to other AM technologies. The specified resolution on most printers typically refers to the resolution in the XY plane. In laser-based systems, this corresponds to the width of the laser beam itself, while in projected light methods, it reflects the optimal resolution of the image, *i.e.*, pixel size (similar to television resolution ratings). The layer thickness represents the resolution in the Z direction, influenced by factors such as the power delivered by the light source and the precision of mechanical components. Depending on the printer type, build sizes are determined by either the vat size or the capacity of the light projector.

1.4.2.1. Stereolithography

Stereolithography was the first available technique in this type of printing to be developed, recognized for its good resolution. A SLA printer is based on a transparent tank filled with light-curing resin, in which the platform immersed in the resin, after being lowered along the Z-axis of the printer, is irradiated with a laser beam (which must draw the entire layer to cure it because it goes point by point) according to the file coming from the printer's software, after being sliced with respect to the standard template library (STL). The curing process is repeated layer by layer until the 3D-mentioned model is completed. The very narrow width of the laser beam allows for high resolution. Printing speed correlates closely with curing depth and light penetration, determined by the material's properties. Enhancements in these parameters are achievable through the utilization of light absorbers and polymerization facilitators[110]. The accuracy of an SLA 3D printer is related to the diameter of the laser beam at the curing point. The layer height range typically falls between 12 and 200 µm, with 100 µm being the preferred choice for commercial resins. SLA works best with resins of low viscosity (<4 Pa s), enabling the resin to flow and replenish between layers[111].

1.4.2.2. Digital Light Processing

This 3D printing technique uses a projector to send the image of the layer of the object that will solidify the resin. For that reason, the major difference between DLP and laser-based SLA is that DLP employs the projection of UV light (or visible light) through a digital micromirror device (DMD) to instantaneously display a single image of the entire layer across the resin. Basically, DLP projects a white image of a designed pattern or a layer of a 3D CAD model that will give rise to the solid part of the object in that layer, and the rest in black will remain uncured. In other words, where there is light, the material hardens and where there is not, the resin remains uncured[112].

DLP provides faster printing speeds compared to SLA when large parts are required. It is worth recalling at his point that DLP is able to cure an entire layer in a single irradiation step while SLA requires to “draw” with a laser the part to be printed. As a result, DLP speed is determined only by the dimensions of the objects along the Z-axis[113]. For the production of a high-resolution structure, precise adjustment of parameters such as curing time per layer, layer thickness, and UV light intensity, is required. These parameters are related to the concentration and type of both photopolymer and photoinitiator present in the resin. Hence, it is important to note that this technology only supports viscosities within the range of 0.1-10 Pa·s[114] and with an adjustable layer height typically ranging from 12 to 200 µm. In this case, 50 or 100 µm is the common layer height for commercial resins, as in SLA. It is imperative to acknowledge that the majority of desktop DLP 3D printers feature a predetermined XY resolution, typically ranging from 35 to 100 µm.

1.4.2.3. Liquid Crystal Display

LCD technology is an innovation based on the principles of the DLP technology which employs digital projection with light-emitting diodes (LEDs)[108]. The main difference is the light source itself because LCD uses a single source lamp from an array of LEDs masked by a LCD screen where the light is not supposed to hit the resin, to form a 2D image of slices[115]. As a result, in those cases where the fabrication of multiple parts is required or when the surface occupied by the part to be printed is large, LCD/DLP resulted to be significantly faster than SLA as the light intensity stays the same across the entire vat.

1.4.3. Design of photosensitive resins for vat photopolymerization: components and their roles

The composition of the light-curing resins used in VPP techniques comprises polymerizable components, which may contain monofunctional monomers and crosslinkers (di- or multi-functional monomers), both of which may be of an oligomeric nature (all of them from now on, monomers), photoinitiators, diluents, and other additives such as fillers. Furthermore, the formulation design of photopolymer constituents is essential for the performance and properties of photopolymerization-based 3D printing systems[6,116].

Photoinitiators are compounds that undergo decomposition (in the case of radical photoinitiators) when the resin is irradiated with UV light, thereby becoming reactive. Polymerization is then initiated by the reaction of the reactive photoinitiator with specific functional groups present in the monomers/oligomers and crosslinking agents (typically acrylates and methacrylates), constituting the backbone of the 3D polymer network. Overall, currently employed photoinitiators can be categorized into two main groups: radical and cationic photoinitiators. In 3D printing, the amounts typically added to the composition of the resins are between 0.5 and 12% by weight enabling cure depths from 0.1 to 2.5 mm[7]. Photoinitiators are vital in triggering a rapid, accurate, and controllable photopolymerization[117] and are also involved in the accuracy of the fabricated part.

Therefore, the selection of a photoinitiator plays an essential role in the photopolymerization because it directly influences, among others, the curing rate. Effective photoinitiator systems must comply with basic requirements, including thermal stability and strong absorption within the desired wavelength region (in DLP/LCD 3D printers the most common wavelength is 405 nm), enabling efficient generation of reactive species upon irradiation. These reactive species then engage with monomers/oligomers and crosslinking agents to initiate the photpolymerization[6].

Another main component of the resin is the UV photoabsorber, an example used in this thesis is Sudan I[7]. Photoabsorbers are required in order to achieve micrometer-scale resolution in the Z direction of the 3D printed pieces since a

UV-light photoabsorber is used to restrict UV-light penetration. Through the optimization of UV penetration depth, a reliable procedure for the fabrication of 3D objects with high model accuracy is established.

In addition to photoabsorbers, diluents can be also used to reduce the viscosity of the resin, to dissolve in a better way some of the components of the resin, or to maintain the resin in the liquid state at room temperature, thereby preventing for instance, the crystallization and/or precipitation of any of the components. Diluents are especially important when reinforcements or oligomers that can be very viscous are added into the resin. Another factor arises when employing a monomer with a melting point above room temperature, leading to crystallization at ambient conditions, thereby compromising the print quality. An illustrative example of the latter is discussed in this thesis where VCL, crystalline and solid at room temperature (RT), has been employed as the main component to produce the thermoresponsive hydrogels and presented a melting point of around 37 °C.

Resin viscosity is also a critical parameter in vat polymerization, affecting both the curing surfaces between two successive layers and the printing time[118–120]. In general, low viscosities are desired to allow the proper coating of the previous printed layer or the surface of the immersive platform[121]. Too high viscosity may lead to air entrapment during platform movement, resulting in defects in the printed piece. To address this issue, diluents[122] or reactive monomers[123] are commonly incorporated into the viscous oligomer system to balance the required viscosity range with the desired properties. In addition, a high viscosity resin will take longer to flow and form a new uniform layer, thus increasing the printing time[119,124]. Besides, diluents and monomers can be volatile, and excessive usage may compromise the original mechanical properties of the oligomer[125], resulting in volumetric shrinkage of the printed pieces[126,127]. Additionally, shear thinning behavior (non-Newtonian behavior in which the fluid viscosity decreases with increasing shear stress) can be advantageous for vat polymerization techniques to enable the spreading of homogeneous layers[128,129].

Moreover, the addition of fillers enables to modulate the properties of the materials at low cost, e.g., to obtain materials with improved properties. Thus, fillers are typically employed to adjust the physical properties of polymer resins

while preserving their printability. As an example of the use of fillers in photosensitive resins, in this doctoral thesis, multi-walled carbon nanotubes (CNTs) were used, and will be discussed in Chapter 7.

Monomers (mono and multifunctional) are also relevant components of the resin because they play a major role on the polymerization step (either by a radical or a cationic polymerization) and also in the crosslinking upon exposure to UV light in the presence of a photoinitiator. The commercial photosensitive resins employed for VPP, comprise photoinitiators able to launch the polymerization when exposed to light[130,131] in the UV range. Therefore, monomers (that will define the reaction kinetics) and the photoinitiator (that will determine the wavelength of the light required), are without any doubt the most critical components. Typically used monomers are acrylate and methacrylate derivatives in which the C=C bonds of the vinyl groups react through a radical polymerization process[132] with fast reaction rates thus reducing the time required to photopolymerize each layer.

Within many available acrylate-based resins, multifunctional acrylates (crosslinking agents) are commonly employed, though multifunctional monomers offer the possibility to introduce crosslinking sites and tune the final properties (mechanical, solubility, swelling, …) of the cured resin. Moreover, it should be noted that the molecular weight of the monomer will significantly impact the viscosity of the liquid resin. This aspect requires also a particular consideration as will be described in this work.

An important aspect of commercial resins is that they result in highly cross-linked networks, thus preventing swelling of the fabricated part in the photosensitive resin itself. Since the part is suspended during printing, swelling of the part would lead to a weakening of the adhesion of the part to the build platform and their possible detachment. For this reason, the use of crosslinking agents is also crucial, as the absence of crosslinkers in the resin may complicate the adhesion of polymerized layers to the platform, resulting in longer exposure times per layer and increased printing durations or even preventing the formation of the part if the polymer formed is soluble in the photosensitive resin.

In this thesis we propose to explore precursors that are not used in commercial resins. As mentioned above, commercial resins yield stable and permanent

printed parts. In contrast to this behavior, in a first block of the thesis, we want to exploit the opportunities associated with the use of labile crosslinkers, which have never been described in vat photopolymerization, in particular, for the printing of sacrificial 3D printed parts (Chapter 3) and the preparation of readjustable networks (Chapter 4). In a second block of the thesis, we iimplemented the 3D printing of hydrogels of the iFABCell technology. The possibility of having iFABCell 3D parts can open new ways in the use of this technology.

1.4.3.1. Fundamental printing parameters in vat photopolymerization

In addition to the main components of a photosensitive resin, the printer parameters should be also fine-tuned according to the resin's characteristics. Intrinsic properties, such as viscosity and the photosensitive properties of the resin, are important to set the optimal parameters of the printing process. The 3D printer parameters that can be modified and optimized include:

a) Layer thickness ranges usually from 12 μm up to 200 μm, impacting both printing speed and printing quality[94]. Lower layer thickness yields better detail definition and smoother surface finish in printed objects, although the required printing time is longer and, as a result, the printing costs are higher. Normally, vat photopolymerization printers operate within a minimum height range of 12-25 μm and a maximum of 200 μm. The hydrogels printed throughout this thesis using this technique have been prepared with layer thicknesses in the range between 50 and 100 μm[104].

b) The layer exposure time is defined as the time that each layer is exposed to a certain light intensity and wavelength. Depending on the type of printer (SLA/DLP/LCD), exposure times vary for the same resin due to the 3D printer specifications (including intensity of the light irradiation and the type technology employed)[133]. This parameter is adjusted according to the physical properties of the resin (such as the reactive groups of the monomers/oligomers, the amount of crosslinking agent, or the resin viscosity just to mention a few of them), requiring more or less exposure time for solidification. To ensure the adhesion of the initial layers to the printing platform, an initial exposure time (also named, bottom exposure time) is set, usually 8 to 12 times longer than the standard exposure

time, and applied to the first 3-7 printing layers. Generally, longer curing time of the base layers will improve the adherence to the building platform.

Photosensitive parameters are also related to the intrinsic properties of the resin. Uniformity of light intensity is an important parameter for the precise formation of 3D solid features, where the shape, size, and surface texture of cured layers correspond to the regions within the optical field with sufficient energy to trigger polymerization[6]. In this regard, the vertical curing precision is related to the curing depth, C_d (μm), obtained from the thickness of the polymerized (or at least gelled) resin, which is theoretically expressed using Jacob's working curve as follows (equation 3.1):[90,91,134–136]

$$C_d = D_p \cdot \ln\left(\frac{E_{max}}{E_c}\right) \quad (3.1)$$

Where D_p (μm) is the penetration depth of the resin, *i.e.*, the distance photons travel in the resin before being absorbed by a resin component[120], E_{max} (mJ·cm^{-2}) is the irradiation intensity at the surface and E_c (mJ·cm^{-2}) is the critical exposure energy required to induce polymerization.

This expression translates into a straight line on a semilogarithmic plot, with C_d on the y-axis versus Exposure (E_{max}) on the x-axis. The point where the Jacobs working curve intersects with the x-axis denotes E_c, whereas D_p represents the slope of the linear fit. An ideal resin for vat polymerization exhibits low E_c values, facilitating reaction initiation with a low energy dose and high D_p values to optimize cured thickness[7]. To determine if a resin is suitable for a specific printer, it is recommended to calculate C_d corresponding to the light source employed and compare it with the targeted layer thickness (z)[137]. The layer thickness obtained must be equal to or less than the curing depth, which should be high enough to reduce and optimize the manufacturing time. It has to be taken into account that the presence of additives such as particles and reinforcements alters the light-curing behavior of the resin (E_c and D_p) due to potential light scattering and/or absorption by the additive. As a result, an adjustment of the layer thickness is required[7].

c) The last technical parameter that is defined is the Z-axis lift time, which denotes the speed at which the build platform is raised from the resin tank after each light-cured layer. If the lift time is excessively short, the model may break

and damage the supports, due to the tension between the building platform and the fluorinated ethylene propylene (FEP) sheet at the tank bottom. Conversely, reducing the speed too much will increase the printing time. The standard speed typically stands around 65 $mm \cdot min^{-1}$.

1.4.4. Workflow of a 3D printing process

A typical vat polymerization-based printing process entails three main stages (see **Figure 1.8**). First, preprocessing involves generating an idea with a CAD design. The second step is the printing process which entails the slicing and the printing steps. The third and final step is postprocessing, which involves cleaning the printed parts (washing and support removal) and conducting a post-curing process.

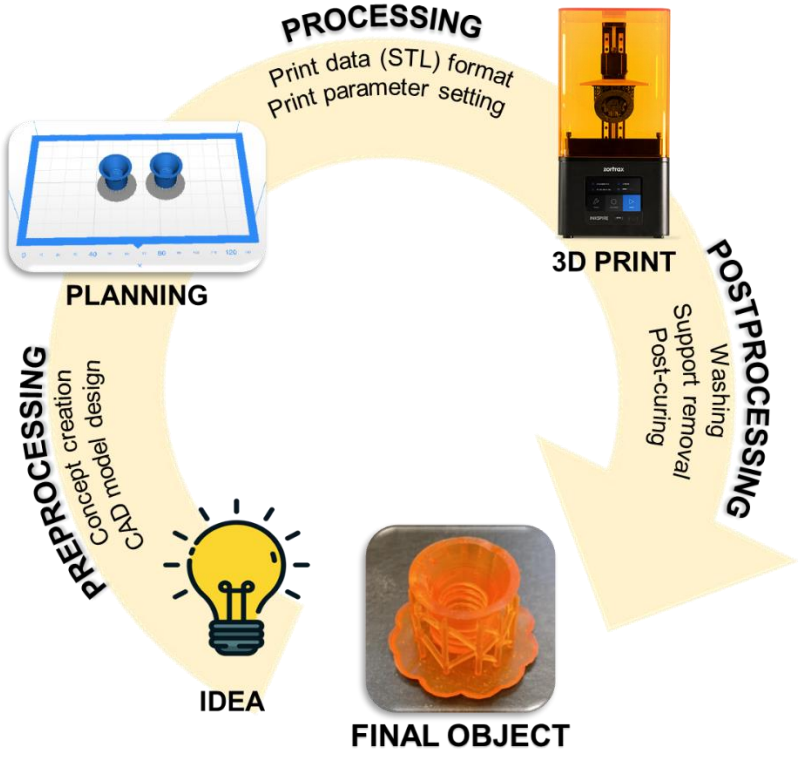

Figure 1.8. Scheme of a typical production process by vat photopolymerization 3D printing.

Prior to 3D printing an object, a 3D model is designed or obtained from a scanned part or even from medical resonance images (Dicom analysis). This 3D model is then converted into the STL format, describing the 3D model's surface with a network of triangles of different sizes, depending on the required resolution[7]. A

finer triangular mesh results in a smoother surface on the printed object. This stage is known as preprocessing.

Processing, the second stage of the production of a 3D printed object[94], involves slicing of 3D part in multiple layers, *i.e.*, transforming the 3D model into multiple 2D layers. Each layer must be supported by the platform, the previous layer, or additional support elements. The layer thickness depends on the printer, the AM technology, and the resolution quality requirements of the final product. Once printing parameters are set, the sliced model is sent to the printer.

After printing process is completed, the model is removed from the platform, and the post-processing step begins. In vat photopolymerization, printed objects directly obtained after printing are immersed in a washing solution, usually 2-propanol, to remove uncured liquid resin[132,138]. Once the parts have been washed and dried to complete the photopolymerization reaction (thus enhancing and fix the mechanical properties), the objects are exposed to additional UV light in a UV-curing chamber (time and temperature will be controlled). It is worth noting that during the fabrication process, the parameters selected for the photopolymerization process are optimized in order to reduce the printing time and thus the final part is only partially cured. The postcuring step is thus critical to ensure a complete polymerization and avoid the release of unreacted components (monomers/oligomers/crosslinking agents).

The cleaning time, temperature, and timing of the curing process significantly influence the mechanical properties of the finished pieces. Additional post-processing steps may include other additional steps such as the removal of supports.

1.5. Organization of this PhD work

This PhD thesis has been organized as follows. In the next chapter, Chapter 2, the hypothesis and objectives of the work are established. Subsequently, Chapter 3 presents the materials and methods used throughout the thesis.

Chapters 4 and 5 are devoted to explore the use of the aforementioned hydrolysable crosslinkers in VPP. Specifically, Chapter 4 focuses on the printing of water-sacrificial parts, while Chapter 5 focuses on the printing of readjustable

networks and/or hydrogels. The resins in these two chapters are based on (meth)acrylates.

Chapters 6 and 7 make use of the team's experience in preparing and evaluating VCL-based networks (iFABCell technology) to prepare novel VCL-based platforms. In particular, Chapter 6, partly making use of what has been learned in Chapters 4 and 5, explores different routes to prepare printable VCL-based resins, *i.e.*, procedures for 3D printing iFABCell parts are developed. Finally, Chapter 7, making use in this case of what was learned in Chapter 6, deals with the preparation of CNT-doped VCL-based iFABCell networks.

Finally, Chapter 8 presents the general conclusions of this doctoral thesis.

References

1. Wu, J. *et al.* Evolution of material properties during free radical photopolymerization. *J Mech Phys Solids* **112**, 25–49 (2018).
2. Andrzejewska, E. Photopolymerization kinetics of multifunctional monomers. *Prog Polym Sci* **26**, 605–665 (2001).
3. Check, C., Chartoff, R. & Chang, S. Inkjet printing of 3D nano-composites formed by photopolymerization of an acrylate monomer. *React Funct Polym* **97**, 116–122 (2015).
4. Kaur, M. & Srivastava, A. Photopolymerization: A review. *JOURNAL OF MACROMOLECULAR SCIENCE Part C—Polymer Reviews Vol. C42* **No. 4**, 481–512 (2002).
5. Lee, H. & Fang, N. Micro 3D Printing Using a Digital Projector and its Application in the Study of Soft Materials Mechanics. *J Vis Exp* (2012) doi:10.3791/4457.
6. Kowsari, K. *et al.* Photopolymer formulation to minimize feature size, surface roughness, and stair-stepping in digital light processing-based three-dimensional printing. *Addit Manuf* **24**, 627–638 (2018).

7. Bartolo, P., Bertsch, A. & Renaud, P. Stereolithography. (2011) doi:10.1007/978-0-387-92904-0_4.

8. Gibson, I., Rosen, D., Stucker, B. & Khorasani, A. *Additive Manufacturing Technologies*. (2020). doi:10.1007/978-3-030-56127-7.

9. Kaur, M. & Srivastava, A. K. PHOTOPOLYMERIZATION: A REVIEW. *Journal of Macromolecular Science, Part C* **42**, 481–512 (2002).

10. Bartolo, P. J. da S. Optical approaches to macroscopic and microscopic engineering. (2001).

11. Zhakeyev, A., Zhang, L. & Xuan, J. Photoactive resin formulations and composites for optical 3D and 4D printing of functional materials and devices. in 387–425 (2020). doi:10.1016/B978-0-12-816805-9.00013-2.

12. Navarro, R. *et al.* Understanding the regioselectivity of Michael addition reactions to asymmetric divinylic compounds. *RSC Adv.* **7**, 56157–56165 (2017).

13. Redondo Marín, J. A. *et al.* Prodendronic Polyamines from Stable or Labile Methacrylates Obtained by Selective Michael Addition onto Asymmetric Diacrylic Compounds. *J Polym Sci A Polym Chem* **52**, (2014).

14. del Prado, A., Navarro, R., Gallardo, A., Elvira, C. & Reinecke, H. Synthesis of randomly aminated polyvinylpyrrolidone and its use in the preparation of hydrolyzable conjugates. *RSC Adv.* **4**, (2014).

15. Redondo, J. A. *et al.* Effect on in vitro cell response of the statistical insertion of N-(2-hydroxypropyl) methacrylamide on linear pro-dendronic polyamine's gene carriers. *European Journal of Pharmaceutics and Biopharmaceutics* **93**, 303–310 (2015).

16. García-Sobrino, R. *et al.* Fabrication of 3D cylindrical thermosensitive hydrogels as supports for cell culture and detachment of tubular cell sheets. *Biomaterials Advances* **144**, 213210 (2023).

17. García-Sobrino, R. *et al.* Cell harvesting on robust smart thermosensitive pseudo-double networks prepared by one-step procedure. *Eur Polym J* **209**, 112925 (2024).

18. Reinecke, H. *et al.* Tecnología iFABCell - ¿una revolución dentro de la Medicina Regenerativa? Preprint at (2023).

19. Kaiser, T. Highly crosslinked polymers. *Prog Polym Sci* **14**, 373–450 (1989).

20. Weerasinghe, M. A. S. N. *et al.* Educational series: turning monomers into crosslinked polymer networks. *Polym Chem* **14**, 4503–4514 (2023).

21. Gu, Y., Zhao, J. & Johnson, J. A. Polymer Networks: From Plastics and Gels to Porous Frameworks. *Angewandte Chemie International Edition* **59**, 5022–5049 (2020).

22. Kopeček, J. Hydrogel biomaterials: A smart future? *Biomaterials* **28**, 5185–5192 (2007).

23. Tibbitt, M. & Anseth, K. Hydrogels as extracellular matrix mimics for 3D culture. *Biotechnol Bioeng* **103**, 655–663 (2009).

24. WICHTERLE, O. & LÍM, D. Hydrophilic Gels for Biological Use. *Nature* **185**, 117–118 (1960).

25. Kopeček, J. & Yang, J. Hydrogels as smart biomaterials. *Polym Int* **56**, 1078–1098 (2007).

26. Hoare, T. R. & Kohane, D. S. Hydrogels in drug delivery: Progress and challenges. *Polymer (Guildf)* **49**, 1993–2007 (2008).

27. Cushing, M. & Anseth, K. Materials science. Hydrogel cell culture. *Science* **316**, 1133–1134 (2007).

28. Maitra, J. & Shukla, V. Cross-linking in hydrogels - a review. *Am J Polym Sci* **4**, 25–31 (2014).

29. Slaughter, B. V, Khurshid, S. S., Fisher, O. Z., Khademhosseini, A. & Peppas, N. A. Hydrogels in Regenerative Medicine. *Advanced Materials* **21**, 3307–3329 (2009).

30. Chang, C., Duan, B., Cai, J. & Na, N. Superabsorbent hydrogels based on cellulose for smart swelling and controllable delivery. *European Polymer Journal - EUR POLYM J* **46**, 92–100 (2010).

31. Nguyen, K. T. & West, J. L. Photopolymerizable hydrogels for tissue engineering applications. *Biomaterials* **23**, 4307–4314 (2002).

32. Ahmad, Z. *et al.* Versatility of Hydrogels: From Synthetic Strategies, Classification, and Properties to Biomedical Applications. *Gels* **8**, (2022).

33. Wei, Y.-Y., An, S.-S., Sun, S. & Jiang, Y. Photo-polymerized and thermal-polymerized silicon hydrogels with different surface microstructure and wettability. *Colloids Surf A Physicochem Eng Asp* **618**, 126284 (2021).

34. Wu, J. *et al.* An intrinsically stretchable humidity sensor based on anti-drying, self-healing and transparent organohydrogels. *Mater Horiz* **6**, 595–603 (2019).

35. Pang, Q. *et al.* Smart Flexible Electronics-Integrated Wound Dressing for Real-Time Monitoring and On-Demand Treatment of Infected Wounds. *Advanced Science* **7**, 1902673 (2020).

36. Shi, J. *et al.* Design of a mechanically strong and highly stretchable thermoplastic silicone elastomer based on coulombic interactions. *J Mater Chem A Mater* **8**, 5943–5951 (2020).

37. Bao, D. *et al.* An anti-freezing hydrogel based stretchable triboelectric nanogenerator for biomechanical energy harvesting at sub-zero temperature. *J Mater Chem A Mater* **8**, 13787–13794 (2020).

38. Moad, G., Rizzardo, E. & Solomon, D. H. 10 - Other Initiating Systems. in *Comprehensive Polymer Science and Supplements* (eds. Allen, G. & Bevington, J. C.) 141–146 (Pergamon, Amsterdam, 1989). doi:https://doi.org/10.1016/B978-0-08-096701-1.00072-0.

39. Li, Y., Rodrigues, J. & Tomás, H. Injectable and biodegradable hydrogels: gelation, biodegradation and biomedical applications. *Chem Soc Rev* **41**, 2193–2221 (2012).

40. Wang, C., Varshney, R. R. & Wang, D.-A. Therapeutic cell delivery and fate control in hydrogels and hydrogel hybrids. *Adv Drug Deliv Rev* **62**, 699–710 (2010).

41. Oh, E. J. *et al.* Target specific and long-acting delivery of protein, peptide, and nucleotide therapeutics using hyaluronic acid derivatives. *Journal of Controlled Release* **141**, 2–12 (2010).

42. Strehin, I., Nahas, Z., Arora, K., Nguyen, T. & Elisseeff, J. A versatile pH sensitive chondroitin sulfate-PEG tissue adhesive and hydrogel. *Biomaterials* **31**, 2788–2797 (2010).

43. Sakiyama-Elbert, S. E. & Hubbell, J. A. Development of fibrin derivatives for controlled release of heparin-binding growth factors. *Journal of Controlled Release* **65**, 389–402 (2000).

44. Hou, Y. *et al.* Thermoresponsive nanocomposite hydrogels with cell-releasing behavior. *Biomaterials* **29**, 3175–3184 (2008).

45. Chirani, N. *et al.* History and Applications of Hydrogels. **Vol. 4**, 13–23 (2015).

46. Ullah, F., Othman, M. B. H., Javed, F., Ahmad, Z. & Akil, H. Md. Classification, processing and application of hydrogels: A review. *Materials Science and Engineering: C* **57**, 414–433 (2015).

47. Liz-Basteiro, P. *et al.* High resolution molds, sacrificial in aqueous media, obtained by vat photopolymerization 3D printing. *Addit Manuf* **75**, 103758 (2023).

48. Koetting, M. C., Peters, J. T., Steichen, S. D. & Peppas, N. A. Stimulus-responsive hydrogels: Theory, modern advances, and applications. *Materials Science and Engineering: R: Reports* **93**, 1–49 (2015).

49. Huglin, M. R. Hydrogels in medicine and pharmacy Edited by N. A. Peppas, CRC Press Inc., Boca Raton, Florida, 1986 (Vol. I), 1987 (Vols 2 and 3). Vol. 1 Fundamentals, pp. vii + 180, £72.00, ISBN 0-8493-5546-X; Vol. 2 Polymers, pp. vii + 171, £72.00, ISBN 0-8493-5547-8; Vol. 3 Properties and Applications, pp. vii + 195, £8000, ISBN 0-8493-5548-6. *British Polymer Journal* **21**, 184 (1989).

50. Troncoso-Afonso, L., Vinnacombe-Willson, G. A., García-Astrain, C. & Liz-Márzan, L. M. SERS in 3D cell models: a powerful tool in cancer research. *Chem Soc Rev* (2024) doi:10.1039/D3CS01049J.

51. Ullah, S. & Chen, X. Fabrication, applications and challenges of natural biomaterials in tissue engineering. *Appl Mater Today* **20**, 100656 (2020).

52. Saldin, L. T., Cramer, M. C., Velankar, S. S., White, L. J. & Badylak, S. F. Extracellular matrix hydrogels from decellularized tissues: Structure and function. *Acta Biomater* **49**, 1–15 (2017).

53. Peppas, N., Hilt, J., Khademhosseini, A. & Langer, R. Hydrogels in Biology and Medicine: From Molecular Principles to Bionanotechnology. *Advanced Materials - ADVAN MATER* **18**, (2006).

54. Seliktar, D. Designing Cell-Compatible Hydrogels for Biomedical Applications. *Science (1979)* **336**, 1124–1128 (2012).

55. Thiele, J., Ma, Y., Bruekers, S. M. C., Ma, S. & Huck, W. T. S. 25th Anniversary Article: Designer Hydrogels for Cell Cultures: A Materials Selection Guide. *Advanced Materials* **26**, 125–148 (2014).

56. Li, Z., Zhou, Y., Li, T., Zhang, J. & Tian, H. Stimuli-responsive hydrogels: Fabrication and biomedical applications. *VIEW* **3**, 20200112 (2022).

57. Glatzel, S., Laschewsky, A. & Lutz, J.-F. Well-Defined Uncharged Polymers with a Sharp UCST in Water and in Physiological Milieu. *Macromolecules* **44**, 413–415 (2011).

58. Costa, R. O. R. & Freitas, R. F. S. Phase behavior of poly(N-isopropylacrylamide) in binary aqueous solutions. *Polymer (Guildf)* **43**, 5879–5885 (2002).

59. Bandyopadhyay, S., Sharma, A., Ashfaq Alvi, M. A., Raju, R. & Glomm, W. R. A robust method to calculate the volume phase transition temperature (VPTT) for hydrogels and hybrids. *RSC Adv* **7**, 53192–53202 (2017).

60. Francis, R., Baby, D. K. & Kumar, D. S. Poly(N-isopropylacrylamide) hydrogel: Effect of hydrophilicity on controlled release of ibuprofen at different pH. *J Appl Polym Sci* **124**, 5079–5088 (2012).

61. Abu-Lail, N. I., Kaholek, M., LaMattina, B., Clark, R. L. & Zauscher, S. Micro-cantilevers with end-grafted stimulus-responsive polymer brushes for actuation and sensing. *Sens Actuators B Chem* **114**, 371–378 (2006).

62. Purushotham, S. & Ramanujan, R. V. Thermoresponsive magnetic composite nanomaterials for multimodal cancer therapy. *Acta Biomater* **6**, 502–510 (2010).

63. Cortez-Lemus, N. A. & Licea-Claverie, A. Poly(N-vinylcaprolactam), a comprehensive review on a thermoresponsive polymer becoming popular. *Prog Polym Sci* **53**, 1–51 (2016).

64. Hoffman, A. S. Stimuli-responsive polymers: Biomedical applications and challenges for clinical translation. *Adv Drug Deliv Rev* **65**, 10–16 (2013).

65. White, E. M., Yatvin, J., Grubbs III, J. B., Bilbrey, J. A. & Locklin, J. Advances in smart materials: Stimuli-responsive hydrogel thin films. *J Polym Sci B Polym Phys* **51**, 1084–1099 (2013).

66. Ramos, J., Imaz, A. & Forcada, J. Temperature-sensitive nanogels: Poly(N-vinylcaprolactam) versus poly(N-isopropylacrylamide). *Polym Chem* **3**, 852 (2011).

67. Shakya, A., Kumar, A. & Nandakumar, K. S. Adjuvant properties of a biocompatible thermo-responsive polymer of N-isopropylacrylamide in autoimmunity and arthritis. *Journal of the Royal Society, Interface / the Royal Society* **8**, 1748–1759 (2011).

68. Imaz, A. & Forcada, J. N-Vinylcaprolactam-Based Microgels for Biomedical Applications. *J Polym Sci A Polym Chem* **48**, 1173–1181 (2010).

69. Meeussen, F. *et al.* Phase behavior of poly(N-vinyl caprolactam) in water. *Polymer (Guildf)* **41**, 8597–8602 (2000).

70. Moerkerke, R. *et al.* Phase Transitions in Swollen Networks. 3. Swelling Behavior of Radiation Cross-Linked Poly(vinyl methyl ether) in Water. *Macromolecules* **31**, 2223–2229 (1998).

71. Martínez-Campos, E. *et al.* Thermosensitive hydrogel platforms with modulated ionic load for optimal cell sheet harvesting. *Eur Polym J* **103**, (2018).

72. Nagase, K., Yamato, M., Kanazawa, H. & Okano, T. Poly(N-isopropylacrylamide)-based thermoresponsive surfaces provide new types of biomedical applications. *Biomaterials* **153**, 27–48 (2018).

73. Langer, R. & Vacanti, J. P. Tissue Engineering. *Science (1979)* **260**, 920–926 (1993).

74. Mason, C. & Dunnill, P. A brief definition of regenerative medicine. *Regenerative Med* **3**, 1–5 (2007).

75. Chen, G. *et al.* Application of the cell sheet technique in tissue engineering (Review). *Biomed Rep* **3**, (2015).

76. Kobayashi, J., Kikuchi, A., Aoyagi, T. & Okano, T. Cell sheet tissue engineering: Cell sheet preparation, harvesting/manipulation, and transplantation. *J Biomed Mater Res A* **107**, (2019).

77. Yamato, M. & Okano, T. Cell sheet engineering. *Materials Today* **7**, 42–47 (2004).

78. Yorukoglu, A. C., Kiter, A. E., Akkaya, S., Satiroglu-Tufan, N. L. & Tufan, A. C. A Concise Review on the Use of Mesenchymal Stem Cells in Cell Sheet-Based Tissue Engineering with Special Emphasis on Bone Tissue Regeneration. *Stem Cells Int* **2017**, 2374161 (2017).

79. Kushida, A., Yamato, M., Kikuchi, A. & Okano, T. Two-dimensional manipulation of differentiated Madin–Darby canine kidney (MDCK) cell sheets: The noninvasive harvest from temperature-responsive culture dishes and transfer to other surfaces. *J Biomed Mater Res* **54**, 37–46 (2001).

80. Kushida, A. *et al.* Decrease in culture temperature releases monolayer endothelial cell sheets together with deposited fibronectin matrix from temperature-responsive culture surfaces. *J Biomed Mater Res* **45**, 355–362 (1999).

81. Tang, Z. & Okano, T. Recent Development of Temperature-Responsive Surfaces and Their Application for Cell Sheet Engineering. *Regen Biomater* **1**, 91–102 (2014).

82. Okano, T., Yamada, N., Okuhara, M., Sakai, H. & Sakurai, Y. Mechanism of cell detachment from temperature-modulated, hydrophilic-hydrophobic polymer surfaces1. *The Biomaterials: Silver Jubilee Compendium* **16**, 109–115 (2006).

83. Nash, M., Healy, D., Carroll, W., Elvira, C. & Rochev, Y. Cell and cell sheet recovery from pNIPAm coatings; motivation and history to present day approaches. Preprint at (2015).

84. Wang, X. *et al.* Recent Advances in Hydrogel Technology in Delivering Mesenchymal Stem Cell for Osteoarthritis Therapy. *Biomolecules* **14**, (2024).

85. Nagase, K., Yamato, M., Kanazawa, H. & Okano, T. Poly(N-isopropylacrylamide)-based thermoresponsive surfaces provide new types of biomedical applications. *Biomaterials* **153**, 27–48 (2018).

86. Egami, M., Haraguchi, Y., Shimizu, T., Yamato, M. & Okano, T. Latest status of the clinical and industrial applications of cell sheet engineering and regenerative medicine. *Arch Pharm Res* **37**, (2013).

87. Haraguchi, Y., Shimizu, T., Yamato, M. & Okano, T. ChemInform Abstract: Scaffold-Free Tissue Engineering Using Cell Sheet Technology. *RSC Adv.* **2**, 2184–2190 (2012).

88. Dzhoyashvili, N., Thompson, K., Gorelov, A. & Rochev, Y. Film Thickness Determines Cell Growth and Cell Sheet Detachment from Spin Coated Poly(N-Isopropylacrylamide) Substrates. *ACS Appl Mater Interfaces* **8**, (2016).

89. Dilberoglu, U. M., Gharehpapagh, B., Yaman, U. & Dolen, M. The Role of Additive Manufacturing in the Era of Industry 4.0. *Procedia Manuf* **11**, 545–554 (2017).

90. Arias-Ferreiro, G., Ares-Pernas, A., Dopico-García, M. S., Lasagabáster-Latorre, A. & Abad, M.-J. Photocured conductive PANI/acrylate composites for digital light processing. Influence of HDODA crosslinker in rheological and physicochemical properties. *Eur Polym J* **136**, 109887 (2020).

91. Arias-Ferreiro, G. *et al.* Lignin as a High-Value Bioaditive in 3D-DLP Printable Acrylic Resins and Polyaniline Conductive Composite. *Polymers (Basel)* **14**, (2022).

92. Sotov, A., Kantyukov, A., Popovich, A. & Sufiiarov, V. LCD-SLA 3D printing of BaTiO3 piezoelectric ceramics. *Ceram Int* **47**, 30358–30366 (2021).

93. Schweiger, J., Edelhoff, D. & Güth, J.-F. 3D Printing in Digital Prosthetic Dentistry: An Overview of Recent Developments in Additive Manufacturing. *J Clin Med* **10**, (2021).

94. Pagac, M. *et al.* A Review of Vat Photopolymerization Technology: Materials, Applications, Challenges, and Future Trends of 3D Printing. *Polymers (Basel)* **13**, (2021).

95. Zhang, Z., Li, P., Chu, F. & Shen, G. Influence of the three-dimensional printing technique and printing layer thickness on model accuracy. *Journal of Orofacial Orthopedics / Fortschritte der Kieferorthopädie* **80**, 194–204 (2019).

96. Arias-Ferreiro, G. *et al.* Printability Study of a Conductive Polyaniline/Acrylic Formulation for 3D Printing. *Polymers (Basel)* **13**, (2021).

97. christian. sandstrom. Ratio Working Paper No . 262 Adopting 3 D Printing for manufacturing – The case of the hearing aid industry. in (2015).

98. Yap, Y. L. & Yeong, W. Y. Additive manufacture of fashion and jewellery products: a mini review. *Virtual Phys Prototyp* **9**, 195–201 (2014).

99. Mishra, P. K. & Jagadesh, T. Applications and Challenges of 3D Printed Polymer Composites in the Emerging Domain of Automotive and Aerospace: A Converged Review. *Journal of The Institution of Engineers (India): Series D* **104**, 849–866 (2023).

100. Espera, A. H., Dizon, J. R. C., Chen, Q. & Advincula, R. C. 3D-printing and advanced manufacturing for electronics. *Progress in Additive Manufacturing* **4**, 245–267 (2019).

101. Gul, J. Z. *et al.* 3D printing for soft robotics – a review. *Sci Technol Adv Mater* **19**, 243–262 (2018).

102. Deshmukh, K., Houkan, M. T., AlMaadeed, M. A. & Sadasivuni, K. K. Chapter 1 - Introduction to 3D and 4D printing technology: State of the art and recent trends. in *3D and 4D Printing of Polymer Nanocomposite Materials* (eds. Sadasivuni, K. K., Deshmukh, K. & Almaadeed, M. A.) 1–

24 (Elsevier, 2020). doi:https://doi.org/10.1016/B978-0-12-816805-9.00001-6.

103. Zhang, J. *et al.* Water soluble photocurable carboxymethyl cellulose-based bioactive hydrogels for digital light processing. *J Appl Polym Sci* **139**, 52155 (2022).

104. Liz-Basteiro, P. *et al.* Vat Photopolymerization 3D Printing of Hydrogels with Re-Adjustable Swelling. *Gels* **9**, (2023).

105. Kodama, H. Automatic method for fabricating a three-dimensional plastic model with photo-hardening polymer. *Review of Scientific Instruments* **52**, 1770–1773 (1981).

106. Ngo, T. D., Kashani, A., Imbalzano, G., Nguyen, K. T. Q. & Hui, D. Additive manufacturing (3D printing): A review of materials, methods, applications and challenges. *Compos B Eng* **143**, 172–196 (2018).

107. Oezkan, B., Sameni, F., Karmel, S., Engstrøm, D. S. & Sabet, E. A systematic study of vat-polymerization binders with potential use in the ceramic suspension 3D printing. *Addit Manuf* **47**, 102225 (2021).

108. Palmara, G., Frascella, F., Roppolo, I., Chiappone, A. & Chiadò, A. Functional 3D printing: Approaches and bioapplications. *Biosens Bioelectron* **175**, 112849 (2021).

109. Zhang, F. *et al.* The recent development of vat photopolymerization: A review. *Addit Manuf* **48**, 102423 (2021).

110. Al Rashid, A., Ahmed, W., Khalid, M. Y. & Koç, M. Vat photopolymerization of polymers and polymer composites: Processes and applications. *Addit Manuf* **47**, 102279 (2021).

111. Sampson, K. *et al.* Multimaterial Vat Polymerization Additive Manufacturing. *ACS Appl Polym Mater* **3**, (2021).

112. Huh, J. T., Yoo, J. J., Atala, A. & Lee, S. J. Chapter 74 - Three-dimensional bioprinting for tissue engineering. in *Principles of Tissue Engineering (Fifth Edition)* (eds. Lanza, R., Langer, R., Vacanti, J. P. & Atala, A.) 1391–1415 (Academic Press, 2020). doi:https://doi.org/10.1016/B978-0-12-818422-6.00076-9.

113. Mou, Y. A. & Koc, M. Dimensional capability of selected 3DP technologies. *Rapid Prototyp J* **25**, 915–924 (2019).

114. Mendes, C., Oliveira, J., Etxebarria, I., Vilas, J. & Lanceros-Méndez, S. State-of-the-Art and Future Challenges of UV Curable Polymer-Based Smart Materials for Printing Technologies. *Adv Mater Technol* **4**, 1800618 (2019).

115. Shan, W., Chen, Y., Hu, M., Qin, S. & Peng, L. 4D printing of shape memory polymer via liquid crystal display (LCD) stereolithographic 3D printing. *Mater Res Express* **7**, 105305 (2020).

116. Nguyen, L. H., Straub, M. & Gu, M. Acrylate-Based Photopolymer for Two-Photon Microfabrication and Photonic Applications. *Adv Funct Mater* **15**, 209–216 (2005).

117. Wang, C.-C., Chen, J.-Y. & Wang, J. The selection of photoinitiators for photopolymerization of biodegradable polymers and its application in digital light processing additive manufacturing. *J Biomed Mater Res A* **110**, 204–216 (2022).

118. Heeger, A. J. Semiconducting and Metallic Polymers: The Fourth Generation of Polymeric Materials (Nobel Lecture). *Angewandte Chemie International Edition* **40**, 2591–2611 (2001).

119. Medellin, A. *et al.* Vat Photopolymerization 3D Printing of Nanocomposites: A Literature Review. *J Micro Nanomanuf* **7**, (2019).

120. Sutton, J., Rajan, K., Harper, D. & Chmely, S. *Lignin-Containing Photoactive Resins for 3D Printing by Stereolithography*. (2018). doi:10.26434/chemrxiv.6820229.

121. Voet, V. *et al.* Biobased Acrylate Photocurable Resin Formulation for Stereolithography 3D Printing. *ACS Omega* **3**, 1403–1408 (2018).

122. Lee, Y., Lee, J.-B., Maeng, W.-Y., Koh, Y.-H. & Kim, H.-J. Photocurable ceramic slurry using solid camphor as novel diluent for conventional digital light processing (DLP) process. *J Eur Ceram Soc* **39**, (2019).

123. Patel, D. *et al.* Highly Stretchable and UV Curable Elastomers for Digital Light Processing Based 3D Printing. *Advanced Materials* **29**, 1606000 (2017).

124. Han, Y., Wang, F., Wang, H., Jiao, X. & Chen, D. High-strength boehmite-acrylate composites for 3D printing: Reinforced filler-matrix interactions. *Compos Sci Technol* **154**, 104–109 (2018).

125. Shuqiang, P. *et al.* 3D Printing Mechanically Robust and Transparent Polyurethane Elastomers for Stretchable Electronic Sensors. *ACS Appl Mater Interfaces* **XXXX**, (2020).

126. Yuan, Y., Li, C., Zhang, R., 刘仁 R. & Liu, J. Low volume shrinkage photopolymerization system using hydrogen-bond-based monomers. *Prog Org Coat* **137**, 105308 (2019).

127. Weng, Z., Huang, X., Peng, S., Zheng, L. & Wu, L. 3D printing of ultra-high viscosity resin by a linear scan-based vat photopolymerization system. *Nat Commun* **14**, 4303 (2023).

128. Li, X. *et al.* Fabrication of zirconia all-ceramic crown via DLP-based stereolithography. *Int J Appl Ceram Technol* **17**, 844–853 (2020).

129. Johansson, E., Lidström, O., Johansson, J., Lyckfeldt, O. & Adolfsson, E. Influence of Resin Composition on the Defect Formation in Alumina Manufactured by Stereolithography. *Materials* **10**, 138 (2017).

130. Chartrain, N., Williams, C. & Whittington, A. A Review on Fabricating Tissue Scaffolds using Vat Photopolymerization. *Acta Biomater* **74**, (2018).

131. Torgersen, J. *Photocured Materials CHAPTER 4. Efficient Photoinitiators for Two-Photon Polymerization*. (2014). doi:10.1039/9781782620075-00075.

132. Manapat, J. Z., Chen, Q., Ye, P. & Advincula, R. C. 3D Printing of Polymer Nanocomposites via Stereolithography. *Macromol Mater Eng* **302**, 1600553 (2017).

133. Bennett, J. Measuring UV curing parameters of commercial photopolymers used in additive manufacturing. *Addit Manuf* **18**, 203–212 (2017).

134. Lee, J., Prud'homme, R. & Aksay, I. Cure depth in photopolymerization: Experiments and theory. *Journal of Materials Research - J MATER RES* **16**, 3536–3544 (2001).

135. Li, Y. *et al.* Theoretical prediction and experimental validation of the digital light processing (DLP) working curve for photocurable materials. *Addit Manuf* **37**, 101716 (2021).

136. Chartrain, N. A., Williams, C. B. & Whittington, A. R. A review on fabricating tissue scaffolds using vat photopolymerization. *Acta Biomater* **74**, 90–111 (2018).

137. Gojzewski, H. *et al.* Layer-by-Layer Printing of Photopolymers in 3D: How Weak is the Interface? *ACS Appl Mater Interfaces* **XXXX**, (2020).

138. Finck, N. S. *et al.* Effects of solvent type and UV post-cure time on 3D-printed restorative polymers. *Dental Materials* **40**, 451–457 (2024).

Chapter 2. Hypothesis and Objectives

2.1. Hypothesis

The research program of this thesis is based on the premise that the group's extensive experience and knowledge in photopolymerization and photocuring processes to obtain tailored hydrogels, such as those developed in iFABCell, combined with expertise in β-amino ester chemistry, will enable the creation of novel advanced photopolymerizable resins and some of which may be the seeds of next-generation iFABCell culture platforms. These resins are expected to facilitate the 3D printing by vat photopolymerization of parts. Moreover, due to the presence of labile crosslinkers within the material structure, these materials will be employed for the preparation of sacrificial parts, as well as to 3D print iFABCell hydrogels. This thesis aims at designing, characterizing, and evaluating each critical element within the proposed resin and printed systems.

2.2. Objectives

The primary aim of this doctoral thesis is to develop advanced resins for 3D printing by vat photopolymerization. To achieve the main objective, a series of specific objectives had to be defined. These objectives are developed in the different chapters of the PhD thesis and entail understanding the state of the art (Chapter 1), developing resin formulations for 3D printing of soluble sacrificial networks (Chapter 4), optimizing and evaluating resins for 3D printing of readjustable networks, which eventually may allow obtaining hydrogels (Chapter 5), optimizing and evaluating the use of different ways to enable the vat photopolymerization 3D printing of thermosensitive hydrogels based on VCL (Chapter 6), and doping printable VCL-based thermosensitive hydrogels with nanofillers such as CNTs (Chapter 7). More in detail, the specific objectives of the thesis research are the following:

- To explore and define a direct and scalable route to obtain printable formulations containing hydrolysable crosslinkers. The 3D printing of these resins, through vat photopolymerization, are expected to lead to sacrificial pieces upon hydrolysis, that, is, to soluble polymer chains after breaking the crosslinking points. (Chapter 4).

- To optimize and evaluate different formulations employing mixtures of both stable and hydrolysable crosslinkers simultaneously in the resin for 3D printing. The purpose of this combination of crosslinking agents is to be able to obtain readjustable networks with high crosslinking degrees after printing and lower/modulated degree after controlled hydrolysis. (Chapter 5).

- To, based on the original formulation of photosensitive resins developed under the iFABCell technology, that lead to thermosensitive hydrogels, develop novel formulations to be employed in vat photopolymerization 3D printing. The main purpose, of this objective, is to address whether it is possible to fabricate thermosensitive hydrogels with unprecedented shapes (Chapter 6).

- To explore the possibility of dope iFABCell printable hydrogels with nanocomposites to address both the printability of the material as well as the novel properties of the materials produced. In particular, to carry out this objective it is proposed the incorporation of carbon nanotubes (CNTs) within the iFABCell formulations to produce CNTs loaded thermoresponsive hydrogels (Chapter 7).

Chapter 3. Experimental section

3.1. Materials

3-(acryloyloxy)−2-hydroxypropyl methacrylate, piperazine, acetic acid, poly(ethylene glycol) methyl ether acrylate (PEGMEA, Mw 480), poly(ethylene glycol) dimethacrylate (PEGDMA, Mw 550), sodium hydroxide (NaOH), carboxyethyl acrylate (CEA), 1-(phenyldiazenyl)naphthalen-2-ol (Sudan I), phenylbis(2,4,6-trimethyl benzoyl) phosphine oxide (BAPO), phosphate-buffered saline (PBS, pH 7.4), VCL, ethylene glycol dimethacrylate (EGDMA), diphenyl(2,4,6-trimethylbenzoyl) phosphine oxide (TPO), 1-hydroxyl cyclohexyl phenyl ketone (HCPK), 4-vinylaniline (VA), and isoamyl nitrite (IAN), icariin (ICA), cyrene, *N*-methyl-2-pyrrolidone (NMP), dimethylacetamide (DMAc), ethyl lactate, ethanol, *N,N*-dimethylformamide (DMF), acetonitrile (MeCN), methanol, and diethyl ether were supplied by Sigma-Aldrich.

Jeffamine ED-600 was supplied by Huntsman. 2-hydroxyethyl acrylate (HEA) and methacrylic acid (MAA) were supplied by TCI. Azo-bis-isobutirenitrile (AIBN) was supplied by Glentham, and dioxane by Panreac. Glycerol monomethacrylate (GMM) was supplied by Polysciences. 184 Silicone Elastomer Base and 184 Elastomer Curing Agent were supplied by Sylgard™. Poly (***ε***-caprolactone), (50.000 g mol^{-1}) (PCL) was supplied by Perstorp. 1, 3-divylimidazolidin-2-one (DVI) was supplied by BASF. *N*-vinylpyrrolidone (VP) was supplied by Acros Organics. Multi-wall carbon nanotubes (CNTs) were purchased from Elicarb (diameter: 15-20 nm). Reagents and solvents were used as received without further purification, unless indicated differently[1,2].

Autofluorescent C166-GFP endothelial murine cell line expressing green fluorescent protein (GFP), was purchased by ATTC-(CRL-2583;RRID#CVCL 6582). Fetal bovine serum (FBS) was purchased from Thermo Scientific. Dulbecco's Modified Eagle Medium (DMEM), the antibiotic (penicillin, streptomycin (P/S), and G418), and glutaMAX were also supplied by Sigma-Aldrich. 12 and 24 well culture plates (treated and untreated, respectively) were purchased from Corning Costar. For neural cultures, Neuro2a mouse neuroblastoma cell line (cat# CCL-131, ATCC; RRID#CVCL_0470) was

purchased from ATTC. 48 and 96 wells culture plates were purchased from Thermo Scientific.

3.2. Synthesis, polymerizations, and fabrications (excluding vat photopolymerization)

3.2.1. Synthesis of hydrolyzable crosslinkers HCL(jef) and HCL(pip)

3-(acryloyloxy)−2-hydroxypropyl methacrylate and diamino-containing structures (jeffamine to produce crosslinker HCL(jef) and piperazine to produce the crosslinker HCL(pip)) were mixed in a 2:1 molar ratio. The reactions were carried out overnight at 37 ºC in the presence of a catalytic amount of acetic acid (0.25 wt. %). A slightly yellow liquid was obtained and stored. ^{1}H Nuclear magnetic resonance (^{1}H NMR) spectroscopy was used to monitor the disappearance of acrylate signals as the reactions proceeded, quantitative yield.

^{1}H NMR HCL(jef) (400 MHz, $CDCl_3$) d: 6.10 (m, 2 H, 1-H), 5.56 (m, 2 H, 1-H), 4.18 (m, 4 H 4-H), 3.92 (m, 2 H, 5-H), 3.80–3.17 (m, OH + 6-H + Hjef), 3.03–2.69 (m, H-*β* + CH-jef), 2.50 (m, H-*α* + CH_2O), 1.92 (m, 6 H, Me), 1.11 (m, Me-jef), 1.0 (m, Me-jef) ppm.

^{1}H NMR HCL(pip) (400 MHz, $CDCl_3$) d: 6.11 (m, 2 H, 1-H), 5.58 (m, 2 H, 1-H), 4.37–3.45 (m, 16 H, 4–6 H + OH + H-*β*), 2.80–2.37 (m, 12 H, 1′-H + 2′-H + H-*α*), 1.87 (m, 6 H, Me) ppm[2].

3.2.2. Synthesis of poly(2-hydroxyethyl acrylate), polyHEA

The synthesis of polyHEA was carried out by conventional radical polymerization HEA in dioxane ([HEA] = 0.57 mol/L), using AIBN as ta thermal initiator ([AIBN] = 0.015 mol/L). The polymerization was allowed to proceed overnight in an oven at 60 ºC, after nitrogen was bubbled for 5 min. The following day, upon cooling to 5 °C separation into two phases was observed, which allows easy removal of dioxane[1].

3.2.3. Synthesis of linear polyvinylcaprolactam, polyVCL

Linear pVCL was obtained by conventional radical polymerization of VCL in ethanol ([VCL] = 1 mol/L), using AIBN as a thermal initiator ([AIBN] = 0,015 mol/L). The polymerization was allowed to proceed overnight in an oven at 60 °C.

The resulting polymer was purified by dialysis with diH_2O using membranes with a molecular weight of 3.5 kDa. Consequently, the polymer was lyophilized.

3.2.4. Photocuring of VCL/VP-based hydrogels in UV chamber

Different relations of VCL/VP hydrogels were prepared, between 100 and 0 molar percentages as shown in **Table 6.4 of Chapter 6**. The crosslinkers added were DVI and EGDMA in molar percentages of 0.57 and 1.07, respectively, against the total monomer content. HCPK was used as a photoinitiator at 0.5% weight. In the case of the hydrogels loaded with CNTs, the formulations depicted above were additionally charged with different weight percentages of CNT were prepared (see **Table 7.2** in **Chapter 7,** 0 wt. % was prepared as control). The photopolymerizable mixtures were stirred for 5 min. Subsequently, CNTs were added and the mixtures were stirred again for 5 min, followed by sonication for 30 min.

All the mixtures were injected into molds and photopolymerized in a curing chamber. The molds were prepared using polystyrene sheets covered with polyethylene film and separated both by commercial silicone with a thickness of 0.3 mm. The photopolymerization was carried out inside a UV chamber that generate close to 3500 μW/cm^2 (model CL-1000L, 230 V), for 40 min and λ=365 nm. After obtaining the hydrogels, the hydrogel mold is removed, and successively washed with distilled water to remove any residual unreacted materials and finally swelled to achieve the equilibrium between the hydrogel and the medium.

3.2.5. Fabrication of (pVCL@ICA) nanoparticles

The nanoparticles were prepared by encapsulating ICA in linear pVCL using SAS-SCCO_2 following previously reported procedures[3]. Basically, particles were formed using a SAS R100 pilot plant from Thar Technologies Variables. A flow of 1 mL/min of a polymer-drug solution was kept constant in all the experiments. Once the desired temperature was reached, CO_2 was pumped at the desired flow rate through a high-pressure pump, until the temperature and pressure stabilized in the SAS reactor. A sample solution of ICA and pVCL was pumped into the reactor through a filter. 20 mL of this solution were exposed to the CO_2 pumping, leading to the obtention of particles. The CO_2 flow was kept for a certain time,

eliminating the residual solvent. Due to depressurization, the solvent dissolved in a supercritical fluid because of its miscibility, producing the formation of nanoparticles by precipitation.

3.2.6. Manufacture of screws by the use of sacrificial molds

To carry out a proof of concept for the use of the printed parts as sacrificial molds, two types of screw molds with different thread pitches (1 and 2 mm) were digitally designed (see **Figure 3.1**) and printed. In both cases, the dimensions of the screw filler were 1.5 cm of height and 1/2 cm of thread/head diameter [2].

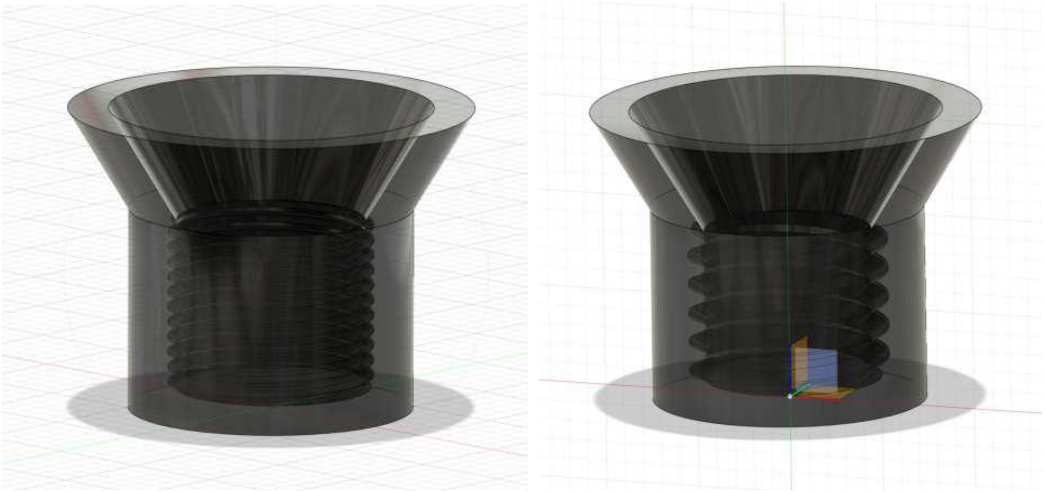

Figure 3.1. Digital designs of the molds of screws with two different thread pitches (1 and 2 mm).

Example 1: Sacrificial molds for the fabrication of 3D structures using thermoplastic polymers.

PCL pellets were introduced into the mold, and the construct was heated up to 100 ºC until PCL was melted. Thereafter, the construct was allowed to cool down to room temperature for 1 h and subsequently immersed overnight in basic aqueous media. Finally, the 3D structured PCL part was recovered from the solution, surface dried, and stored.

Example 2: Chemical crosslinking inside the sacrificial 3D printed molds: Fabrication of silicone networks.

The silicone-based elastomeric kit Sylgard 184, which is a liquid two-component system (a polymer, named base, and a curing agent that crosslinks with the

base), was used. Both components 1) polymer (base) and 2) curing agent, were mixed in a 10:1 (base:curing agent) ratio by weight. The mixture was stirred manually and left under vacuum for 15 min to avoid contact with the entrapped oxygen. The mixture was then added to the printed sacrificial molds and placed in the oven at 60 ºC overnight to form the crosslinked silicone elastomer. Later, the construct (mold with the cured Sylgard 184) was immersed overnight in basic water. Finally, the silicone network was recovered from the solution, dried, and stored.

Example 3: Preparation of VCL-based thermosensitive hydrogels inside the sacrificial molds

The VCL-based thermosensitive hydrogel used in this case is pc-$VCL_{100}VP_0$, system depicted in **section 6.2.3** in **Chapter 6.** The mixture was stirred for 5' and preheated beforehand at 50 ºC until VCL melted to liquid. The mixture was then added to the printed sacrificial molds and placed in the UV curing chamber for 40 min and λ=365 nm. Later, the construct (mold with the photopolymerized thermosensitive hydrogel) was immersed overnight in basic water. Finally, the VCL-based thermosensitive hydrogel was recovered from the NaOH solution, immersed in distilled water for 24 h, dried, and stored.

3.3. Vat photopolymerization 3D printing

3.3.1. Designing of the resins for the preparation of either sacrificial or readjustable networks

For each resin a total of 20 g of precursor mixture was prepared. Examples of each type of system are detailed below:

As an example of a resin from the HCL(jef) or HCL(pip) and PEGMEA (the resins were labeled as $HCL(jef)_XPEGMEA_{100-X}$, where X the weight percentage of HCL), formulation $HCL(jef)_{30}PEGMEA_{70}$ was prepared by mixing 6 g of HCL(jef) and 14 g of PEGMEA.

As an example of resin from binary blends, the $HCL(jef)_{15}HEA_{85}$ formulation was prepared by mixing 3 g of HCL(jef) and 17 g of HEA.

As an example of resin from the ternary blends, $HCL(jef)_{15}HEA_Xmonomer_{85-X}$, where monomer is PEGMEA, CEA, or MAA, and X is the weight percentage of

HEA (0<X<85), HCL(jef)$_{15}$HEA$_{60}$CEA$_{25}$ was prepared by mixing 3 g of HCL(jef), 12 g of HEA, and 5 g of CEA[2].

As an example of ink for the HCL(jef)$_X$HEA$_{60}$ system, the formulation HCL(jef)$_{10}$HEA$_{60}$ was prepared by mixing 1.0 g of PEGDMA (1.8 mmol), 2.0 g of HCL (1.9 mmol), 5.0 g of PEGMEA (10.4 mmol) and 12.0 g of HEA (103.3 mmol). For this formulation, the reference formulation containing GMM instead of HCL(jef) was prepared by mixing 1.0 g of PEGDMA, 0.6 g of GMM (3.8 mmol), 5.0 g of PEGMEA and 12.0 g of HEA[1].

In all cases, 2.67 mg of Sudan I (1.35 wt. %) was added and the vessel was covered with aluminum foil. Then, 0.2 g (1 wt. %) of photoinitiator (BAPO) was added and the mixture was stirred for 5–10 min until it was completely homogeneous. The resin was then ready to be tested in the Zortrax Inkspire printer.

3.3.2. Photosensitive mixtures for the preparation of VCL-based hydrogels

For reasons of confidentiality, this section has been omitted.

3.3.3. 3D printing of the photosensitive resins

The photopolymerizable mixtures were stirred for 5 minutes. Resins were added into the tank and the following printing parameters were selected and maintained constant for all of the experiments: layer height 100 µm, raft height 1 mm, raft offset 4 mm, exposure off time 5 s, bottom layers 5 pcs, platform lower speed 100 mm/min and 5 platform lift speed 100 mm/min. The printer was a Zortrax Inkspire (0.5 $mW \cdot cm^{-2}$) using Z-Suite as slicer program for the sacrificial or either readjustable network. Creality LD-002H (5.5 $mW \cdot cm^{-2}$), using Chitubox as slicer program was used for printing the VCL-based hydrogels.

For reasons of confidentiality, part of this section has been omitted.

After printing, the printed networks were washed in 2-propanol for 5’ to remove any residual monomer, and a post-curing process for 30 min at room temperature for sacrificial or either readjustable networks.

3.4. Methods

3.4.1. Nuclear magnetic resonance (NMR)

^{1}H NMR spectra were recorded at room temperature in a Bruker Advance III HD-400 spectrometer using $CDCl_3$ as the solvent for HCL(jef) and HCL(pip), and D_2O for the analysis of the product resulting from the solubilization tests, described in section 3.4.10.

The hydrolysis of the polyHEA ester was monitored by ^{1}H NMR. 100 mg of polymer was dissolved in 0.6 mL of D_2O at 2 wt. % of NaOH. This sample was monitored from time = 0 as indicated in **Figures 5.10a and 5.10b in Chapter 5**. ^{1}H NMR spectra were recorded at room temperature (^{1}H 399.86 MHz) using D_2O with 2 wt. % NaOH as solvent. Chemical shifts (d in ppm) are given from internal solvent, D_2O, 4.8 ppm[1].

3.4.2. Rheology of photosensitive resins

Rheological characterization of the uncured formulations was carried out at 25 ºC using a strain-controlled rheometer (Waters, ARG2, TA Instruments) with a cone and plate geometry (40 mm diameter). The viscosity was measured at shear rates ranging between 0.3 and 100 s^{-1}. For every resin, at least three viscosity measurements were performed to confirm the reproducibility of the methodology. In the case of hydrated samples, hydrogels were subjected to rheological analysis with a plate geometry (20 mm diameter). At first, the hydrogels were placed in distilled water in the fridge at 5 ºC for 2 h. The temperature sweep was performed from 10 ºC to 45-75 ºC at a heating rate of 2 ºC/min. The variation in storage and loss modulus was collected under constant oscillation stress of 10 Pa and a frequency of 1 Hz (viscoelastic linear region).

3.4.3. Jacobs working curves

To obtain the Jacobs working curves[5–7], circular samples (diameter 2 cm) were cured with the Zortrax Inkspire 3D printer or the Creality LD-002H 3D printer between the tank and a glass, with a constant intensity of 0.5 $mW \cdot cm^{-2}$ for the Zortrax and 5.5 $mW \cdot cm^{-2}$ for the Creality, and varying the exposure times between 10 and 35 s in the Zortrax case, and between 20 and 120 s in the Creality case. Every sample was fabricated in duplicate. After polymerization, the

remaining solvent was extracted and the film was cleaned with paper. The curing depth (C_d, μm) was obtained from the thickness of the samples, which was measured with a thickness gauge (Tactix 251420). The C_d is related to the irradiated light energy on the surface, E_{max}, through **Equation 3.1**.

$$C_d = D_p \cdot \ln\left(\frac{E_{max}}{E_c}\right) \qquad (\mathbf{3.1})$$

where E_{max} (mJ·cm^{-2}) is given by the product of the exposure time and the energy of the lamp. E_c (mJ·cm^{-2}) is the starting point for the transition from liquid to solid and D_p (μm) represents the penetration depth. Bearing in mind the properties of the 3D printed objects, it is necessary to obtain good adhesion between layers. To achieve this, the use of layers with sufficient depth is essential, *i.e.*, $C_d > z$, in our case Z = 100, because the stiffness of a polymer at the gel point (or below it) is too low to endure the printing process[5,8,9]. Equation 3.1 can be plotted using a semilogarithmic scale in the y-axis (C_d) versus E_{max} on the *x*-axis. As a result, the interception of the Jacobs working curve with the *x*-axis represents E_c, whereas D_p is the slope of the linear line[1].

3.4.4. Raman spectroscopy

Raman spectra were acquired on five different spots per sample with an InVia 50 Renishaw Raman Microscope equipped with laser at 532 nm (25 mW), with 10 accumulations, 1 cm^{-1} resolution. Samples were prepared on microscopy glass slides and at least 5 replicas.

3.4.5. Transmission electron microscopy

Transmission electron microscopy (TEM) was carried out on a JEM 2100 (Jeol) at 100 kV. Samples were dispersed in DMF via ultrasonic treatment to obtain a light grey dispersion, then 2 μL of the samples were dropcasted onto TEM carbon grids previously exposed to UV-Ozone Procleaner Plus for 5 min and dried under vacuum.

3.4.6. Fourier transform infrared (FT-IR) spectroscopy

Attenuated total reflectance-infrared spectroscopy (ATR-FTIR) was conducted on dried samples using an FT-IR Spectrometer (Spectrum Two) from

PerkinElmer, equipped with a diamond crystal ATR accessory. Spectra were recorded with a resolution of 4 cm^{-1} in the range of 4000–500 cm^{-1} for each sample.

3.4.7. Thermogravimetry

Thermal analyses were carried out in a thermogravimetric analyzer (TGA) controlled by a METTLER instrument. 1-10 mg of powdered sample was heated from 0 up to 800 ºC, by equilibrating at 100 ºC for 20 min. The experiments were performed under oxygen flow for hydrolysable hydrogels and under nitrogen flow for loaded hydrogels, using a constant temperature increment of 10 $ºC \cdot min^{-1}$.

3.4.8. Scanning electron microscopy

Scanning electron microscopy (SEM) measurements were performed using a XL30 ESEM (Phillips), at an acceleration voltage of 25 kV.

3.4.9. Dimensional accuracy analysis

Dimensional accuracy analysis of cylinders was carried out by measuring dimensions (diameter and height) with a micrometer. In the case of the 3D printed screws, ImageJ was used to analyze photographs of representative screw molds.

3.4.10. Solubilization tests

3D printed pieces (2.0×2.0×0.2 cm^3) were immersed overnight in 15 mL of basic aqueous media (2 wt. % NaOH) at room temperature. After this time, the solubilization of the piece was visually analyzed to observe the disappearance of the mold. The dissolved material of the mold was analyzed by ^1H NMR (see **Figures 4.8 and 4.9 in Chapter 4**)[2].

3.4.11. Extractable analysis

An extractable release study of the different types of 3D printed hydrogels was carried out. The hydrogels were extracted at 4 °C in distilled water. The experiments were performed by duplicate and a volume of between 20 mL and 100 mL per sample was used. The extraction was carried out for 72 h, replacing every 24 h the distilled water to obtain 3 dilutions, which were analyzed separately. The total concentration was obtained by adding those obtained for

each solution. The concentration of extractables was determined using a NanoDrop One UV-visible spectrophotometer.

The quantification of extractable (VCL and pVCL) in hydrogels that used NMP as a solvent for their preparation and in hydrogels containing HCL(jef) as a crosslinker, was performed by first determining the amount of VCL by measuring absorbance at 260 nm using this calibration line: $[VCL](mg \cdot mL^{-1})=(A_{VCL}(260)-0.75)/49.41$. To determine the amount of pVCL (or sol fraction) the absorbance measurement at 205 nm was used. Since both VCL and PVCL exhibit absorbance at 205 nm, it was necessary to determine the individual absorbances of each. For this purpose, the absorbance of VCL at 205 nm was calculated using the calibration line $A_{VCL}(205)=34.65 \cdot [VCL](mg \cdot mL^{-1})+0.65$, where $[VCL](mg \cdot mL^{-1})$ was the value previously obtained from the absorbance at 260 nm. The absorbance corresponding to pVCL at 205 nm is given by $A_{pVCL}(205)=A(205)-A_{VCL}(205)$, and its concentration was determined using the corresponding calibration line: $[pVCL] (mg \cdot mL^{-1}) = (A_{pVCL}(205)+0.4)/39.2$.

For hydrogels obtained using Cyrene as a solvent in their preparation, each hydrogel was assumed to have 10% Cyrene of the total weight. Since Cyrene absorbs at 260 nm, the absorbance at this wavelength corresponding to VCL was determined as follows: $A_{VCL}(260)=A(260)-A_{Cyrene}(260)$. $A_{Cyrene}(260)$ was determined from the following calibration line; $A_{Cyrene}(260) = 0.028 \cdot [Cyrene](mg \cdot mL^{-1})+0.0792$, where [Cyrene](mg/mL) corresponds to the 10% mentioned above. In addition, Cyrene absorbs at 205 nm, the wavelength used to determine pVCL, so: $A_{pVCL}(205)=A(205)-A_{Cyrene}(205)-A_{VCL}(205)$. $A_{Cyrene}(205)$ was obtained from the calibration line; $A_{Cyrene}(205) = 0.36 \cdot [Cyrene](mg \cdot mL^{-1}) + 1.60$, where $Cyrene](mg \cdot mL^{-1})$ is the previously obtained value. $A_{VCL}(205)$ and $[pVCL](mg \cdot mL^{-1})$ were determined as explained above.

Finally, in the case of VCL hydrogels with VP it was considered that both vinyl-lactams had the same reactivity and that the VCL/VP ratio in the extractable, as well as the ratio of units in the sol fraction, is the same, *i.e.*, 1 (since it is the vpp-$VCL_{50}VP_{50}$ formulation). Therefore, the calibration lines were made with equimolar VCL+VP mixtures, as well as with an equimolar copolymer p(VCL-co-VP) prepared as described in **section 6.2.3.2** in **Chapter 6.** In this case, the

absorbance at 235 nm was used for the determination of [VCL+VP], using this calibration line: [VCL-VP](mg/mL)=(A(235)-0.048)/34417. For the sol fraction, the wavelength of 210 was selected, taking into account that both monomers and copolymers presented absorption bands at this wavelength, and its concentration was determined in a similar way as has been described above: the absorbance of the monomers was determined using the concentration determined above and this calibration line $A_{VCL+VP}(210)=11684\cdot[VCL\text{-}VP](mg\cdot mL^{-1})-0.008$. Therefore, $A_{p(VCL\text{-}co\text{-}VP)}(210)=A(210)-A_{VCL+VP}(210)$, and the concentration of sol fraction was calculated using the corresponding calibration line $[poly(VP\text{-}co\text{-}VCL](mg\cdot mL^{-1})=(A(210)+0.02)/2581.1$.

3.4.12. Swelling tests

Swelling tests of the VCL-based hydrogels were performed in PBS (pH=7.4). Hydrated hydrogels were die-cut into a 7 mm diameter cylinders prior to testing. After that, the hydrogels were immersed in 15 mL of PBS at different temperatures (from 5 to 80 ºC). The pieces were weighted at different times to follow the swelling process. All the samples were measured by triplicate (minimum). Swelling (S) was determined from **Equation 3.2.**

$$S=\frac{(w_S-w_D)}{w_D} \qquad (\mathbf{3.2})$$

where wS and wD are the weights of the swollen and dry systems, respectively[1].

The 3D printed pieces (2.0×2.0×0.2 cm^3) were immersed in 15 mL of the corresponding media (PBS, buffer pH 10 or 2 wt. % NaOH in water), either at room temperature or at 60 °C. The pieces were weighted at different times to monitor the swelling process. S was also determined from **Equation 3.2.**

The VPTT values were determined from the onset point at which a significant change in the slope of the swelling ratio curve appears.

3.4.13. Mechanical tests

Two types of mechanical tests were carried out in this doctoral thesis, tensile strength tests and compression tests. Mechanical tests on the hydrolysable hydrogels were carried out in a "Universal testing machine", INSTRON brand, with Load cells of 100 N, 1 kN, and 5 kN, depending on the material

resistence, tensile test speed: 100 mm/min and compression test speed: 10 mm/min[2].

The size of the tensile test pieces (5 pieces for each test) was V test type of the ASTM D638–14 (Standard Test Method for Tensile Properties of Plastics), that is, W (Width of narrow section) = 3.18 ± 0.03 mm (0.125 ± 0.001 in.), L (Length of narrow section) = 9.53 ± 0.08 mm (0.375 ± 0.003 in.), G (Gage length) = 7.62 ± 0.02 mm (0.300 ± 0.001 in.), and R (Radius of fillet) = 12.7 ± 0.08 mm (0.500 ± 0.003 in.)[2].

The size of the compression specimens (always 5 specimens for each test) was 29 cm in diameter and 12.5 cm in height. 4 sweeps were run until reaching 25% of deformation of the pieces, following the norm UNE 53536:2001[10].

The mechanical properties of VCL-based hydrogels were analysed based on dynamic compression tests. Measurements were performed on gels hydrated at 20 ºC immersed in distilled water, using a universal test system (MTS System, ® QTest1/L Elite) in compression mode. Cylindrical samples with a diameter of 7 mm and a thickness of around 0.5 to 0.7 mm were used (hydrogels were die-cut prior to the assay at 20 ºC to ensure correct dimensions). Samples were placed between compression plates, with the upper one being 5 mm of diameter. Each sample was subsequently deformed to a specific compressive strain level at 0.5 mm/min. All measurements were performed in quintuplicate and analysed with a 100 N Charge Cell associated with TestWorks software.

3.4.14. Oscillatory rheology

Oscillatory rheological characterization was carried out using another strain-controlled rheometer (Malvern Kinexus Ultra Plus Rheometer) with a parallel-plate geometry (20 mm diameter) at a fixed temperature of 20 °C using a Peltier temperature controller. The hydrogels were measured at a shear rate between 0.1 and 100 s^{-1}. Frequency sweeps recorded at 2 Pa from 0.01 to 10 Hz. Stress sweeps were performed from 1 Pa up to hydrogel failure at 1 Hz. For every type of hydrogel, three measurements were performed to confirm the reproducibility of the measurements.

3.4.15. Conductivity tests

Electrical conductivity at room temperature was measured using a conventional four-point probe method (Ossila, Sheffield) with a target current set in the range between 10 and 100 μA using 10 V as the maximum voltage. The hydrogels were cut into circles with a diameter of 8 mm and kept in water until they were measured. The final thickness of the wet samples was then measured with a caliper before the measurement. Electrical conductivities reported for each polymer formulation are averages of at least three different samples.

3.4.16. Ultraviolet-visible spectroscopy

Transmittance values of hydrogels were determined in a UV–Vis SPECORD 205 spectrophotometer associated with the WinASPECT software, which was used at a visible wavelength (600 nm) in PBS at 37 ºC by triplicate. The hydrogels were stabilized in the medium 24 h before the test to ensure a complete polymer-medium equilibrium.

3.5. Biological characterization of the hydrogels: Cell culture on hydrogels based on VCL-VP

3.5.1. Biological evaluation with C166-GFP cells. General overview

C166-GFP (ATCC® CRL-2583™) is a mouse endothelial cell line transfected with GFP to achieve their constitutive expression in culture, and therefore, autofluorescence that enables real-time monitoring via fluorescence microscopy. Culture conditions were DMEM supplemented with 10% fetal bovine serum plus 1% antibiotics (penicillin and streptomycin sulfate). After sample esterilization, cells were seeded on the networks with a density of 2.0×10^4 cells/cm^2 and incubated at 37 °C with 5% CO_2. Cells were monitored using an inverted fluorescence microscope (Olympus IX51) with a FITC filter ($\lambda_{ex}/\lambda_{em}$ 488/568 nm).

For thermally induced cell sheet detachment, cell-cultured hydrogels were turned upside down and located in new TCP wells. Subsequently, cold medium was added to each well in order to reach $T \leq 27$ °C. A temperature probe (SC1, Biocote, UK) was used to monitor this process. After 45 min, the hydrogels were removed and samples were reincubated at 37 °C with CO_2.

Transplanted cells in new TCP well were monitored daily as described before.

Metabolic activity of cell transplants was measured by Alamar Blue assay following the manufacturer's instructions (Biosource, CA, USA).

This approach is non-toxic, scalable, and utilizes the intrinsic reducing capacity of living cells, providing a quantitative assessment of cell viability and cytotoxicity. In summary, 10% of the culture volume of Alamar Blue dye was added to each well containing viable transplanted cells and incubated for 90 minutes. Assays were performed, on each sample type, in triplicate. The fluorescence ($\lambda_{ex}/\lambda_{em}$ 535/590 nm) of each well was measured using a plate-reader (Synergy HT, Brotek)[11].

In addition, cell proliferation has been measured through dsDNA fluorometric quantification (FluoReporter® Blue), based on Hoechst nuclei staining.

3.5.1.1. Hydrogel sterilization and seeding

Hydrogels with a diameter of 10 mm, cutted to fit into a 12-well plate, were die-cut in distilled water at 37° C. Subsequently, for sterilization, the networks were first washed through three washes with 70% ethanol for 10 minutes each. Following this step, the hydrogels underwent extensive washing three times with PBS at pH 7.4. The samples were then irradiated with UV light for 20 minutes on each side. Following the UV treatment, a final wash with high-glucose Dulbecco's Modified Eagle Medium (DMEM; D6429) was performed. The samples were then immersed in complete DMEM and incubated overnight in a cell incubator at 37 °C and 5% CO_2.

C166-GFP cell line, was utilized as a cytocompatibility model, and seeded as described before.

3.5.1.2. Quantitative analysis of cell adhesion by image analysis

Focal adhesion of the cells was studied through image analysis by monitoring the surface of the hydrogels at two different times 4 and 24 h after cell seeding. Samples were imaged in triplicate for quadrant analysis with ImageJ software taking five quadrant images with resolution of (x, y) = (750, 550) µm. Cells were labeled as adhered (stretched) or not adhered (rounded) according to the displayed morphology.

3.5.1.3. Cell sheet detachment using a controlled temperature decrease

After 48 h of cell culture proliferation, the cultures were transferred to new tissue culture plates using a controlled temperature decrease method. First, fresh culture medium was added to the new plate, comprising 70% of the total volume to maintain moisture on the contact surface. Subsequently, the hydrogels were inverted and placed onto the new plate, allowing the cell culture to contact the surface of the well plate. The remaining 30% of culture medium was then added. This process ensured that the samples were maintained at 15-20 °C for 40 min. Finally, the hydrogels were removed, and the plates containing the cell transplants were reincubated at 37 °C and 5% CO_2.

3.5.1.4. Cell proliferation study, quantify dsDNA. Fluorimetry assay

The quantification of double stranded DNA content of the samples was analyzed, 48 h after seeding stage using the FluoReporter® Blue Fluorometric dsDNA Quantitation Kit (F-2962). The analysis was developed in accordance with the kit's instructions. Briefly, the samples were frozen overnight at -80 °C. Subsequently, they were thawed at RT and then covered with 300 µl of distilled water to ensure complete coverage of the hydrogel layer with proliferating cells. The plates were then incubated at 37 °C for 1 h, followed by a 20 min freezing period and subsequent thawing at RT. For quantitative analysis, an additional 300 µL of Hoechst 33258 reagent mixed with the kit's TNE buffer in a 1:4 ratio was added. DNA content analysis was performed in triplicate using a plate-reader with excitation/emission wavelengths set at 346/460 nm.

3.5.1.5. Metabolic activity. Alamar Blue

Metabolic activity was analyzed using Alamar Blue assay (Biosource, CA, USA), in accordance with the manufacturer's instructions. Widely recognized for its non-toxicity and scalability, this method quantifies cellular reduction capacity, primarily indicative of mitochondrial activity, and thus provides an estimate of cell viability and cytotoxicity. The study was carried out in triplicate, with 10% of the staining reagent added to the total volume, followed by a 90 min incubation period. Fluorescence measurements (λex/λem 535/590 nm) were performed in three independent experiments using a plate reader.

3.5.2. Neural culture evaluation

3.5.2.1. Cell culture

To evaluate hydrogels' toxicity and their effects on proliferation, migration, and differentiation of neural cells, we used Neuro2a mouse neuroblastoma cell line. Neuro-2a cells were cultured in DMEM supplemented with 10% FBS, 1% P/S, and 1% glutaMAX at 37 ºC in a humidified incubator containing 5% CO_2. After 3 to 5 passages, cells were seeded on 96 or 48 well plates bearing the hydrogels washed and sterilized as described in section 3.5.1.

3.5.2.2. Cell viability assay

The effect of hydrogels on Neuro2a viability was measured via the (4,5-dimethylthiazol-2-yl)-2,5-diphenyltetrazolium bromide (MTT) assay. Briefly, 10,000 Neuro-2a cells per well were seeded on top of the hydrogels in 96-well plates in a 10-20 µL drop, left for 10 min to adhere to the hydrogel, and then 100 µL of the culture medium was added. After 48 h, the hydrogel and the culture well were separately incubated with 0.5 mg/mL of MTT reagent (Sigma-Aldrich) for 1 h at 37 ºC and solubilized with 100 µL of hydrochloric acid 0.1 M diluted in isopropanol for 20 min shaking at RT. Finally, absorbance at 570 and 660 nm was determined using a plate reader luminometer (Infinite M200, Tecan Group LTD. Mannendorf, Switzerland). Analyses were replicated in two independent experiments.

3.5.2.3. Video Time Lapse analysis of proliferation, differentiation, and migration

20,000 Neuro2a cells per well were seeded on top of the hydrogel in 48 wells culture plates, followed by the addition of the culture medium. After allowing them to adhere for 4 h, they were taken to a Leica DMI6000B automatic inverted microscope prepared for Video Time Lapse (temperature and humidity maintenance, motorised stage) and equipped with a Leica DFC 350 FX ultra-high sensitivity monochrome digital camera. The system was scheduled to capture images every 20 minutes for 48 hours at 5 positions in each well. As a result, 725 images were taken for each hydrogel–bearing well using a 20X objective (HCX PL FLUOTAR 20x/0.40 CORR PH). One additional well without hydrogels was also seeded and imaged as a control. The resulting images were analyzed using

FIJI 2.14.0 software (Schindelin *et al.*, 2012), following the evolution of selected cell clusters over 48 h and assessing their morphology throughout the process.

References

1. Liz-Basteiro P, Reviriego F, Martínez-Campos E, et al. Vat Photopolymerization 3D Printing of Hydrogels with Re-Adjustable Swelling. *Gels*. 2023;9(8). doi:10.3390/gels9080600
2. Liz-Basteiro P, Sanz-Horta R, Reviriego F, et al. High resolution molds, sacrificial in aqueous media, obtained by vat photopolymerization 3D printing. *Addit Manuf*. 2023;75:103758. doi:https://doi.org/10.1016/j.addma.2023.103758
3. García-Sobrino R, Casado-Losada I, Caltagirone C, et al. Osteoblastic Cell Sheet Engineering Using P(VCL-HEMA)-Based Thermosensitive Hydrogels Doped with pVCL@Icariin Nanoparticles Obtained with Supercritical CO2-SAS. *Pharmaceutics*. 2024;16(8). doi:10.3390/pharmaceutics16081063
4. Garcia C, Gallardo A, López D, et al. Smart pH-Responsive Antimicrobial Hydrogel Scaffolds Prepared by Additive Manufacturing. *ACS Appl Bio Mater*. 2018;1(5):1337-1347. doi:10.1021/acsabm.8b00297
5. Arias-Ferreiro G, Ares-Pernas A, Lasagabáster-Latorre A, et al. Printability Study of a Conductive Polyaniline/Acrylic Formulation for 3D Printing. *Polymers (Basel)*. 2021;13(13). doi:10.3390/polym13132068
6. Arias-Ferreiro G, Ares-Pernas A, Dopico-García MS, Lasagabáster-Latorre A, Abad MJ. Photocured conductive PANI/acrylate composites for digital light processing. Influence of HDODA crosslinker in rheological and physicochemical properties. *Eur Polym J*. 2020;136:109887. doi:https://doi.org/10.1016/j.eurpolymj.2020.109887
7. Ligon S, Liska R, Stampfl J, Gurr M, Mülhaupt R. Polymers for 3D Printing and Customized Additive Manufacturing. *Chem Rev*. 2017;117. doi:10.1021/acs.chemrev.7b00074
8. Arias-Ferreiro G, Lasagabáster-Latorre A, Ares-Pernas A, et al. Lignin as a High-Value Bioaditive in 3D-DLP Printable Acrylic Resins and Polyaniline

Conductive Composite. *Polymers (Basel)*. 2022;14(19). doi:10.3390/polym14194164

9. Gojzewski H, Guo Z, Grzelachowska W, et al. Layer-by-Layer Printing of Photopolymers in 3D: How Weak is the Interface? *ACS Appl Mater Interfaces*. 2020;XXXX. doi:10.1021/acsami.9b22272

10. Rubber, vulcanized or thermoplastic. Determination of compression stress-strain properties. UNE 55536:2001.

11. Martínez-Campos E, Santos-Coquillat A, Pérez-Ojeda ME, et al. Thermosensitive hydrogel platforms with modulated ionic load for optimal cell sheet harvesting. *Eur Polym J*. 2018;103:400-409. doi:https://doi.org/10.1016/j.eurpolymj.2018.04.021

Chapter 4. High-resolution molds, sacrificial in aqueous media, obtained by vat photopolymerization 3D printing

4.1. Introduction

Currently, a myriad of vat photopolymerization (VPP) resins are available, which allow for printing materials with variable properties, ranging from elastic/flexible to tough or stable at high temperatures. However, as far as we know, there is a pending need to develop VPP resins that enable the preparation of sacrificial parts. Up to date, all the final models printed by VPP result in non-reprocessable and non-soluble materials. In contrast to VPP, this type of sacrificial materials has homologs in FDM, *i.e.*, high impact polystyrene (HIPS), soluble in limonene, and poly (vinyl alcohol), (PVA) soluble in water[1,2]. These materials have been widely used for the fabrication, for instance, of supports or molds that need to be removed after use. However, the poor x-y resolution of FDM limited by the nozzle diameter (in the range of 200-400 microns) produces low-quality molds in comparison to VPP[3]. Therefore, taking into account the high precision of VPP, it would be highly desirable to provide resins that can be employed for the fabrication of high-resolution sacrificial molds. It is worth mentioning that those (permanent non-sacrificial) molds made with VPP do not allow for the fabrication of intricate structures because they need to be integrally removed once the part has been fabricated. In this sense, sacrificial molds will significantly improve the complexity of the structures that could be produced.

In VPP processes, a minimum amount of crosslinkers is required to obtain pieces with a suitable resolution and desirable mechanical properties. Indeed, VPP resins are usually formulated with a high content of multifunctional crosslinkers to form stable non-swellable structures, that is, covalently linked polymer networks that remain unaltered during the lifetime of the 3D printed object. Based on this requirement, it is hypothesized that the design of sacrificial printed parts in VPP can be based on the use of labile crosslinkers. In this manner, the resin would comprise enough crosslinker for printing, with a minimum required for good definition and mechanical properties, but the printed part could be sacrificed by breaking the labile crosslinker's bridges, thus converting the polymer network into soluble polymer chains. If the crosslinker is hydrolysable, like those used in this

work, the printed part will be sacrificial in water, a non-toxic and ubiquitous solvent, which is attractive toward its commercial implementation.

Based on our previous experience[4,5], in this work methacrylic crosslinkers containing hydrolysable β-amino esters were employed, which can satisfy the aforementioned needs.

4.2. Results and discussion

The strategy employed to fabricate 3D printed pieces (sacrificial in aqueous media) is illustrated in **Figure 4.1** using representative structures of the components used in the formulations of the photopolymerizable resins developed in this work. In this study, the key components are a hydrolysable crosslinker such as HCL(jef), carrying a jeffamine-derived spacer and *β*-amino ester bonds activated for hydrolysis, and hydrophilic monofunctional monomers (in this case PEGMEA) that allows for tuning the characteristics of the resin and, in turn, of the printed piece and eventually of the hydrolytic process.

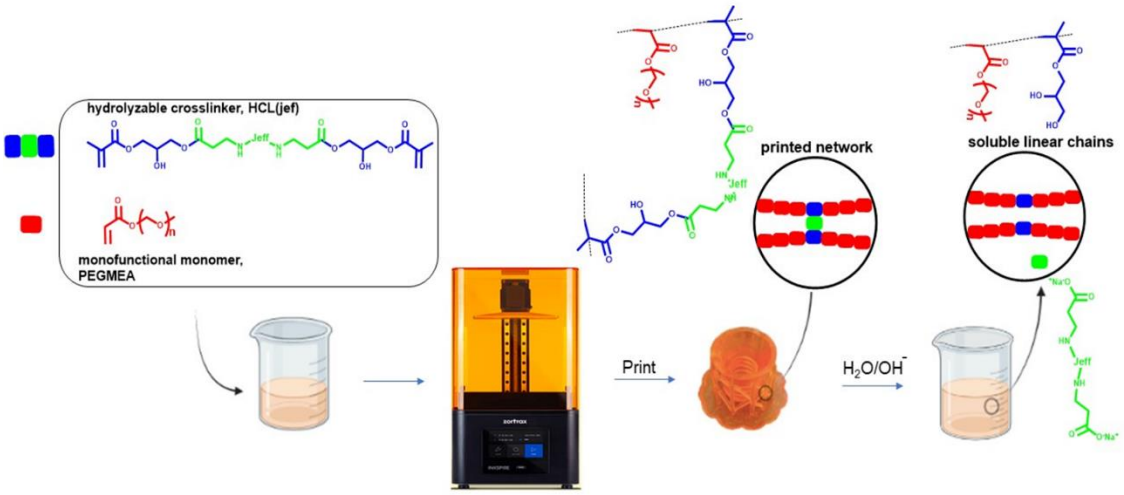

Figure 4.1. Strategy to prepare sacrificial (in water) 3D printable polymeric materials illustrated for resins containing HCL(jef) as hydrolysable crosslinker and PEGMEA as monofunctional monomer. After polymerization (3D printing), a polymer network is obtained, which is sacrificial in basic water because the crosslinking bridges are hydrolysable thus leading to soluble linear chains.

4.2.1. Synthesis of hydrolysable crosslinkers

A generic route to obtain methacrylates bearing hydrolysable side chains by means of a Michael addition of amines on asymmetric acrylic structures

comprising simultaneously methacrylate and acrylate groups has been previously reported by our group[4,5]. This route takes advantage of the very high selectivity of the reaction towards the acrylate group. The obtained methacrylates bear β-amino ester groups in their side chain, which are known to have a high activation towards hydrolysis[6,7]. A similar route was devised in this work, to obtain a dimethacrylate containing β-amino esters in the spacer moiety, by Michael addition of diamines to 3-(acryloyloxy)-2-hydroxypropyl methacrylate (also called 1-(acryloyloxy)-3-(methacryloyloxy)-2-propanol), (1), as asymmetric structure, in a 1:2 molar ratio. Diamines only react with the acrylate group. This route has been previously described to prepare crosslinkers for different applications (neither for 3D printing purposes nor for sacrificial purposes)[8,9]. Jeffamine ED-600 (2) and piperazine (3) were selected as diamines, to obtain the structures shown in **Figure 4.2**, which are denoted as HCL(jef) and HCL(pip) (HCL, stands for hydrolysable crosslinkers).

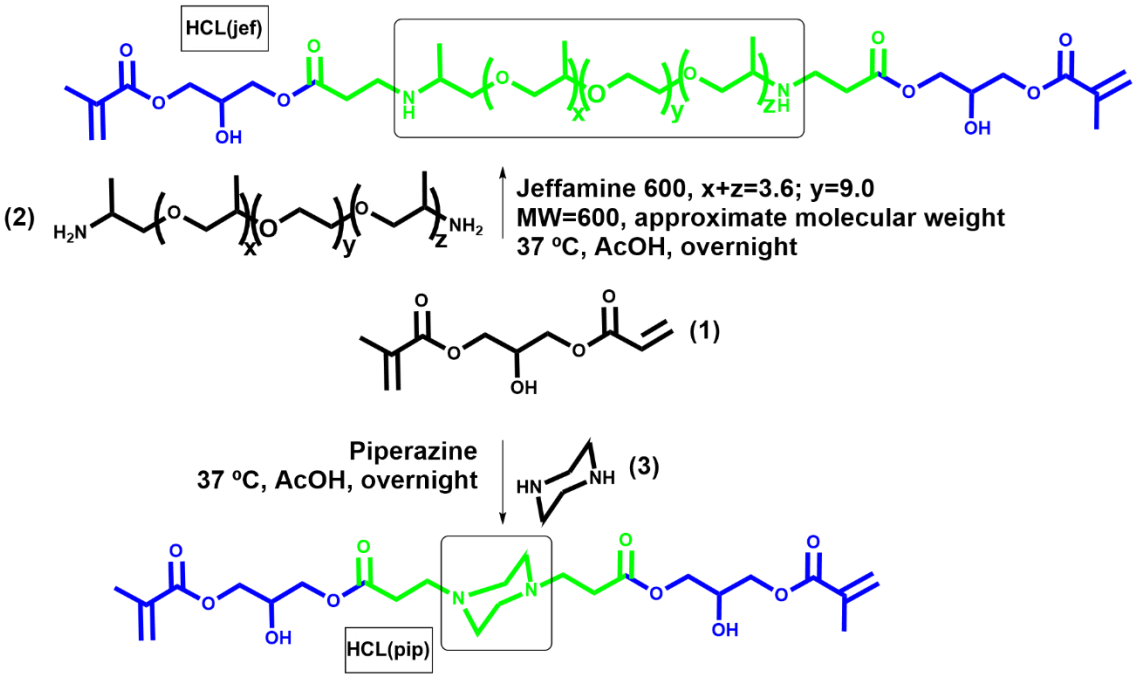

Figure 4.2. Synthetic procedure to obtain the hydrolysable crosslinkers HCL(jef) and HCL(pip), by using two different diamines. The colors in this figure are related to **Figure 4.1**.

It is worth mentioning that this reaction proceeded quantitatively, from relatively cheap commercial chemicals, and without the use of solvents allowing for the use of the reaction product, without needing for further purification. These

characteristics of the reaction make them very promising for future scalability purposes in resin preparation.

4.2.2. Initial tests and adjustments using a binary system comprising HCL and PEGMEA

To impart versatility to the range of final properties, the photocurable resin can be formulated by incorporating, in addition to HCL, other monofunctional monomers in different weight ratios. Properties such as the resin viscosity, mechanical properties of the printed part or water solubility after hydrolysis, can be modulated by a correct choice of these components, as well as the weight ratio of the different precursors. Taking into account that many of the commercial LCD/DLP resins use precursors derived from poly ethylene glycol (PEG) such as PEG-based acrylates or crosslinkers[10,11], PEGMEA has been initially selected as monofunctional monomer, to be combined with HCL in different HCL/PEGMEA weight ratios. It should be noted that jeffamine is also a PEG-related structure. In the context of our design, PEG-based chain segments will ensure negligible toxicity and will favor the solubility in water of the final residual chains. It must be noted that, after photopolymerization and the formation of the polymerized crosslinked solid part, the hydrolysis of the two synthesized crosslinkers yield glycerol methacrylate type units (see final blue structure in **Figure 4.1**).

Formulations with different HCL/PEGMEA weight ratios were prepared, and the influence of this composition ratio on the printability and properties of the printed pieces was studied. The resins have been labeled as HCL(abc)$_X$PEGMEA$_{100-X}$, with abc being jef or pip, and X the weight percentage of HCL in the formulation of the photopolymerizable resin.

4.2.2.1. Analysis of the VPP printability of HCL/PEGMEA resins

In a first series of experiments, a rheological study was carried out to measure the viscosity of the photosensitive resins as a function of the shear rate. The results are summarized in **Figure 4.3**.

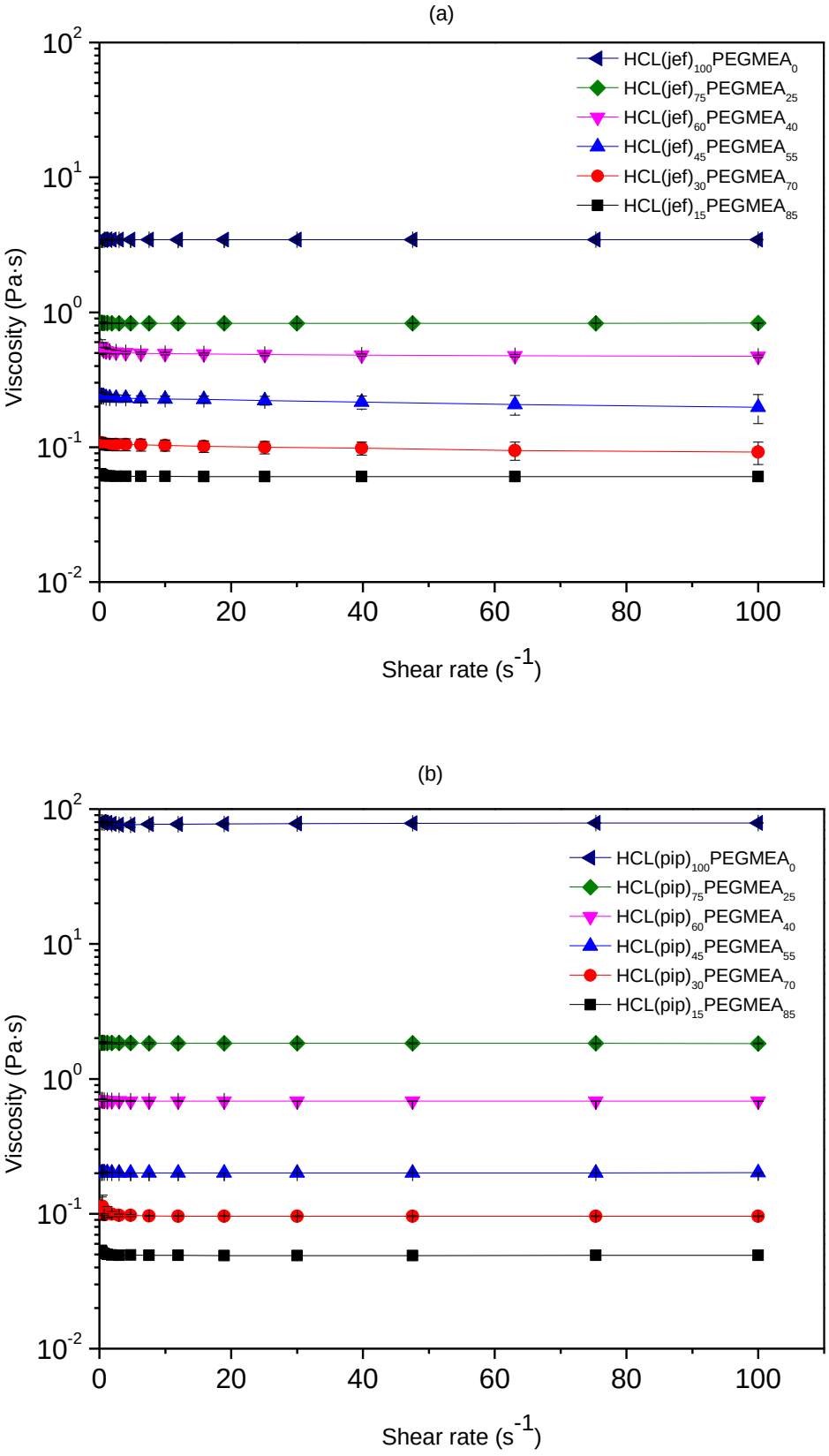

Figure 4.3. Viscosity values as a function of shear rate and a) HCL(jef)/PEGMEA ratio, b) HCL(pip)/PEGMEA ratio.

According to our findings, all the resins showed a Newtonian behavior. It was observed that an increasing proportion of HCL in the mixture produces photopolymerizable resins with higher viscosity. Particularly interesting is the resin comprising exclusively HCL where the viscosity of $HCL(pip)_{100}PEGMEA_0$ is more than an order of magnitude higher than that of $HCL(jef)_{100}PEGMEA_0$. Representative viscosity values obtained for a shear rate of 1 s^{-1} are depicted in **Figure 4**. Low viscosities are known to be required for VPP printing[12,13]. Within the exception of the 100-0 systems prepared using both hydrolysable crosslinking agents, *i.e.*, ($HCL(jef)_{100}PEGMEA_0$ and $HCL(pip)_{100}PEGMEA_0$) and $HCL(pip)_{75}PEGMEA_{25}$, the viscosities of the resins were determined to be less than 1 Pa·s. It is worth mentioning, that according to previous literature, resins with lower ratios of HCL have viscosities close to or even less than 0.1 Pa·s, which are highly suitable values for DLP/LCD printing[14].

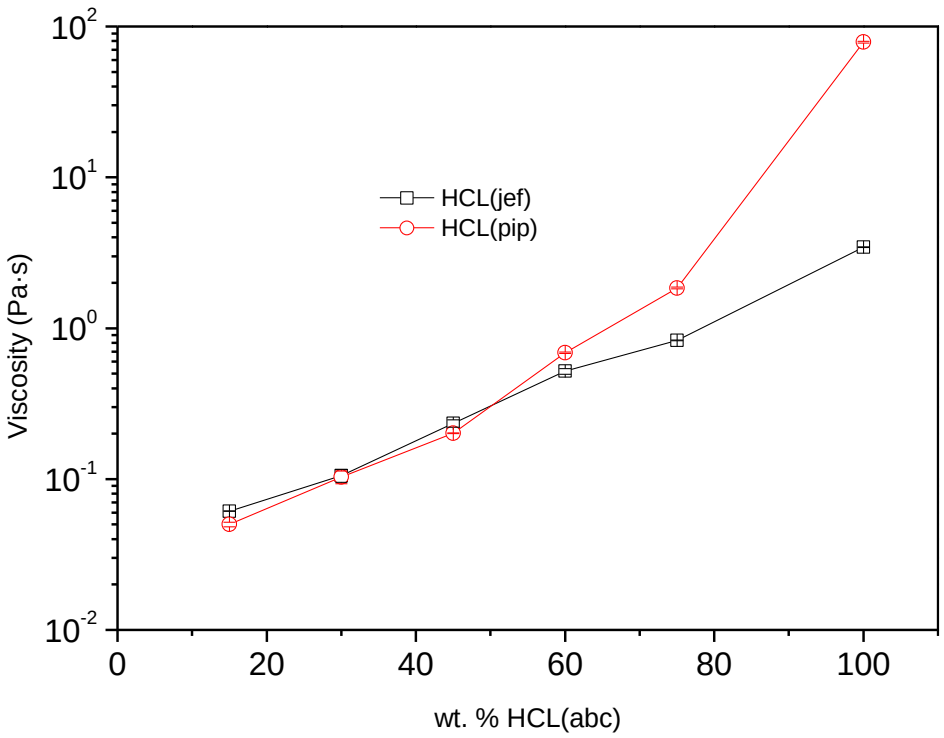

Figure 4.4. Viscosity values for a shear rate of 1 s^{-1} for the different HCL/PEGMEA ratios. Error bars are contained inside the symbols (indicating a narrow data dispersion), hollow points are used to enable the error visualization.

In summary, resins with HCL weight percentages of 45 and lower presented appropriated viscosities for printing. In view of these results, and the interest in

using the lowest possible amount of HCL in the formulation of the resin for scaling, printability and characterization tests of the printed pieces, this study was carried out with photopolymerizable resins with HCL wt. % of 45 or lower. It is worth mentioning that a minimum of 20 s of exposure time in each layer was required to allow for the photopolymerization to proceed in order to ensure the correct anchoring of the 3D printed part onto the fabrication platform. Printability of each resin was tested using a rather simple printing design (2.0x2.0x0.2 cm^3, see **Figure 4.5a**).

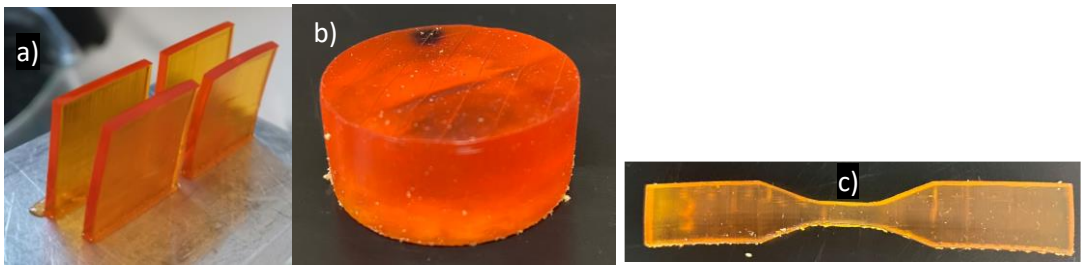

Figure 4.5. (a) Printed specimen prepared in this study: 2.0x2.0x0.2 cm^3 (left image). (b) and (c) samples for compression and tensile tests (center and right images respectively). The dimensions of the last two specimens are described in the Experimental Section.

According to previous studies, the photoabsorber Sudan I was added at 1.35 wt. %, to limit the UV-light penetration[15]. In those cases where Sudan I was not used, pieces with a poorer resolution were obtained (see **Figure 4.6**). The optimized printing parameters are described in the Experimental Section. As mentioned in this Section, the Zortrax Inkspire (LCD 3D printer) was used, but in the first tests it was found that with other LCD 3D printers such as the Creality LD-002H and LD-002R, the same result was achieved, confirming the universality of the resin.

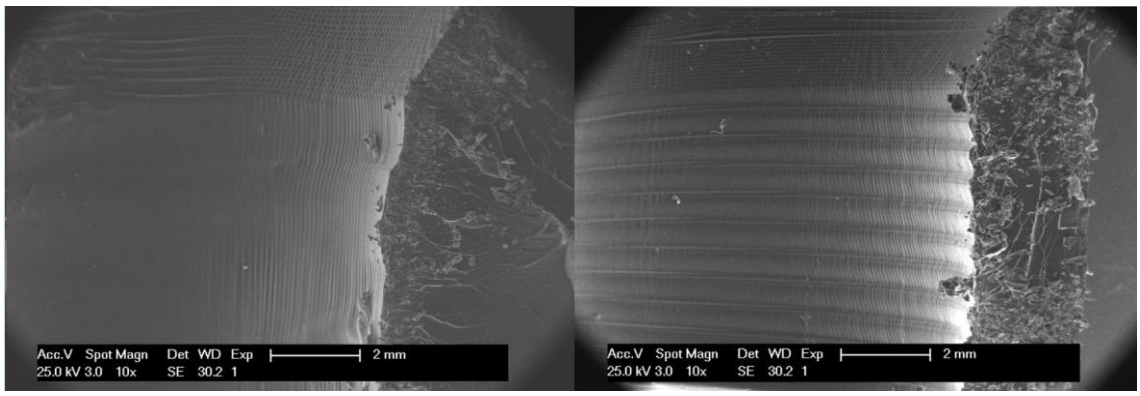

Figure 4.6. SEM images of a piece printed from resin without UV absorber (left) and a piece printed from resin with UV absorber (Sudan I, right).

From these experiments, it could be concluded that the minimum amount of HCL necessary for DLP/LCD printing with these resins, to achieve minimum printability and workability, was 15 wt. % (pieces were not correctly formed below this content). This cutoff percentage is in good agreement with other previous studies[16–20]. The rest of the resins with percentages of HCL higher than 15% by weight could be equally properly printed.

In addition to the amount of crosslinking, another critical aspect is to check the complete light-curing of the resin after 3D printing. To address this aspect FT-IR analysis was carried out (**Figure 4.7**) for the resin and a printed and post-cured piece (30 min, RT). As can be observed, the signals of the polymerizable double bonds within the interval 1675-1600 cm^{-1} range disappear, which confirms the complete polymerization of the resin upon post-curing.

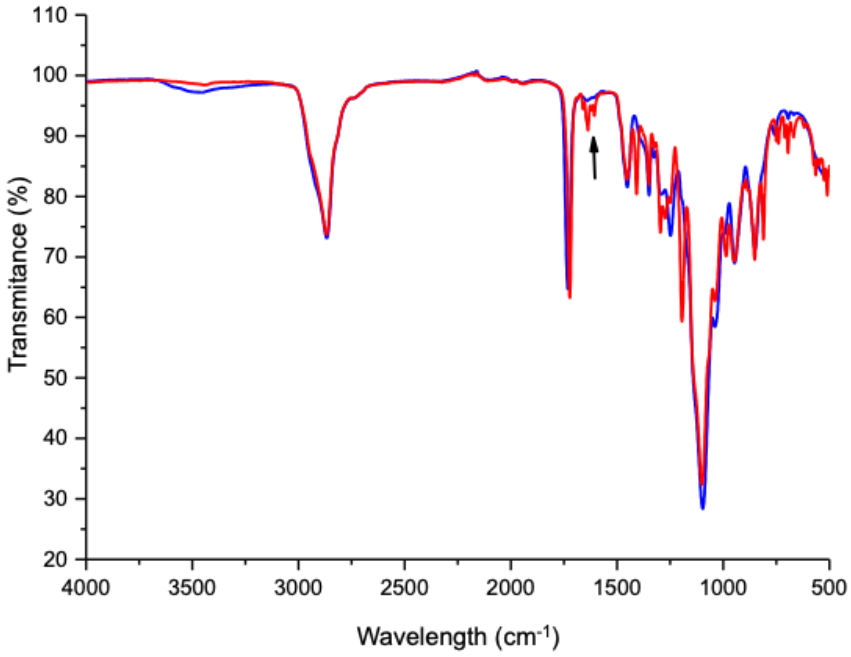

Figure 4.7. FT-IR spectra of the ink and of a printed and post-cured part of $HCL(jef)_{15}PEGMEA_{85}$.

4.2.2.2. Properties of parts 3D printed using HCL/PEGMEA resins

The sacrificial character of these 3D printed samples obtained in dimensions 2.0 x 2.0 x 0.2 cm^3 was preliminarily tested by immersing them in aqueous basic medium (NaOH 2 wt. %). In all cases, the samples were solubilized overnight at room temperature. The solubilized structures were further characterized by ^1H-

NMR spectroscopy. The spectrum obtained was consistent with the proposed mechanism (see **Figure 4.8 and Figure** 4.9).

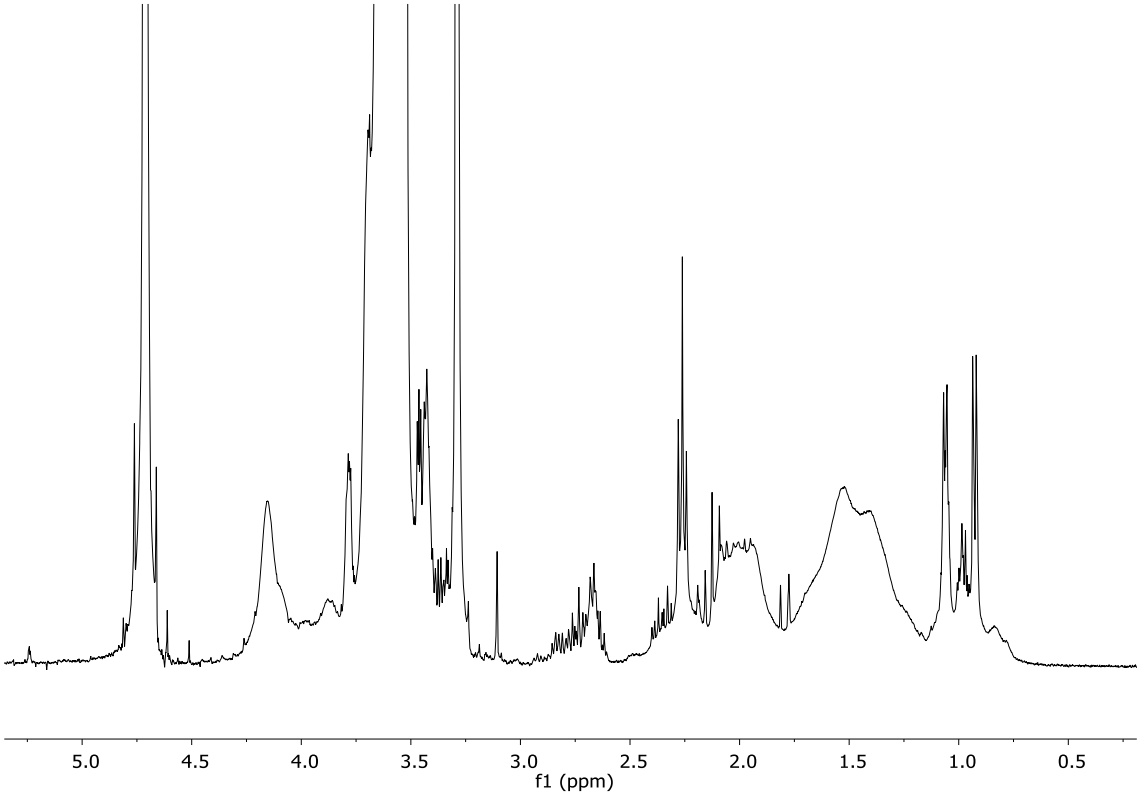

Figure 4.8. ^{1}H NMR of the solution resulting from the hydrolysis of HCL(jef)$_{15}$PEGMEA$_{85}$ in basic water.

This spectrum is consistent with the proposed degradation mechanism (see **Figure 4.9**). There is a main polymeric residue very rich in PEGMEA units. The wide and more intense signals centered on 3.62 and 1.51 ppm correspond respectively to the protons of the O-CH_2-CH_2-O and -CH_2- chain of such PEGMEA units. O-CH_3 is also observed at 3.35 ppm. Signals at 4.2 ppm are also observed that can be assigned to the residual glycerol carrier unit, as well as the α-CH_3 of the methacrylic structure (splitted wide signals in the range of 0.7-0.9 ppm). In the spectrum, there are also signals that can be assigned to the dicarboxylic residue derived from Jeffamine, such as the 2.29 ppm signal that can be assigned to the NaOOC-CH_2-, or the well-defined signals in the 0.9-1.1 region, which can be assigned to the different -CH_3 of the residue (contained both in the polymer chain and the crosslinking agent). It should be noted that these signals are well defined, what confirms that it is a non-polymeric residue. In addition, the integrals of the signals are consistent with the compositions of the system.

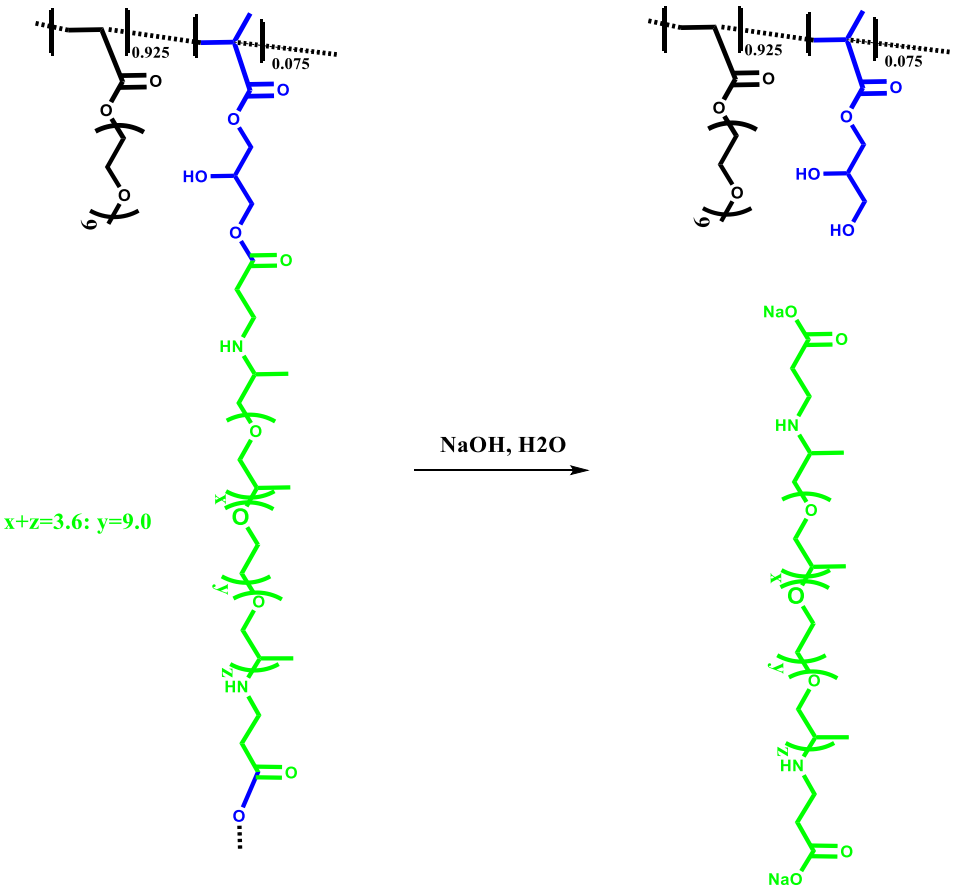

Figure 4.9. Hydrolytic mechanism of the HCL(jef)$_x$PEGMEA$_{100-x}$ system.

Interestingly, a reference network prepared by substituting HCL(jef) by the stable crosslinker PEGDMA did not solubilize after 24 h, but instead became a swollen network (See **Figure 4.10**).

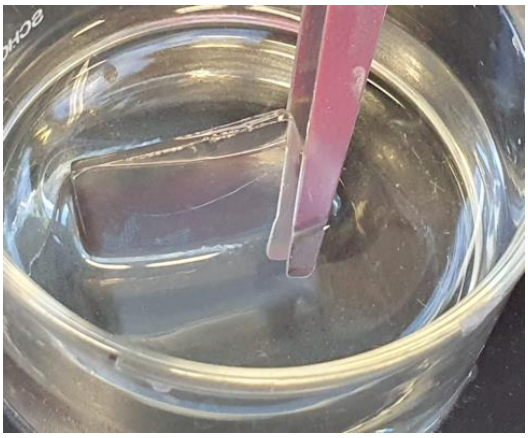

Figure 4.10. Photograph of a reference sample after 24 hours in basic water: in this reference sample HCL(jef) has been replaced by polyethylene glycol dimethacrylate (PEGDMA) in the same percentage by weight (15%).

Provided the fabrication conditions as well as the solubility of the resin in basic conditions, the printed parts obtained from these resins were mechanically characterized by both tensile and compression tests (photographs of the specimens are shown in **Figure 4.11** and **Figure 4.5**). **Table 4.1** shows the mechanical characteristics of the 3D printed materials obtained using both crosslinking agents. According to the results summarized in **Table 4.1** and **Figure 4.11**, the higher the amount of HCL the higher the mechanical strength, being the HCL(pip) system less brittle than the HCL(jef) one. For both families, higher HCL content, leads to photopolymerized parts with higher modulus, although low values can be considered (in the interval of 1-16 MPa). It is observed that, for the same HCL wt. %, the HCL(pip) family shows a higher modulus (both Young's and compression) than the HCL(jef) family. Most probably, this difference is related to the fact that HCL(jef), being longer (higher molar mass) than HCL(pip), leads to less molar crosslinking density than HCL(pip) for photopolymerizable resins with a similar weight percentage. It is interesting to note that when comparing systems of both families with similar molar crosslinking, the moduli are closer (*i.e.*, HCL(jef)$_{30}$PEGMEA$_{70}$ as compared to HCL(pip)$_{15}$PEGMEA$_{85}$, or HCL(jef)$_{45}$PEGMEA$_{55}$ as compared to HCL(pip)$_{30}$PEGMEA$_{70}$, see **Table 4.1**). 3D printed parts using both crosslinking agents are rather brittle, showing values of deformation at break, in tension tests, in the order of 5%. The values of stress at break are higher in the HCL(pip)PEGMEA system, and in both cases, it increases with the amount of HCL, which is in good agreement with the results obtained in the tensile strength tests. The compression measurements, recorded up to 25% of deformation, also ended up breaking the tested 3D printed specimens. In any case, the HCL(pip) based 3D printed parts were slightly stronger than those prepared using HCL(jef), and required higher loads to break as shown in **Figure 4.11** and summarized in **Table 4.1**.

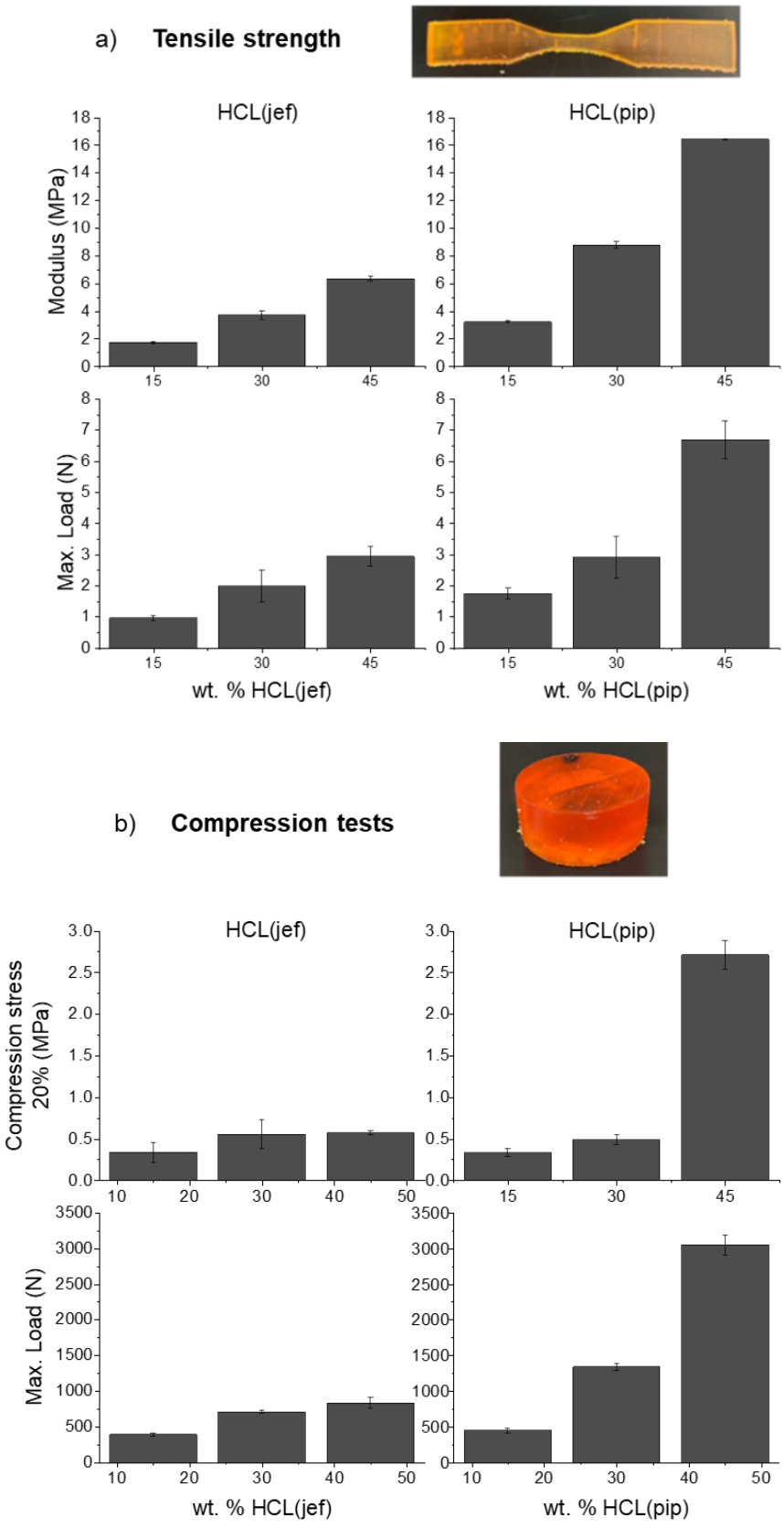

Figure 4.11. Tensile (a) and compression (b) results of HCL(abc)$_X$PEGMEA$_{100-X}$ as a function of the HCL(abc) content in the resin.

Table 4.1. Data of the HCL(abc)$_X$PEGMEA$_{100-X}$ systems. Data are plotted in **Figure 4.11**.

Label	HCL %		Tension				Compression			Sacrificial?[a)]
	Wt.	Mol	E (MPa)	Strain break (%)	Maximum Load (N)		K (MPa)	Compression stress (MPa) 20%	Maximum Load (N)	
HCL(jef)							**HCL(jef)**			
HCL(jef)$_{15}$PEGMEA$_{85}$**	15	7.5	1.74 ± 0.09	5.78 ± 0.49	0.97 ± 0.07		1.61 ± 0.09	0.34 ± 0.12	393 ± 19	Yes
HCL(jef)$_{30}$PEGMEA$_{70}$***	30	16.7	3.72 ± 0.31	5.54 ± 0.52	2.00 ± 0.51		4.36 ± 0.12	0.55 ± 0.17	662 ± 37	Yes
HCL(jef)$_{45}$PEGMEA$_{55}$	45	27.6	6.35 ± 0.16	5.70 ± 0.44	2.95 ± 0.31		5.41 ± 0.40	0.57 ± 0.02	937 ± 5	Yes
HCL(pip)							**HCL(pip)**			
HCL(pip)$_{15}$PEGMEA$_{85}$***	15	14.1	3.21 ± 0.08	6.30 ± 0.42	1.75 ± 0.18		2.77 ± 0.16	0.34 ± 0.05	449 ± 29	Yes
HCL(pip)$_{30}$PEGMEA$_{70}$*	30	28.6	8.78 ± 0.26	4.33 ± 0.34	2.91 ± 0.67		6.28 ± 0.25	0.49 ± 0.06	1342 ± 51	Yes
HCL(pip)$_{45}$PEGMEA$_{55}$	45	43.3	16.4 ± 0.05	5.73 ± 0.63	6.68 ± 0.60		16.4 ± 0.7	2.71 ± 0.17	3051 ± 141	Yes

a) Immersion in basic aqueous media (NaOH 2 wt. %). All samples were solubilized overnight.

* Successfully tested as molds to prepare PCL screws (according to **section 4.2.5**).

** Successfully tested as molds to prepare PCL and silicone screws (according to **section 4.2.5).**

*** Successfully tested as molds to prepare PCL, silicone, and hydrogel screws (according to **section 4.2.5**).

4.2.3. Evaluation of other HCL(jef)-based photopolymerizable resins. Modulation of the properties of the printed parts

The HCL(abc)$_X$PEGMEA$_{100-X}$ systems studied in the previous section have shown to be perfectly printable, although the printed parts showed low moduli (they exhibited some flexibility) and limited deformation before breaking. An optimization of the properties of the printed parts was addressed through the evaluation of other monofunctional monomers and combinations of them. For this purpose, HCL(jef) was selected as crosslinking agent and, thus, incorporated in the formulations in a fixed wt. percentage of 15% (minimum crosslinking required for printability). It is worth mentioning that a lower content of HCL(jef) will favour subsequent hydrolysis since the system will swell to a higher extent and the crosslinking density will be lower. HCL(jef) was chosen because the properties of HCL(jef)$_{15}$PEGMEA$_{85}$ and HCL(pip)$_{15}$PEGMEA$_{85}$ are similar.

As alternative monofunctional monomers to PEGMEA the selected monomers were: HEA, CEA, and MAA (see structures in **Figure 4.12**). A study on the preparation of resins with 15 wt. % HCL(jef) and different combinations of HEA, CEA, and/or MAA has been carried out in two stages: binary and ternary formulations, that is, first analysing the effect of each monomer separately and secondly evidencing the possibility of modulating the properties by using mixtures of two different monomers.

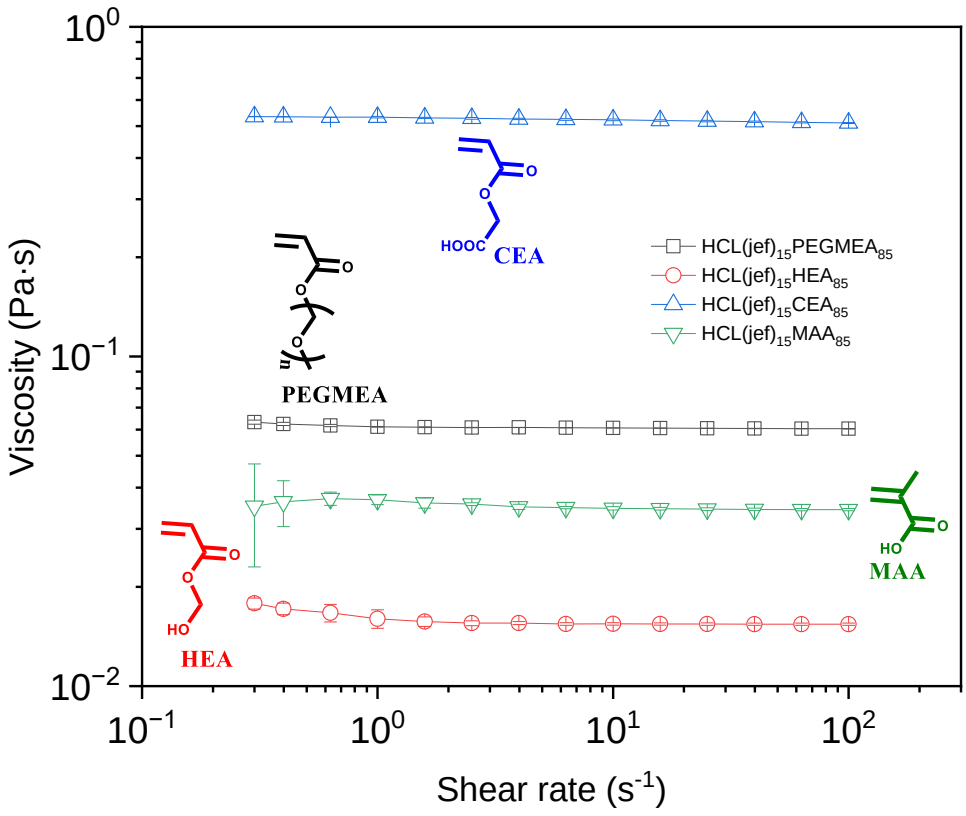

Figure 4.12. Viscosity values as a function of shear rate for the HCL(jef)$_{15}$PEGMEA$_{85}$, HCL(jef)$_{15}$HEA$_{85}$, HCL(jef)$_{15}$CEA$_{85}$, and HCL(jef)$_{15}$MAA$_{85}$ resins. Error bars are contained inside the symbols, hollow points are therefore used.

4.2.3.1. Design and evaluation of HCL(jef)-based binary photopolymerizable resins

In a first series of experiments, binary resins were prepared containing, in addition to 15 wt. % of HCL(jef), one of the four selected monomers. These binary systems were labeled as HCL(jef)$_{15}$PEGMEA$_{85}$, HCL(jef)$_{15}$HEA$_{85}$, HCL(jef)$_{15}$CEA$_{85}$, and HCL(jef)$_{15}$MAA$_{85}$. HEA was selected as a low molecular weight model of PEGMEA, for two reasons: on one hand, for the selected fixed HCL(jef) content of 15 wt. %, the monofunctional monomer size will define the crosslinking molar density, *i.e.*, monomers with higher molar masses will result in higher crosslinking molar density. Thus, the HCL(jef)$_{15}$PEGMEA$_{85}$ and HCL(jef)$_{15}$HEA$_{85}$ correspond to molar ratios of 7.5/1 and 1.9/1 respectively. This difference in crosslinking density will have a great influence on the final properties of the printed parts, as already indicated by the comparative analysis of HCL(jef) and HCL(pip)

described in section 4.2.2. On the other hand, HEA, compared to PEGMEA, leads to polymer chains with a higher glass transition temperature (Tg). Thus, the Tg of PEG-(meth)acrylate type homopolymers has been reported to be around -70 ºC (which is in agreement with the flexible nature of the HCL(jef)$_{15}$PEGMEA$_{85}$ samples)[21], whereas that of poly-HEA is around -2 ºC[22,23]. Therefore, CEA and MAA were selected as precursor monomers for polymers with higher Tg values of 30 and 228 ºC, respectively[24]. Therefore, a range of polymer precursors with increasing values of Tg was employed in this study. It was expected that the rigidity and strength of the printed parts can be controlled with this selection. Furthermore, CEA and MAA are ionizable moieties and are expected to facilitate the dissolution process (involving both swelling and hydrolysis).

4.2.3.1.1. Analysis of the VPP printability of HCL(jef)-based binary resins

Once the rationale behind the selection of the monomers was provided, the resins were rheologically evaluated to analyse whether the viscosities of the resins remain suitable for printing when exchanging PEGMEA by other monomers. **Figure 4.12** shows the viscosity values as a function of the shear rate for the 4 systems. It is observed that all the photopolymerizable mixtures have Newtonian behaviours and, except for the HCL(jef)$_{15}$CEA$_{85}$ system, presented viscosities below 0.1 Pa·s. The viscosity of the HCL(jef)$_{15}$CEA$_{85}$ system, though somewhat higher (close to 0.5 Pa·s), also proved suitable for printing.

4.2.3.1.2. Properties of parts 3D printed using HCL(jef)-based binary resins

All formulations could be printed using the conditions selected in section 4.2.2 and the resulting 3D printed parts could be solubilized overnight at room temperature in basic aqueous media. For the mechanical characterization of the resulting printed materials, specimens for compression and tensile tests were printed and evaluated (see **Figure 4.5**). The simple handling of the parts already showed clear differences: the HCL(jef)$_{15}$PEGMEA$_{85}$ system, as described above, gave rise to somewhat brittle printed parts. Moreover, as will be discussed, the 3D printed parts containing HEA and CEA exhibited improved mechanical properties. As a result, stronger, either elastic or flexible printed parts with different degrees of strength (CEA derivatives stronger than HEA derivatives) (**Figure 4.13**) can be obtained from the HEA and CEA systems. Finally, systems

containing MAA gave rise to very rigid parts. These differences in the values of the mechanical properties are shown in **Figure 4.13** and **Table 4.2**. The Young's and compression modulus of the pieces obtained from the resins containing PEGMEA and HEA are one or two orders of magnitude lower than those of the pieces obtained with resins containing CEA and MAA, respectively. The strain at break (%) data of the elastic HCL(jef)$_{15}$HEA$_{85}$ systems are much higher than those obtained with the HCL(jef)$_{15}$PEGMEA$_{85}$ pieces, which is in good agreement with the greater fragility of these last pieces. Systems containing HEA give rise to 3D printed parts with higher modulus and less brittleness than pieces containing PEGMEA, what can be associated to the difference in crosslinking molar density, which is more than three times higher for the HCL(jef)$_{15}$PEGMEA$_{85}$ system than for HCL(jef)$_{15}$HEA$_{85}$. The pieces of the HCL(jef)$_{15}$CEA$_{85}$ system, which are also elastic, have even higher strain at break values (~142%) for maximum load than HCL(jef)$_{15}$HEA$_{85}$ (~38%). The parts of the HCL(jef)$_{15}$MAA$_{85}$ system hardly deform before breaking at higher loads than any other system, which is indicative of the aforementioned high rigidity. Compression data at 20% deformation for the HCL(jef)$_{15}$CEA$_{85}$ and HCL(jef)$_{15}$MAA$_{85}$ systems were not included because the maximum load of the apparatus (5000 N) was reached before reaching that percentage of deformation.

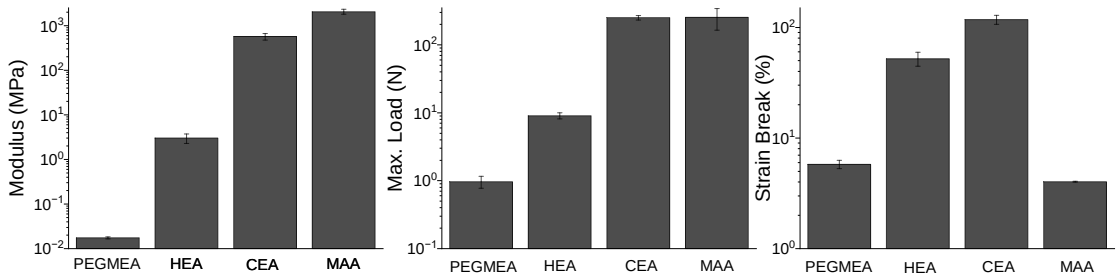

Figure 4.13. Mechanical characteristics of the 3D printed specimen resulting from tensile-strain tests for the following systems: HCL(jef)$_{15}$PEGMEA$_{85}$, HCL(jef)$_{15}$HEA$_{85}$, HCL(jef)$_{15}$CEA$_{85}$, and HCL(jef)$_{15}$MAA$_{85}$.

Table 4.2. Data of the binary systems.

Label	Wt. %	Mol %	Tension				Compression			$T_{5\%}$ (ºC)	Sacrificial?[b)]
			E (MPa)	Elongation (%)	Maximum Load (N)		K (MPa)	Compression stress (MPa) 20%	Maximum Load (N)		
HCL(jef)$_{15}$PEGMEA$_{85}$**	85	92.5	1.74 ± 0.09	5.78 ± 0.49	0.97 ± 0.07		1.61 ± 0.09	34 ± 12	393 ± 19	202	Yes
HCL(jef)$_{15}$HEA$_{85}$**	85	98.1	2.59 ± 0.22	38.3 ± 4.7	9.05 ± 0.93		2.81 ± 0.18	55 ± 17	467 ± 33	228	Yes
HCL(jef)$_{15}$CEA$_{85}$*	85	97.6	121 ± 17	142 ± 21	50.2 ± 5.9		93.2 ± 11.3	a)	a)	183	Yes
HCL(jef)$_{15}$MAA$_{85}$*	85	98.6	2200 ± 403	0.01 ± 0.01	308 ± 20		218 ± 4	a)	a)	217	Yes[c)]

a) The maximum load of the apparatus (5000 N) was reached before reaching 20% of deformation.

b) Immersion in basic aqueous media (NaOH 2 wt. %). All samples were solubilized overnight.

c) The aqueous solution remains as a gelatinous liquid, indicative of a very poorly crosslinked gel.

* Successfully tested as molds to prepare PCL screws (according to section 4.2.5)

** Successfully tested as molds to prepare PCL and silicone screws (according to section 4.2.5).

Since the systems prepared herein are intended to be used as sacrificial molds, it is interesting to analyse the thermal stability of the 3D printed parts, so that a thermal range can be established for a specific application. Printed samples were characterized by TGA. From the thermograms (**Figure 4.14**), the values of $T_{5\%}$, that is, the temperature at which the sample has lost 5% of its mass, were determined and collected in **Table 4.2**. This temperature has been used as the temperature where degradation begins. It can be seen that all the systems remain stable up to ~180 ºC with some differences depending on the employed monomer. Whereas the HCL(jef)$_{15}$CEA$_{85}$ system can be used below 183 ºC, the other systems can be used at temperatures around 200 ºC for HCL(jef)$_{15}$PEGMEA$_{85}$ and up to 220 ºC for HCL(jef)$_{15}$HEA$_{85}$ and HCL(jef)$_{15}$MAA$_{85}$ (see **Table 4.2.** Data of the binary systems.).

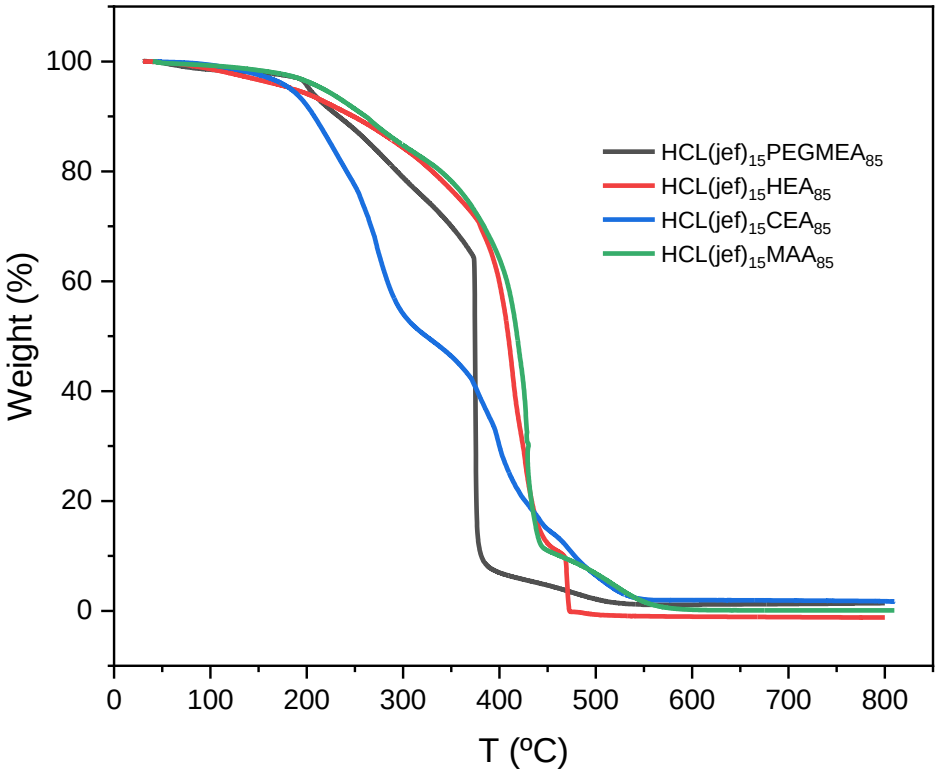

Figure 4.14. Thermograms of the different binary systems investigated using HCL(jef) as crosslinking agent and the monomers PEGMEA, HEA, CEA, and MAA.

4.2.3.2. Incorporation of two monofunctional monomers to the photopolymerizable resin. HCL(jef)-based ternary systems

The study of binary systems depicted above evidenced that the mechanical properties of the printed parts can be modulated, at least to a certain extent, by combining HCL(jef) with different monofunctional monomers with variable side chain lengths and hydrophilicity/charge. As described above, printed parts with Young's modulus of 1.74, 2.59, 121, and 2200 MPa were obtained by using photopolymerizable resins comprising HCL(jef) and PEGMEA, HEA, CEA, and MAA respectively. Whereas the parts fabricated using PEGMEA were fragile, those obtained with MAA were very rigid. Moreover, the HEA and CEA systems made it possible to print robust parts with different degrees of flexibility (the HEA system being more flexible than the CEA system). In this context, more continuous or finer modulation of the properties can be achieved by using ternary systems, *i.e.*, elaborating photosensitive resins comprising HCL(jef) (fixed at 15 wt. %) and dual combinations of the four monofunctional monomers in different ratios. For clarity purposes, the possible combinations have been restricted to HEA-based ternary systems with different wt. % of HEA and the third component selected from PEGMEA, CEA, or MAA, see **Table 4.3**. The rationale behind this selection relies on the fact that $HCL(jef)_{15}HEA_{85}$ is the binary resin with the lowest viscosity (see **Figure 4.12**), and the expected contribution of HEA to the improvement of the thermal stability, robustness, and flexibility, as well as to its homology with PEGMEA. Thus, in systems with CEA and MAA, it is expected that the ternary combinations will lead to parts with gradual Young modulus from highly rigid systems with only MAA to highly flexible and robust systems with only HEA, through systems with intermediate flexibility and very robust with only CEA. The PEGMEA system has been included for comparative purposes.

The ternary systems have been therefore labeled as $HCL(jef)_{15}HEA_{X}monomer_{85-x}$, where monomer is PEGMEA, CEA, or MAA, and X is the weight percentage of HEA ($0 \leq X \leq 85$).

Table 4.3. Data of the ternary systems.

Label	Wt. %[a)]	HCL(jef) molar %	Tension			Compression			$T_{5\%}$ (ºC)	Sacrificial?[b)]
			E (MPa)	Elongation (%)	Maximum Load (N)	K(MPa)	Compression stress (MPa) 20%	Maximum Load (N)		
$HCL(jef)_{15}HEA_XPEGMEA_{85-X}$	85-0**	1.9	2.59 ± 0.22	38.3 ± 4.7	9.05 ± 0.93	2.81 ± 0.18	55 ± 17	467 ± 33	228	Yes
	60-25***	2.4	2.52 ± 0.03	26.0 ± 1.1	4.82 ± 0.22	2.60 ± 0.17	56 ± 4	453 ± 28	271	Yes
	40-45	3.2	1.94 ± 0.20	19,0 ± 3.2	3.04 ± 0.49	2.28 ± 0.20	47 ± 4	444 ± 31	261	Yes
	20-65	4.4	1.87 ± 0.09	13.3 ± 2.1	2.10 ± 0.29	2.27 ± 0.01	43 ± 1	421 ± 22	264	Yes
	0-85**	7.5	1.74 ± 0.09	5.78 ± 0.49	0.97 ± 0.07	1.61 ± 0.09	34 ± 12	393 ± 19	202	Yes
$HCL(jef)_{15}HEA_XCEA_{85-X}$	85-0**	1.9	2.59 ± 0.22	38.3 ± 4.7	9.05 ± 0.93	2.81 ± 0.18	55 ± 17	467 ± 33	228	Yes
	60-25	2.0	7.52 ± 1.87	44.1 ± 0.1	12.8 ± 1.0	26.6 ± 2.3	351 ± 67	4055 ± 740	196	yes
	40-45**	2.1	100 ± 22	64.1± 3.5	15.5 ± 5.4	64.2 ± 8.2	c)	c)	195	Yes
	20-65	2.2	107 ± 13	103 ± 10	26.4 ± 7.3	86.6 ± 9.3	c)	c)	190	Yes
	0-85*	2.4	121 ± 17	142 ± 21	50.2 ± 5.9	93.2 ± 11.3	c)	c)	183	Yes
$HCL(jef)_{15}HEA_XMAA_{85-X}$	85-0**	1.9	2.59 ± 0.22	38.3 ± 4,7	9.05 ± 0.93	2.81 ± 0.18	55 ± 17	467 ± 33	228	Yes
	60-25	1.7	50.9 ± 9.7	3.05 ± 0.32	29.3 ± 1.8	75.9 ± 2.0	c)	c)	201	Yes
	40-45**	1.6	1019 ± 122	0.15 ± 0.02	104 ± 8	d)	d)	d)	195	Yes
	20-65	1.5	1642 ± 221	0.07 ± 0.01	221 ± 16	d)	d)	d)	224	Yes
	85-0*	1.43	2200 ± 403	0.01 ± 0.01	308 ± 20	d)	d)	d)	217	Yes[e)]

a) HEA-PEGMEA, HEA-CEA or HEA-MAA wt. % for a fixed wt. % of HCL(jef) of 15.

b) Immersion in basic aqueous media (NaOH 2 wt.%). All samples were solubilized overnight.

c) The maximum load of the apparatus (5000 N) was reached before reaching the 20% of deformation.

d) Data not shown because experiment reached 5000 N at deformations below 3%.

e) The aqueous solution remains as a gelatinous liquid, indicative of a very poorly crosslinked gel.

* Successfully tested as molds to prepare PCL screws (according to **section 4.2.5**).

** Successfully tested as molds to prepare PCL and silicone screws (according to **section 4.2.5**).

*** Successfully tested as molds to prepare PCL, silicone, and hydrogel screws (according to **section 4.2.5**).

4.2.3.2.1. Analysis of the VPP printability of HCL(jef)-based ternary resins

The rheological study confirmed that all the ternary resins show a Newtonian behaviour, and that the viscosity values obtained are intermediate between the values of the binary systems, being dependent on the composition (see **Figure 4.15**). Of interest is the variation of the viscosity in the system $HCL(jef)_{15}HEA_XCEA_{85-X}$, from 0.5 Pa·s. of the resin with only CEA ($HCL(jef)_{15}CEA_{85}$) to values close to 0.01 of the system made of only HEA ($HCL(jef)_{15}HEA_{85}$; please note that the Y-axis is displayed as a logarithmic scale). Taking into account the background of the study of binary systems (section 4.2.3.1), it can be considered that all resins have appropriate viscosities for printing. This was further confirmed by printing all of them into stable pieces (2.0x2.0x0.2 cm^3). It also should be mentioned that the explored compositions did not significantly affect the solubilization process and, therefore, all samples were solubilized overnight at room temperature in basic aqueous media.

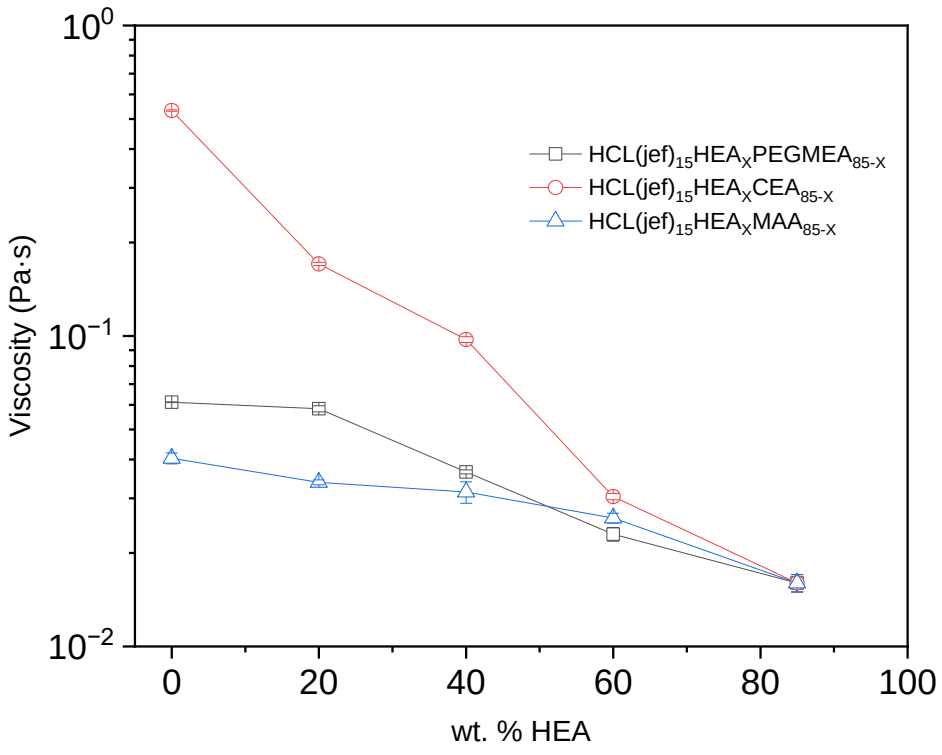

Figure 4.15. Viscosity values for a shear rate of 1 s^{-1} for the different resins. Please note that the wt. % of HCL is always 15%. Error bars are contained inside the symbols, hollow points are therefore used.

4.2.3.2.2. Properties of parts 3D printed using HCL(jef)-based ternary resins

The 3D printed parts obtained with the different systems were thermally and mechanically characterized by TGA, tensile, and compression tests respectively (specimens were prepared according to the Experimental Section and **Figure 4.5**). The mechanical properties of the different systems obtained from the tensile-strain tests have been depicted in **Figure 4.16**. Upon thoroughly analysing system by system, it is possible to evidence that in HCL(jef)$_{15}$HEA$_X$PEGMEA$_{85-X}$ an increase in the flexibility of the printed materials is observed in the photopolymerizable resins with higher HEA content. As described before, the HCL(jef)$_{15}$PEGMEA$_{85}$ binary system is very brittle, breaking at 5% strains with very low load (0.97 N), while HCL(jef)$_{15}$HEA$_{85}$ is significantly more flexible and elastic, breaking at 38% strain and under load one order of magnitude higher (9 N, also low). Systems with both components show intermediate and compositionally correlative properties, being the compositions close to HCL(jef)$_{15}$HEA$_{85}$ eligible for their use as molds according to their resistance. The differences associated with the composition must be ascribed, at least in part, to the change in the molar crosslinking density, which progressively decreases with increasing amount of HEA.

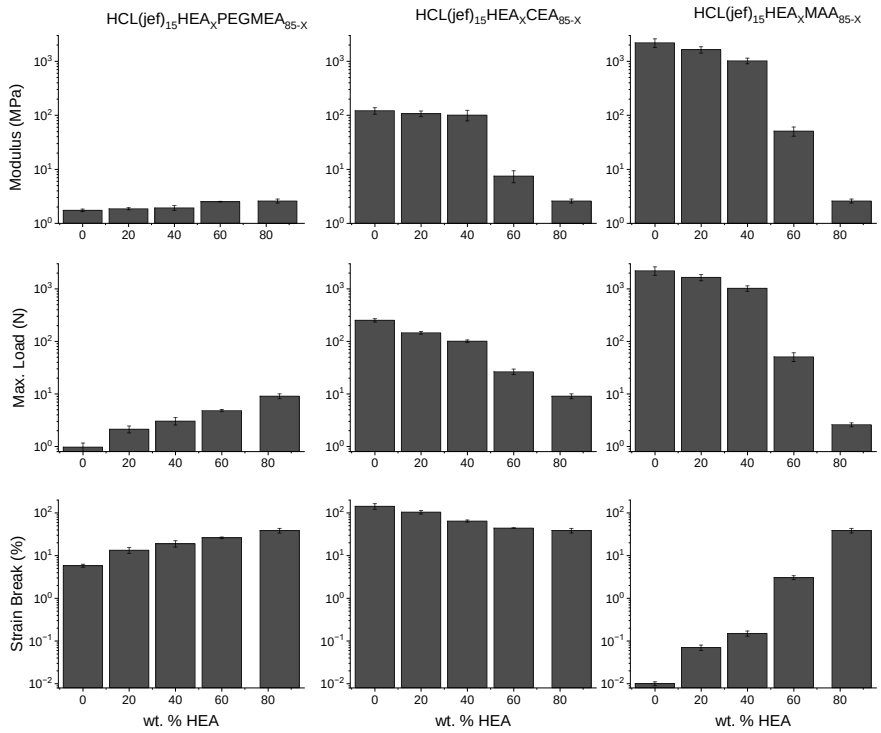

Figure 4.16. Parameters from tensile tests of ternary systems as function of the HEA content.

Regarding thermal stability (**Figure 4.17a, b, and c**), ternary systems have shown significantly higher stability than the binary controls, and can be used up to temperatures of 260-270 ºC. This unexpected increase in the thermal resistance still requires further investigation but nevertheless will allow for their use in a larger range of temperatures.

(a)

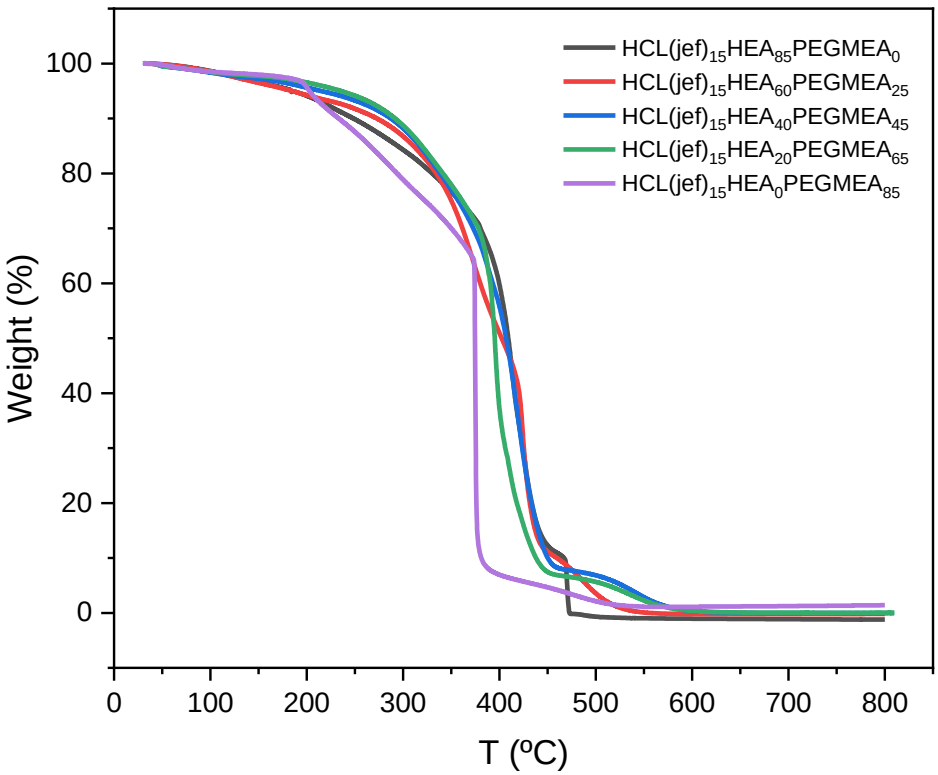
HCL(jef)15HEA85PEGMEA0
HCL(jef)15HEA60PEGMEA25
HCL(jef)15HEA40PEGMEA45
HCL(jef)15HEA20PEGMEA65
HCL(jef)15HEA0PEGMEA85
Weight (%)
T (ºC)
0
20
40
60
80
100
0
100
200
300
400
500
600
700
800

(b)

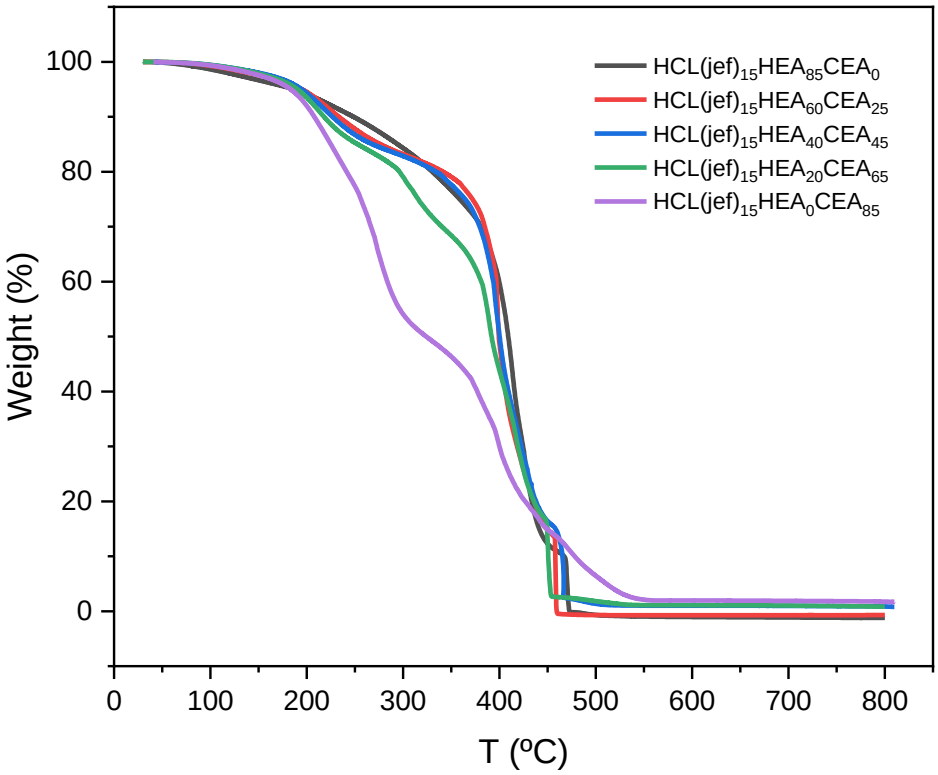
HCL(jef)15HEA85CEA0
HCL(jef)15HEA60CEA25
HCL(jef)15HEA40CEA45
HCL(jef)15HEA20CEA65
HCL(jef)15HEA0CEA85
Weight (%)
T (ºC)
0
20
40
60
80
100
0
100
200
300
400
500
600
700
800

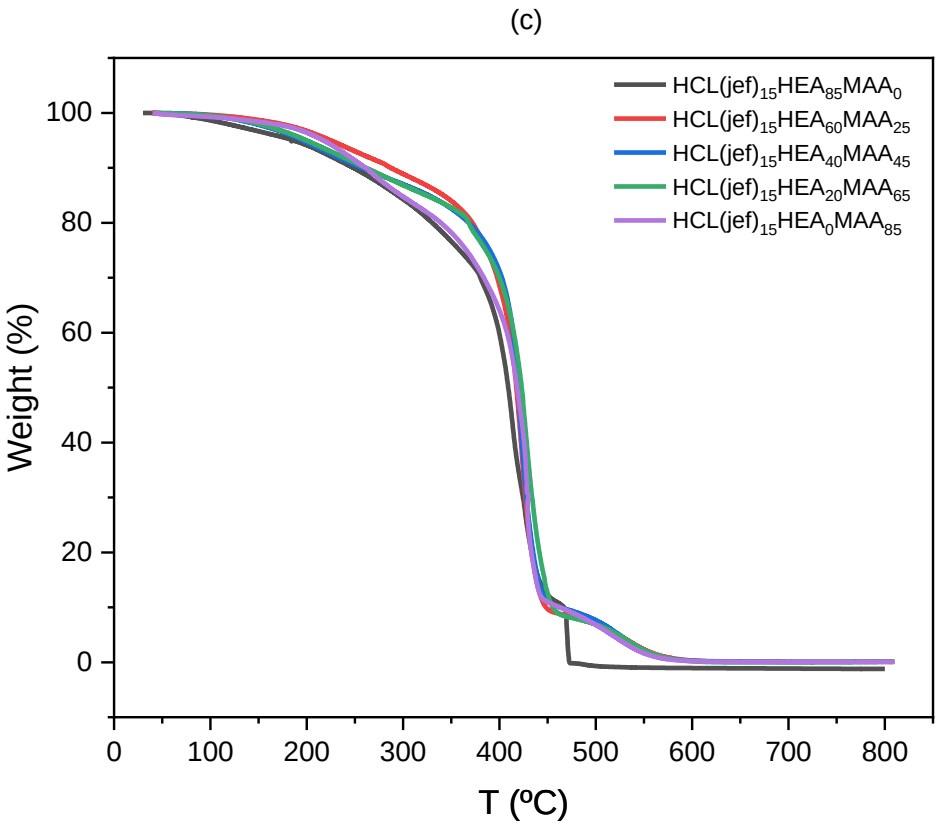

Figure 4.17. Thermograms of a) $HCL(jef)_{15}HEA_XPEGMEA_{85-X}$, b) $HCL(jef)_{15}HEA_XCEA_{85-X}$, and c) $HCL(jef)_{15}HEA_XMAA_{85-X}$ respectively.

The $HCL(jef)_{15}HEA_XCEA_Y$ system is flexible and elastic in all compositions. Nevertheless, an increase in the molar amount of CEA produced parts with improved modulus, improved deformation capacity before breaking (it is more elastomeric) and, therefore, the load at break increases. Intermediate compositions have intermediate properties correlated with the composition. The thermal stability of these series of resins presented maximum temperatures of use of around 190 ºC.

Finally, 3D printed parts fabricated from $HCL(jef)_{15}HEA_XMAA_{85-X}$ ternary photopolymerizable resins were, in comparison with the previous systems, rather rigid. More precisely, moduli of the parts were -independently of the material composition- near the binary control $HCL(jef)_{15}MAA_{85}$ and above 1 GPa. These materials are brittle, they break at minimal deformations, although they require very high loads to do so. The thermal stability is similar to the binary controls.

A global analysis indicates that it is possible to modulate the mechanical properties of printed parts, from elastic and highly flexible parts ($HCL(jef)_{15}HEA_XCEA_{85-X}$ system), to very rigid parts (MAA-rich formulations in the $HCL(jef)_{15}HEA_XCEA_{85-X}$ system), and therefore robust flexible and rigid parts can be manufactured. All materials can be used at temperatures below 180 ºC. If higher temperatures are required, there are options to select materials with ranges of use up to 270 ºC.

4.2.4. Dimensional accuracy analysis

We have carried out dimensional measurements on cylinder-type representative samples, printed from the digital design mentioned in **Table 4.4**. The measurements have been made in triplicate. It can be seen that in most cases, the dimensional accuracy is excellent. Only in the pieces that contain CEA is a small deviation observed. This behavior may be related to the measurement method and the high elasticity of CEA derivatives, which may make the measurement less reliable.

Table 4.4. Dimensional accuracy data.

	Cylinders		Screw' molds
	Diameter	**Height**	**Thread pitch**
Dimensions from the digital design	**29.00**	**12.00**	**2.00**
Label	**Measured diameter**	**Measured height**	**Measured thread pitche**
$HCL(jef)_{15}PEGMEA_{85}$	29.01 ± 0.01	12.50 ± 0.01	n.d.
$HCL(pip)_{45}PEGMEA_{55}$	29.05 ± 0.02	12.50 ± 0.01	n.d.
$HCL(jef)_{15}HEA_{85}$	29.00 ± 0.01	12.51 ± 0.11	2.00 ± 0.04
$HCL(jef)_{15}CEA_{85}$	28.69 ± 0.11	12.51 ± 0.11	n.d.
$HCL(jef)_{15}HEA_{40}PEGMEA_{45}$	29.01 ± 0.05	12.50 ± 0.05	2.00 ± 0.13
$HCL(jef)_{15}HEA_{40}CEA_{45}$	29.96 ± 0.11	12.50 ± 0.13	2.13 ± 0.14
$HCL(jef)_{15}HEA_{40}MAA_{45}$	29.05 ± 0.02	12.46 ± 0.02	n.d.

n.d.: non-determined

4.2.5. Proof of concept of the use of photopolymerizable resins for the preparation of high-resolution sacrificial molds

Provided an adequate printability and sacrificial nature (based on their hydrolysis and solubility in basic aqueous solutions) of all the systems described in the previous sections, selected formulations were used for the preparation of sacrificial molds. SLA/LCD/DLP are without any doubt the current commercially available technology with the best resolution. Different sectors ranging from

dentistry to jewelry employ this technology for the fabrication of molds requiring high level of detail. In addition to the part resolution, for some particular applications where mold removal supposes a challenge such as those parts with intricate internal structures or with delicate surface patterns, the use of soluble molds could be an interesting alternative.

For this proof of concept, a mold with an internal screw shape was selected (mold designs are described in the Experimental Section). To test the dimensional accuracy on these samples, the thread pitches of three printed screws have been analyzed for representative formulations (**Figure 4.18**), obtaining values very close to those of the digital design (these measurements have been included in **Table 4.4**).

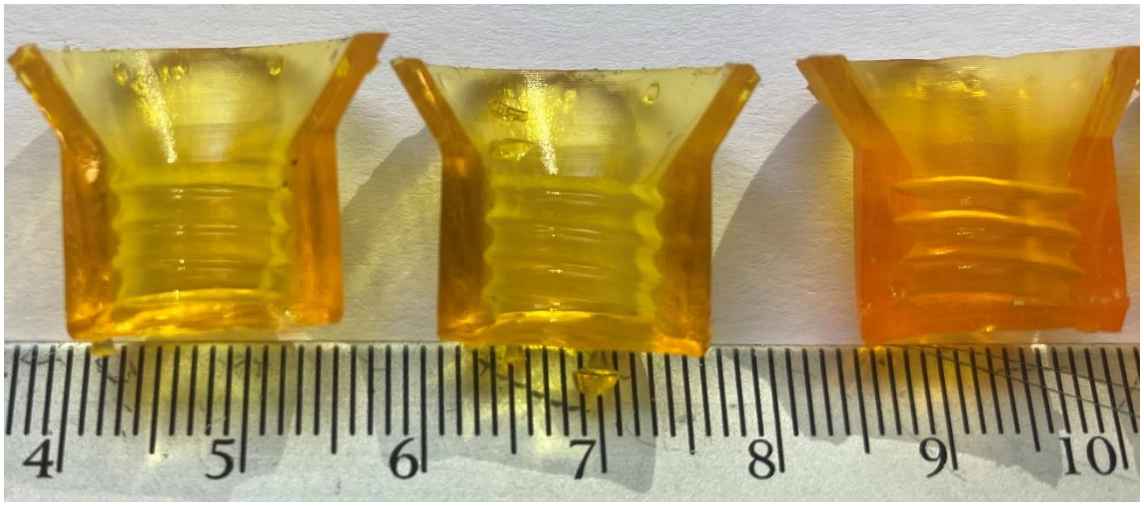

Figure 4.18. Screw' molds printed from HCL(jef)$_{15}$HEA$_{85}$, HCL(jef)$_{15}$HEA$_{40}$PEGMEA$_{45}$, HCL(jef)$_{15}$HEA$_{40}$CEA$_{45}$ formulations, from the left to the right.

More interestingly, to test the versatility of these fabricated molds three different applications that require different processing methods were evaluated.

First, the fabrication of rigid screws made using a thermoplastic polymer able to melt and flow into the mold were explored. As thermoplastic polymer PCL was selected. PCL is a semicrystalline polymer, biocompatible, FDA approved and extensively used for biomedical applications. The mold was filled with solid PCL pellets, heated at 100 ºC (above the PCL melting point) for the time necessary for the molten polymer to completely fill the mold, after which it was allowed to cool to room temperature. Finally, the screw-shaped PCL was recovered by complete solubilization of the resin in basic conditions overnight. It is worth

mentioning that PCL upon melting decreases significantly the viscosity and, as depicted in **Figure 4.19c and Figure 4.19f,** was able to completely fill the mold.

Secondly, reactive processable materials were equally explored. More precisely, elastic silicone screws prepared by filling the mold with the commercial liquid two-component formulation Sylgard 184, followed by overnight curing at 60°C. Similar to the example depicted above the silicon-based screws were recovered by overnight immersion in a basic aqueous medium (**Figure 4.19d and Figure 4.19g**).

These preparative processes selected to evidence the potential of these materials have been evaluated with representative samples of the two families of materials described above. The selected compositions have been indicated in **Table 4.1, Table** 4.2**, and Table 4.3** with one or two asterisks (indicating whether it has only been used in the preparation of PCL screws or if it has been used to obtain screws of both types, respectively). Interestingly, in all cases the fabrication of the desired part was successfully achieved, that is, the conditions employed for the preparation (temperature and time) did not alter the 3D printed structure and, upon immersion in basic aqueous solution, the mold could be completely removed in all the explored cases.

This experiment, although a proof-of-concept, highlight the potential of these soluble materials for their use in many different applications where the high-resolution of VPP 3D printing is required.

4.2.5.1. Use of sacrificial molds to photocure VCL-based hydrogels

As mentioned in the introduction and objectives of the thesis, part of this thesis work is focused on the possibility of obtaining VCL-based 3D thermosensitive hydrogels by 3D printing through vat photopolymerization (Chapter 6). In this context, the development carried out in this chapter may allow to obtain tailored 3D hydrogels not by direct printing but by the alternative use of sacrificial molds. It should be remembered that these VCL-based 3D thermosensitive hydrogels, which are the supports of the iFABCell technology mentioned in the Introduction, have been prepared in the past as flat films by photocuring, using an optimized formulation containing, in addition to VCL and the photoinitiator, a mixture of EGDMA and DVI as crosslinkers.

With this background, we therefore wondered whether the sacrificial molds described in this chapter could be used as molds for the photocuring process of the VCL-based photopolymerizable mixture. For this purpose, the mold was simply filled with the liquid resin formulation and photocured under the standard conditions used to obtain flat hydrogels: 40' at 365 nm of wavelength. It should be noted that the liquid formulation and the mold were preheated beforehand to 50 °C, as indicated in experimental. Using these experimental conditions the polymerization, take place thus leading to a solid screw-shaped filler that could be recovered again by overnight immersion in a basic aqueous medium (**Figure 4.19e and Figure 4.19h**). This experiment can be considered as a proof of concept that sacrificial molds can be used to obtain VCL-based 3D thermosensitive hydrogels, being an alternative to the direct 3D printing that will be studied in **Chapter 6**. In addition, this study shows that sacrificial molds are compatible with the light curing process which is an exothermic radical polymerization process.

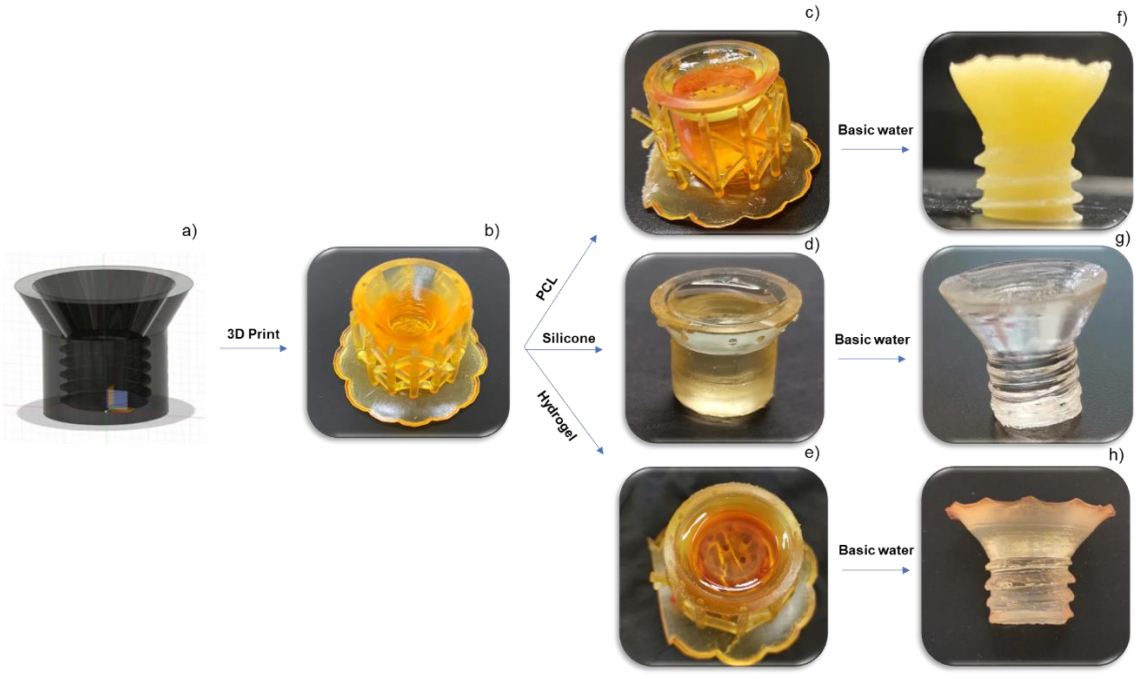

Figure 4.19. Scheme of the proof on concept to prepare PCL or silicone screws using the sacrificial molds described in this work. a) Digital design of the mold. b) Printed mold. c) Printed mold filled with the molten PCL (100 ºC). d) Printed mold filled with the two components liquid Sylgard 184 (please note that in this case the print support columns have been removed). e) Printed mold filled with the VCL-based liquid resin. f) Final PCL screw. g) Final silicone screw. h) Final VCL-based hydrogel screw.

4.3. Conclusions

A direct and scalable route to obtain printable formulations containing hydrolysable crosslinkers has been demonstrated. The 3D printing of these resins, through VPP, has given rise in all cases to sacrificial pieces in basic water, that is, soluble, fulfilling the starting hypothesis that sacrificial networks could be obtained using hydrolysable crosslinkers. The versatility of the approach was shown when it comes to intervening in the components of the formulations, which has allowed the properties of the printed parts to be tuned in terms of moduli, stress required for breakage or their elasticity. Moreover, the 3D printed parts presented a thermal resistance up to 180-240 ºC which establish the limits in their use.

The proposed strategy involves the preparation of sacrificial molds and using them to recover the 3D part with the complementary counter shape. As materials for the targeted part, we have explored the use of a molten thermoplastic, (followed by cooling and solubilization), a bi-component silicone system, (followed by chemical crosslinking and solubilization), or a VCL-based thermosensitive hydrogel liquid formulation, (followed by photopolymerization and solubilization). Please note that these VCL-based hydrogels are the focus of an important part of this thesis.

The three alternatives explored evidenced that the templates have shown thermal stability in the PCL range, as well as chemical stability during the chemical and photocrosslinking reaction. These three systems illustrate proofs of concepts that can be extended to other chemical systems and shapes (provided by the additive manufacturing versatility and the high-resolution of VPP), offering a wide myriad of applications.

References

1. Julinová, M., Vaňharová, L. & Jurča, M. Water-soluble polymeric xenobiotics – Polyvinyl alcohol and polyvinylpyrrolidon – And potential solutions to environmental issues: A brief review. *J Environ Manage* **228**, 213–222 (2018).

2. Wang, J. *et al.* A Method for Manufacturing Flexible Microfluidic Chip Based on Soluble Material. *J Nanomater* **2021**, 1280338 (2021).

3. Decrossas, E. *et al.* Evaluation of 3D printing technology for corrugated horn antenna manufacturing. in *2016 IEEE International Symposium on Electromagnetic Compatibility (EMC)* 251–255 (2016). doi:10.1109/ISEMC.2016.7571653.

4. Navarro, R. *et al.* Understanding the regioselectivity of Michael addition reactions to asymmetric divinylic compounds. *RSC Adv.* **7**, 56157–56165 (2017).

5. Redondo, J. A. *et al.* Prodendronic polyamines from stable or labile methacrylates obtained by selective Michael addition onto asymmetric diacrylic compounds. *J Polym Sci A Polym Chem* **52**, 2297–2305 (2014).

6. Lim, Y., Choi, Y. H. & Park, J. A Self-Destroying Polycationic Polymer: Biodegradable Poly(4-hydroxy-l-proline ester). *J Am Chem Soc* **121**, 5633–5639 (1999).

7. Al Thaher, Y., Latanza, S., Perni, S. & Prokopovich, P. Role of poly-beta-amino-esters hydrolysis and electrostatic attraction in gentamicin release from layer-by-layer coatings. *J Colloid Interface Sci* **526**, 35–42 (2018).

8. Shemper, B. S. *et al.* Synthetic clay nanocomposite-based coatings prepared by UV-cure photopolymerization. *J Appl Polym Sci* **93**, 1252–1263 (2004).

9. Hwang, J.-Z. *et al.* A new UV-curable PU resin obtained through a nonisocyanate process and used as a hydrophilic textile treatment. *Journal of Polymer Research* **19**, 9900 (2012).

10. Martinez, P. R., Goyanes, A., Basit, A. W. & Gaisford, S. Fabrication of drug-loaded hydrogels with stereolithographic 3D printing. *Int J Pharm* **532**, 313–317 (2017).

11. Chiappone, A. *et al.* 3D Printed PEG-Based Hybrid Nanocomposites Obtained by Sol-Gel Technique. *ACS Appl Mater Interfaces* **8**, (2016).

12. Ligon, S. C., Liska, R., Stampfl, J., Gurr, M. & Mülhaupt, R. Polymers for 3D Printing and Customized Additive Manufacturing. *Chem Rev* **117**, 10212–10290 (2017).

13. Li, J. *et al.* Synthesis and properties of a low-viscosity UV-curable oligomer for three-dimensional printing. *Polymer Bulletin* **73**, 571–585 (2016).

14. Tu, J., Makarian, K., Alvarez, N. J. & Palmese, G. R. Formulation of a Model Resin System for Benchmarking Processing-Property Relationships in High-Performance Photo 3D Printing Applications. *Materials* **13**, (2020).

15. Garcia, C. *et al.* Smart pH-Responsive Antimicrobial Hydrogel Scaffolds Prepared by Additive Manufacturing. *ACS Appl Bio Mater* **1**, 1337–1347 (2018).

16. Borrello, J., Nasser, P., Iatridis, J. C. & Costa, K. D. 3D printing a mechanically-tunable acrylate resin on a commercial DLP-SLA printer. *Addit Manuf* **23**, 374–380 (2018).

17. Arias-Ferreiro, G., Ares-Pernas, A., Dopico-García, M. S., Lasagabáster-Latorre, A. & Abad, M.-J. Photocured conductive PANI/acrylate composites for digital light processing. Influence of HDODA crosslinker in rheological and physicochemical properties. *Eur Polym J* **136**, 109887 (2020).

18. Wu, H., Chen, P., Yan, C., Cai, C. & Shi, Y. Four-dimensional printing of a novel acrylate-based shape memory polymer using digital light processing. *Mater Des* **171**, 107704 (2019).

19. Ni, R., Qian, B., Liu, C., Liu, X. & Qiu, J. A cross-linking strategy with moderated pre-polymerization of resin for stereolithography. *RSC Adv.* **8**, 29583–29588 (2018).

20. Tai, H. *et al.* Thermoresponsive and Photocrosslinkable PEGMEMA-PPGMA-EGDMA Copolymers from a One-Step ATRP Synthesis. *Biomacromolecules* **10**, 822–828 (2009).

21. Zhang, J. *et al.* Evolution of Microphase Separation with Variations of Segments of Sequence-Controlled Multiblock Copolymers. *Macromolecules* **50**, (2017).

22. Aran, B., Sankır, M., Vargün, E., Sankır, N. D. & Usanmaz, A. Tailoring the swelling and glass-transition temperature of acrylonitrile/hydroxyethyl acrylate copolymers. *J Appl Polym Sci* **116**, 628–635 (2010).

23. Chen, T. & Kusy, R. P. Effect of methacrylic acid:Methyl methacrylate monomer ratios on polymerization rates and properties of polymethyl methacrylates. *J Biomed Mater Res* **36**, 190–199 (1997).

24. Fang, C., Yan, Q., Liu, Z., Lu, Y. & Lin, Z. The influence of monobutyl itaconate and β-carboxyethyl acrylate on acrylic latex pressure sensitive adhesives. *Int J Adhes Adhes* **84**, 387–393 (2018).

Part of this work has been published at Pedro Liz-Basteiro, Raúl Sanz-Horta, Felipe Reviriego, Enrique Martínez-Campos, Helmut Reinecke, Carlos Elvira, Juan Rodríguez-Hernández, Alberto Gallardo, High resolution molds, sacrificial in aqueous media, obtained by vat photopolymerization 3D printing, Additive Manufacturing, Volume 75, 2023, 103758, ISSN 2214-8604, https://doi.org/10.1016/j.addma.2023.103758.

Chapter 5. Vat photopolymerization 3D printing of hydrogels with re-adjustable swelling

5.1. Introduction

As mentioned in the previous chapter, 3D printing by means of VPP commonly employs resins with high contents of di- or multifunctional polymerizable crosslinkers[1,2], thus yielding parts with a highly crosslinked network structure with dimensional stability and little or no swelling capacity. However, crosslinked networks capable of swelling in water, that is, hydrogels, are materials of great interest in biomedicine and in other applications[3–6].

To print hydrogels, the crosslinking density should be designed, in principle, according to the characteristics of the targeted swelling. According to literature data, selected as an example, if it is desired to print an acrylate-based hydrogel that mimics soft tissues, that is, with a certain amount of water (for example, containing double the amount of water of a polymer), the photocurable formulation must contain around 1 wt. % of a crosslinker such as ethylene glycol dimethacrylate[7]. This percentage, which is much lower than those crosslinking densities obtained using standard resins, may not be compatible with certain aspects of VPP because the technique usually requires a minimum amount of crosslinkers to obtain parts with adequate resolution and desirable mechanical properties[2,8–10]. On certain occasions, low crosslinking is related to poor adhesion to the platform.

In order to overcome this issue, one strategy that can allow for the printing of hydrogel-type networks with the desired swelling capacity using VPP 3D printing[11] involves the preparation of formulations containing a mixture of stable and labile crosslinkers. In this way, the crosslinker content in the resin would be enough for printing pieces with good definition and mechanical properties, although the printed part could be subsequently readjusted by selectively breaking the labile crosslinking bridges. As a result, the final network will have a crosslinking density defined by the amount of stable crosslinker. If the labile character refers to hydrolytic sensitivity, as is the case in this work, the printed network will be able to readjust in water, a non-toxic and ubiquitous solvent, rendering it very attractive for commercial implementation.

In addition, the network readjustment may be of interest for certain applications, such as filling cavities in regenerative medicine[12], the use of hydrogels as supports and reservoirs in hydroponics and aquaponics[13], or for pharmaceutical and cosmetic manufacturing[14,15], which could benefit from a controlled increase in size upon swelling in water.

When designing the printing of a network precursor of a hydrogel, it must be taken into account that the size of the fresh printed part is smaller than that of the swollen networks. If the swelling is isotropic[16,17], the swollen part replicates the shape of the printed part, and the original dimensions and their increase via swelling can be designed to obtain a final custom hydrogel.

Based on the previous experience explained in **Chapter 4**, in this work, different formulations containing mixtures of stable and hydrolysable crosslinkers have been optimized and evaluated for 3D printing. The resulting printed parts were characterized in terms of the size variation and water content. Although LCD 3D printing has been used in this work, the procedure studied here could be extended following slight modifications of the photosensitive resin composition to other VPP techniques, such as SLA and DLP.

5.2. Results and discussion

5.2.1. Design of the photopolymerizable resin and optimization of the 3D printing parameters

Figure 5.1 schematically shows the strategy used in this chapter as well as the structures of the components of the formulation, which includes a stable, SCL, and a hydrolysable crosslinker, HCL (as mentioned in the Introduction section). Three-dimensional printing via VPP renders type A networks, which have a crosslinking density defined by the sum of SCL and HCL. This A network, before any swelling readjusting, is capable of uptaking some amount of water to become a type B network. B networks are then capable of readjusting their swelling upon selective hydrolysis of the hydrolysable crosslinking agents to give rise to C, with network C being the network with the maximum readjustment in swelling (only the permanent crosslinking agents remain ensuring the hydrogel's integrity). Thus, the adjustable network design is based on the simultaneous use of the SCL and HCL. In this way, the adjustable character of hydrogels refers to the ability to

modulate the degree of swelling, starting from an initial value (network B in **Figure 5.1**), through the controlled hydrolysis of the HCL bridges. The final (and maximum) swelling is defined by the residual SCL bridges (after hydrolysis of all the HCL; network C in **Figure 5.1**).

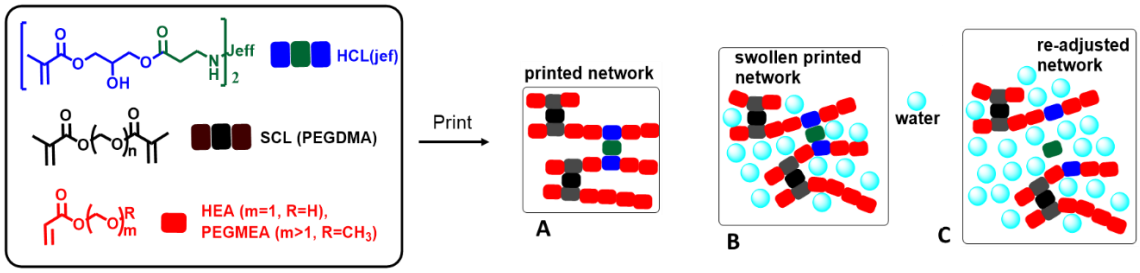

Figure 5.1. Scheme of the strategy used in this work for printing re-adjustable hydrogels via VPP. (A) A 3D printed part obtained directly after printing and post-curing. (B) Initial swelling in PBS. (C) A 3D printed part upon swelling in basic media due to the HCL hydrolysis. The jeff tag refers to the spacer of the Jeffamine (R of H_2N-R-NH_2).

In addition to the crosslinkers, monofunctional monomers responsible for modulating certain properties of the final hydrogel were added to the formulation. Results from **Chapter 4** were used to select the components and the starting parameters[18]. The HCL(jef) containing a Jeffamine derivative carrying activated *β*-aminoesters for hydrolysis was chosen because it has shown its effectiveness in the preparation of sacrificial templates in the previous chapter. PEG derivatives (PEGDMA as the crosslinker and PEGMEA as the monofunctional monomer, from now on PEGDMA and PEGMEA respectively), as well as their ethoxylated low molecular weight homologue (HEA), were chosen as structures of the SCL (PEGDMA) and monofunctional monomers (PEGMEA and HEA) in order to build PEO-related structures. In this sense, Jeffamine is also a PEO-related structure.

The crosslinking percentage was established as 15 wt. % (total amount of the SCL + HCL(jef)), as this value has been shown in the previous chapter to be the minimum required to print parts with good resolution and acceptable mechanical properties[18].

Initially, the influence of the monofunctional monomers (HEA and PEGMEA) on the printing process and the properties of the printed pieces has been addressed. For this purpose, the HCL/PEGDMA weight percentages were set at 7.5/7.5, and the samples were prepared by varying the HEA/PEGMEA weight ratio, as shown

in **Table 5.1**. Using the format of the previous chapter, this series would be labelled HCL(jef)$_{7.5}$PEGDMA$_{7.5}$ HEA$_X$PEGMEA$_{85-X}$ where 0 ≤ X ≤ 85. However, for ease of reading, the label was shortened to HCL(jef)$_{7.5}$-HEA$_X$ since HCL+PEGDMA is always 15.

Table 5.1. Data concerning the HCL(jef)$_{7.5}$-HEA$_X$ series, including the penetration depth (D_p) and critical exposure (E_c) calculated from the Jacobs working curves.

Label	PEGDMA/HCL(jef)/ HEA/PEGMEA wt. %	PEGDMA/HCL(jef)/ HEA/PEGMEA mol %	Crosslinker mol% (PEGDMA + HCL(jef))	ν (Pa·s)	D_p (μm)	E_c (mJ·cm^{-2})
HCL(jef)$_{7.5}$-HEA$_0$	7.5/7.5/0/85	6.9/3.6/0/89.5	10.5	0.041	102	3.82
HCL(jef)$_{7.5}$-HEA$_{20}$	7.5/7.5/20/65	4.2/2.2/52.4/41.2	6.4	0.034	105	3.49
HCL(jef)$_{7.5}$-HEA$_{40}$	7.5/7.5/40/45	3.0/1.6/75.0/20.4	4.6	0.026	165	4.35
HCL(jef)$_{7.5}$-HEA$_{60}$	7.5/7.5/60/25	2.3/1.2/87.7/8.8	3.5	0.019	221	4.69
HCL(jef)$_{7.5}$-HEA$_{85}$	7.5/7.5/85/0	1.8/1.0/97.2/0	2.8	0.012	311	4.89

ν = Viscosity for a Shear Rate of 1 s^{-1} (deviation error 0.001)

First of all, in order to evaluate the photopolymerizable resin printability, a rheological study was carried out to measure the viscosity as a function of the shear rate. All the samples have shown Newtonian behavior (see **Figure 5.2**). Although there is a certain dependence on the composition (the higher the amount of HEA, the lower the viscosity), the viscosities remain in all cases below 0.050 Pa·s, evidencing their suitability for DLP/LCD printing, which requires low viscosities[19,20]. The values of the shear rate measured for a frequency of 1 s^{-1} have been quoted in **Table 5.1**.

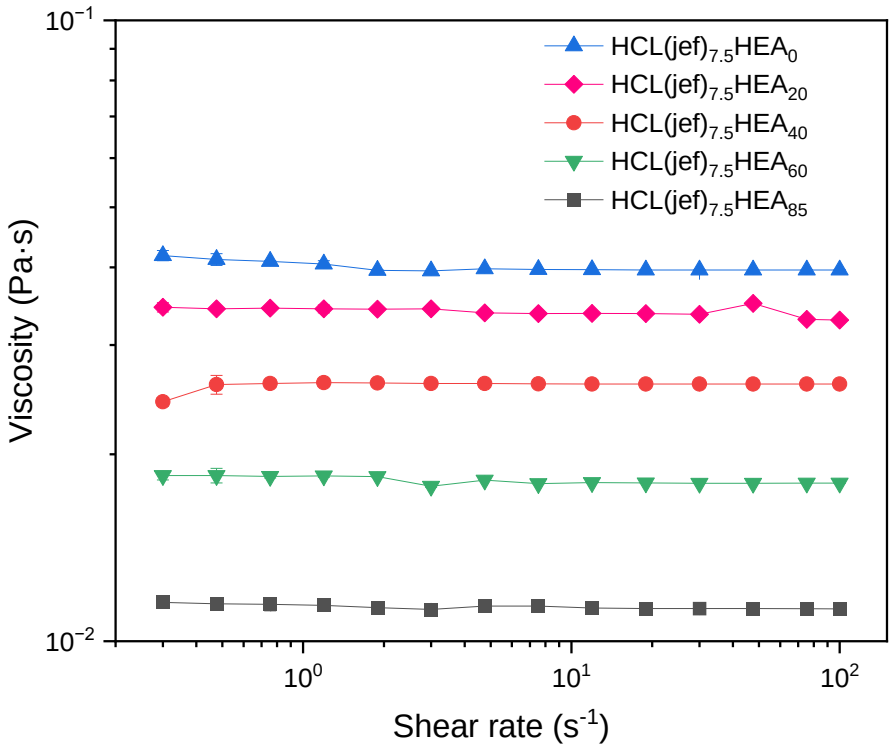

Figure 5.2. Viscosity values as a function of the shear rate for the $HCL(jef)_{7.5}HEA_X$ system.

In order to select the optimal printing parameters, and more specifically, the exposure time for a layer of 100 µm, the Jacobs working curves[21–24] (see **Figure 5.3**) were determined as described in the Experimental Section. These lines, which represent the cured depth (C_d) against the energy that the printer lamp radiates on the surface of the part for different exposure times, allow for the selection of the most appropriate exposure times for the layer height selected in the printing parameters. As can be observed in **Figure 5.3**, for each exposure time, the C_d decreases as the amount of HEA decreases. This working line provides information about the E_c ($mJ \cdot cm^{-2}$), the starting point for the transition from liquid to solid, and the D_p (µm), the penetration depth. The parameters calculated from these curves are presented in **Table 5.1**.

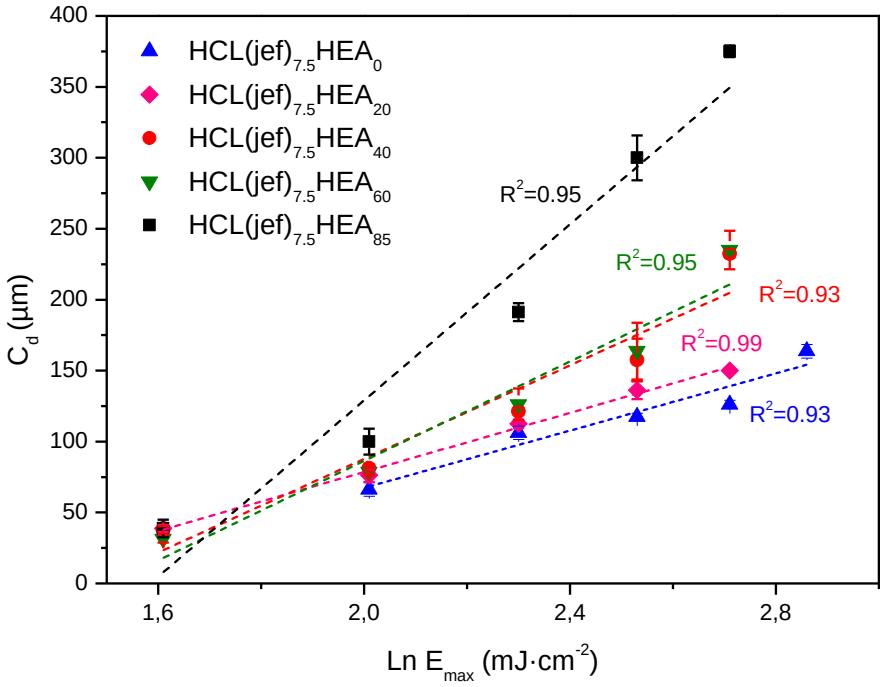

Figure 5.3. Working curves for the HCL(jef)$_{7.5}$HEA$_X$ series when exposed to 405 nm light (0.5 mW·cm^{-2}). Data correspond to (from right to left in each group of data) exposure times of 35, 30, 25, 20, 15 and 10 s. Linear regressions are included.

The HEA/PEGMEA weight ratio does not have a great influence on the E_c, although it does on the Cd. The greater the amount of HEA, the greater the D_p for each exposure time. **Table 5.1** shows that the variation in the HEA/PEGMEA ratio has a great influence on the molar crosslinking density: the more HEA, the lower the molar crosslinking density, which means, in principle, that it will require longer irradiation times (or energy) to reach a gel structure. In addition, by varying the HEA/PEGMEA ratio, the ratio between the low molecular weight monomer (HEA) and the macromonomer (PEGMEA) is also being varied. It has been described that the degree of functionality of the components (mono- vs. difunctional) and their molecular weight have a profound influence on both the gel point and the curing depth[25].

Based on the graph shown in **Figure 5.3**, and taking into account that the objective is to obtain a layer height of 100 microns, 20 s was chosen as the common exposure time for all the printings. For this exposure time, the different systems result in curing depths close to the target value.

To assess the printability and make an initial characterization of the dimensional readjustment, pieces with dimensions of 2.0×2.0×0.2 cm^3 were printed for the different formulations. According to previous studies[26], and to the study of the previous chapter, the photoabsorber Sudan I was added at 1.35 wt. %, to limit the UV light penetration. Please note that Sudan I was already used in the previous study to obtain the Jacobs working curves. The optimized printing parameters employed to print the parts are summarized in the Experimental Section.

It is worth mentioning that an increase in the amount of HEA in the photopolymerizable mixture leads to more resistant and less brittle parts. This fact may be associated with the large variation in the crosslinking molar density, *i.e.*, an increase in the HEA content involves a reduction in the crosslinking molar density.

5.2.2. 3D printed part swelling: Toward a selective rupture of the hydrolysable crosslinking agents

The pieces printed according to section 5.2.1. were immersed either in PBS or in basic water (2 wt. % of NaOH) and gravimetrically monitored to determine their water content and calculate the corresponding swelling according to Equation 3.2. In PBS, a gradual increase in swelling was observed until reaching an equilibrium value varying in the 100–170% swelling range, depending on the composition. This equilibrium value, which is reached between 24 and 96 h (depending on the system), is plotted in **Figure 5.4**. Interestingly, although the crosslinking density decreases with an increasing HEA content, this does not translate into a correlative increase in swelling. Swelling increases slightly up to 40 wt. % HEA but then decreases, remaining in all cases above 100%. To the naked eye, it is observed that very HEA-rich hydrogels have a transparent outer layer and a colored core, which is probably slightly swollen. This behavior can be explained as follows. With an increasing HEA content, on the one hand, there is initially a slight increase in swelling in PBS due to the significant decrease in the molar percent crosslinking. From 40%, on the other hand, these variations in the degree of crosslinking are not as high, and swelling decreases due to the greater water absorption capacity of PEGMA-based systems compared to HEA-based systems for similar degrees of crosslinking[27–29].

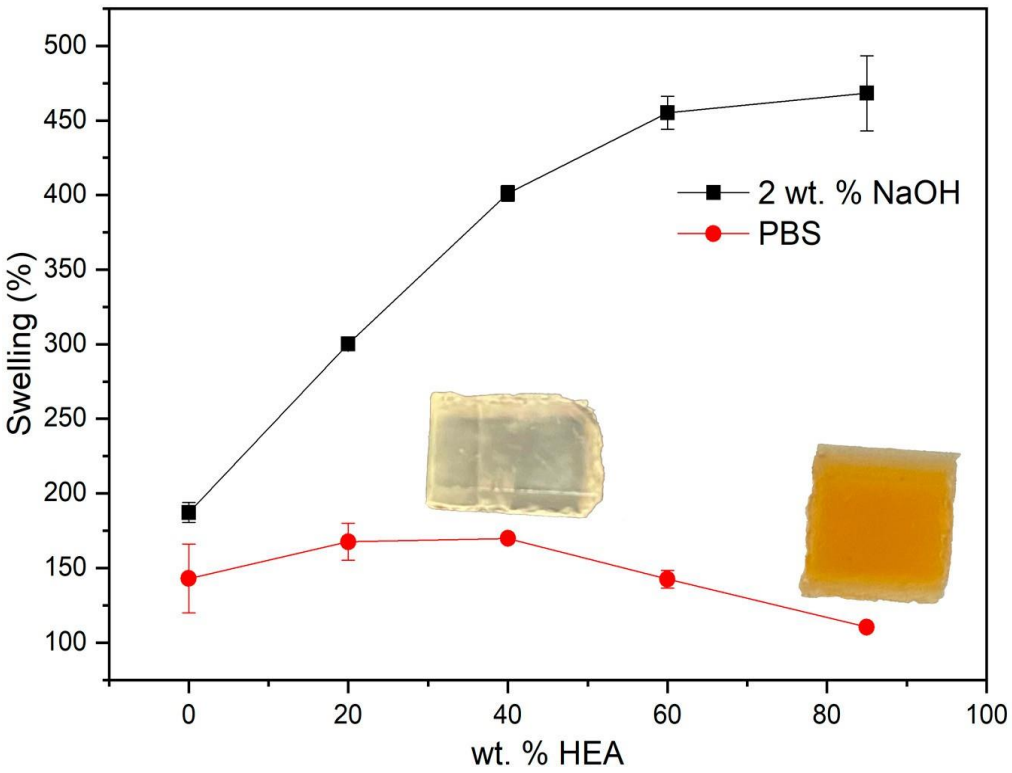

Figure 5.4. Red circles: swelling at equilibrium in PBS. Black squares: swelling after 24 h in water with 2 wt. % NaOH; in both cases, data are for samples of the HCL(jef)$_{7.5}$-HEA$_X$ series.

In a basic medium, much higher and faster swelling is observed than in PBS. In this case, an increase in the molar amount of PEGDMA in the photopolymerizable mixture (see **Table 5.1**) produces parts with lower swelling capacity. Since *β*-aminoesters are sensitive to the pH, that is, they are hydrolyzed much faster at a basic pH, the behavior of the samples represented in **Figure 5.4** is compatible with the idea that the samples in PBS correspond to the type B networks in **Figure 5.1**, that is, swollen networks that have not undergone HCL hydrolysis. On the other hand, where the samples are in basic medium, there is already HCL(jef) hydrolysis and the networks are initially between B and C (when the hydrolysis of the HCL(jef) is not complete), and finally correspond to the type C networks in **Figure 5.1**. HCL hydrolysis gives rise to networks with a lower degree of crosslinking than type B networks, and therefore, with a greater swelling capacity. These C-type networks have, in principle, a crosslinking density, after HCL(jef) hydrolysis, defined by the amount of the SCL (see **Table 5.1**). This could

explain why an increase in the molar amount of PEGDMA within the resin can produce parts with less pronounced swelling after hydrolysis.

Once the HCL(jef)$_{7.5}$-HEA$_X$ series was studied, a fixed HEA/PEGMEA weight ratio was selected (60/25, for a total wt. % of 85) and the PEGDMA/HCL(jef) weight ratio was varied (between 2/13 and 15/0) to analyze the role of the amount of HCL in the initial swelling and to determine whether the swelling of the partially hydrolyzed part can be modulated. The rationale behind the selection of the HEA/PEGMEA weight ratio of 60/25 was based on the fact that being HEA-rich systems are less fragile, this composition still contains a significant amount of hydrophilic PEGMEA macromonomer. This series has been labeled as HCL(jef)$_X$HEA$_{60}$, where X is the weight percentage of the HCL(jef). The characteristics of the samples studied in this second group are collected in **Table 5.2**. It can be seen that the molar crosslinking density (moles of PEGDMA + moles of HCL) increases with the amount of PEGDMA.

Table 5.2. Data concerning the HCL(jef)$_X$HEA$_{60}$ series, including the penetration depth (D_p) and critical exposure (E_c) calculated from the Jacobs working curves.

Label	PEGDMA/HCL(jef)/ HEA/PEGMEA wt. %	PEGDMA/HCL(jef) mol %	ν (Pa·s)	D_p (μm)	E_c (mJ·cm^{-2})
HCL(jef)$_{13}$HEA$_{60}$	2/13/60/25	0.6/2.1	0.024	221	4.69
HCL(jef)$_{10}$HEA$_{60}$	5/10/60/25	1.5/1.6	n.d.	n.d.	n.d.
HCL(jef)$_{7.5}$HEA$_{60}$	7.5/7.5/60/25	2.3/1.2	0.019	176	4.52
HCL(jef)$_5$HEA$_{60}$	10/5/60/25	3.1/0.8	n.d.	n.d.	n.d.
HCL(jef)$_2$HEA$_{60}$	13/2/60/25	4.0/0.3	n.d.	n.d.	n.d.
HCL(jef)$_0$HEA$_{60}$	15/0/60/25	4.6/0	0.012	133	5.08

ν = Viscosity for a Shear Rate of 1 s^{-1} (deviation error 0.001), n.d.: non-determined

A rheological study was carried out again on three representative samples to address the printability of the prepared resins, as quoted in **Table 5.2** (viscosity values for a shear rate of 1 s^{-1}). All of them exhibited Newtonian behavior (see **Figure 5.5**) and a slight dependence on the composition, *i.e.*, an increase in the amount of PEGDMA leads to a decrease in resin viscosity. However, the viscosities in all cases remain in the range of 0.012–0.024 Pa·s, suitable values for VPP[19,20].

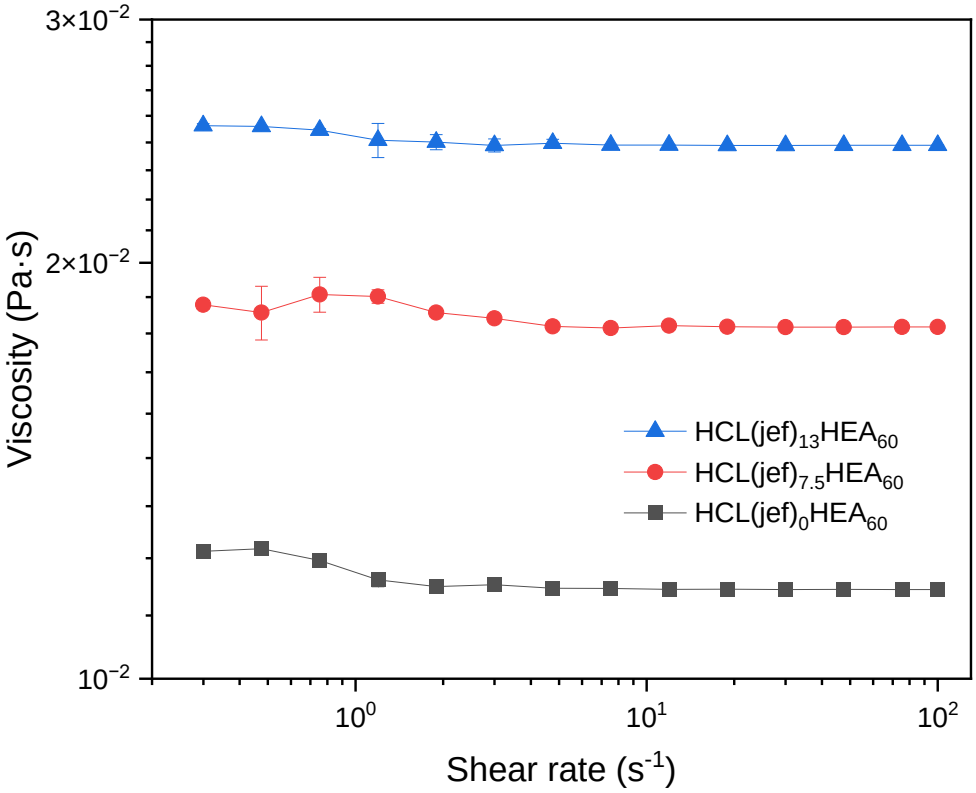

Figure 5.5. Viscosity values as a function of the shear rate for the $HCL(jef)_xHEA_{60}$ system.

From the Jacobs working curves (see **Figure 5.6**), the D_p and E_c values quoted in **Table 5.2** were obtained. These results are in good agreement with those obtained with the $HCL(jef)_{7.5}HEA_X$ system, *i.e.*, a higher nominal molar crosslinking density leads to greater curing depths. Again, a time of 20 s was found to be the most appropriate one to carry out the printing of all the pieces with common parameters.

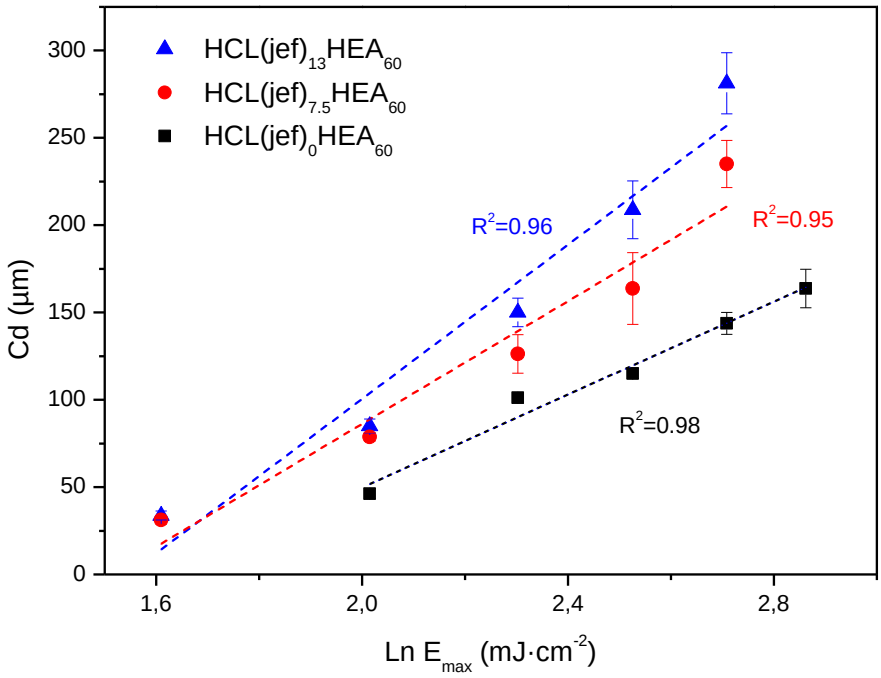

Figure 5.6. Jacobs working curves of the HCL(jef)$_X$HEA$_{60}$ series when exposed to 405 nm light (0.5 mW·cm^{-2}). Data correspond to (from right to left in each group of data) exposure times of 35, 30, 25, 20, 15, and 10 s. Linear regressions are included.

Pieces of 2.0×2.0×0.2 cm^3 could be successfully printed using the conditions described in the experimental section. Following the procedure described in this experimental section, these 3D printed pieces were immersed either in PBS or in basic water (2 wt. % of NaOH), and the swelling was determined via gravimetry as a function of the time (**Figure 5.7**). As occurred with the HCL(jef)$_{7.5}$-HEA$_X$ series, these samples were found to reach equilibrium in PBS after a few days, with moderate swelling values in the range 100–200%. After 24 h in a basic medium, the swelling was, however, much higher and appeared to depend on the amount of PEGDMA. An increase in the amount of PEGDMA within the photopolymerizable resin resulted in 3D printed parts with lower swelling capacity. Again, the overall behavior in PBS and 2 wt. % NaOH was compatible with the re-adjustable hypothesis. In PBS, the hydrogel would correspond to a type B network (see **Figure 5.1**), whereas in the basic medium, there is hydrolysis of HCL(jef), with the networks initially falling between B and C, and eventually becoming type C. The dependence on the amount of PEGDMA is consistent with this process, because the swelling of the C type network is defined by the amount

of SCL, that is, of PEGDMA. In the case of PBS, when there are B type networks, the global molar crosslinking density comprising the contribution of both stable and hydrolysable crosslinkers (SCL + HCL(jef)) increases only slightly with an increasing amount of PEGDMA, which explains the small swelling differences in PBS. The results of high swelling after treatment with an alkaline medium for networks with less PEGDMA are consistent with the literature data for similar HEA networks prepared with a very low crosslinking percentage[30].

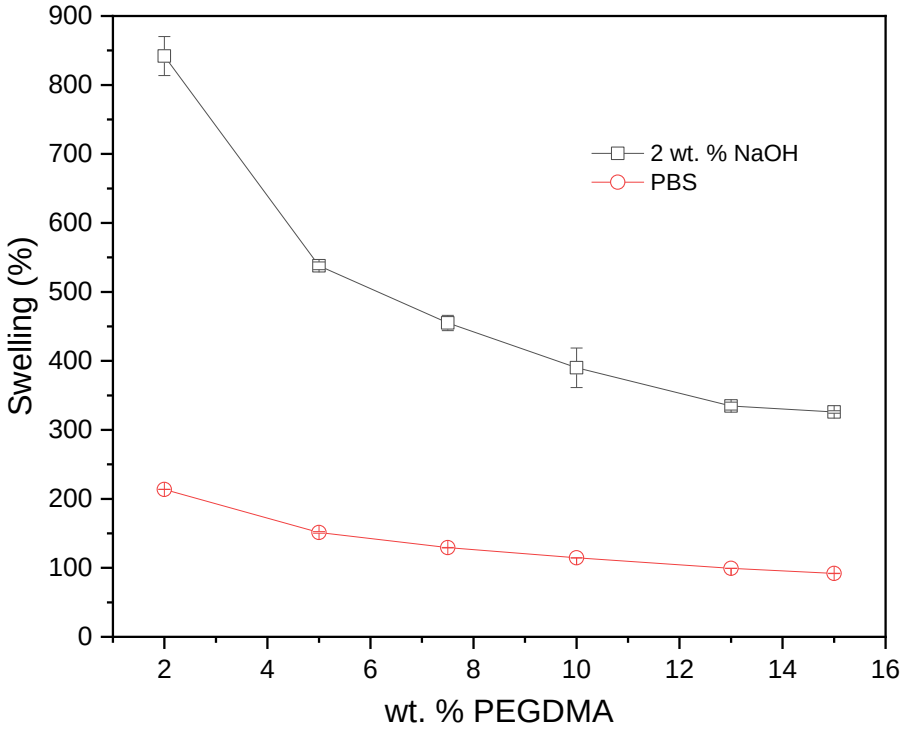

Figure 5.7. Red spheres: swelling at equilibrium in PBS. Black squares: swelling after 24 h in water with 2 wt. % NaOH; in both cases, the samples correspond to the $HCL(jef)_XHEA_{60}$ series. Error bars are contained inside the symbols, hollow points are therefore used.

While it appears that after 24 h in basic media the swelling started to stabilize, longer studies revealed an unexpected behavior. All the samples for both series described above did not reach the swelling equilibrium in 2 wt. % NaOH (see **Figure 5.8**). In most of the cases, a continuous gradual increase in swelling values was observed.

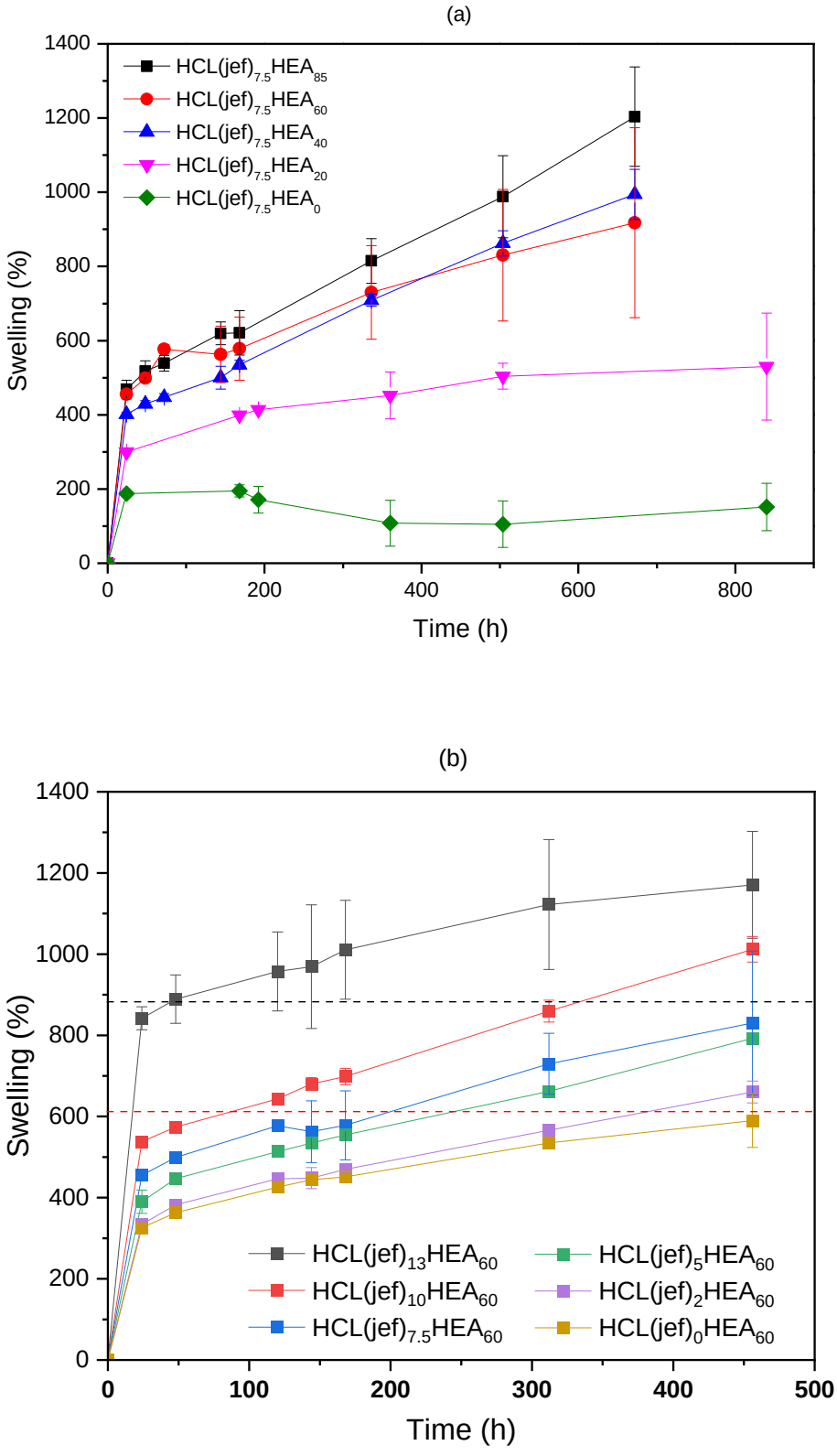

Figure 5.8. Swelling vs. time (from 1 h up to 20 days) in water with 2 wt. % NaOH for the (a) $HCL(jef)_{7.5}HEA_X$ and (b) $HCL(jef)_XHEA_{60}$ series.

Aiming to understand this behavior, reference structures were prepared from a formulation in which the HCL(jef) was replaced by twice the number of moles of the glycerol monomethacrylate, GMM (**Figure 5.9**). It is worth mentioning that GMM has the same structure as the HCL(jef) units upon hydrolysis in basic media, *i.e.*, in the C network. By using these reference models, we expected to be able to determine a reference swelling for the C structure.

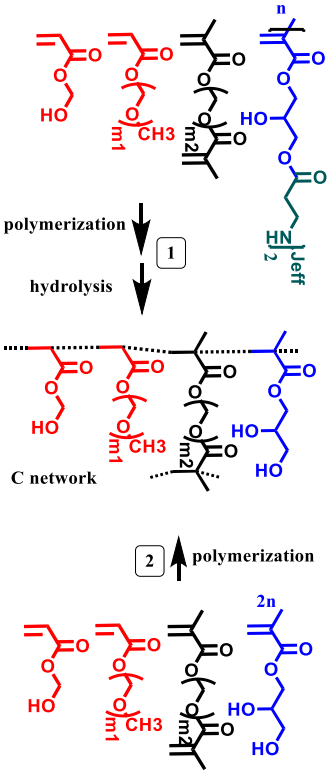

Figure 5.9. 1: Scheme of the polymerization and hydrolysis of the HCL(jef)$_X$HEA$_{60}$ or HCL(jef)$_{7.5}$HEA$_{60}$ systems. 2: Scheme of the preparation of reference structures carrying GMM. The jeff tag refers to the spacer of the Jeffamine (R of H_2N-R-NH_2).

For this purpose, reference systems of the HCL(jef)$_{13}$-HEA$_{60}$ and HCL(jef)$_{10}$-HEA$_{60}$ samples were prepared (see the experimental section for examples of the system formulation and reference formulation). These reference networks were immersed in PBS until reaching equilibrium (using gravimetry), and these swellings in the equilibrium state are plotted in **Figure 5.8b** as dashed horizontal lines. These values are the values that a type C network should reach after breaking all the HCL maintaining the wt. % of the HCL(jef)$_{13}$HEA$_{60}$ and HCL(jef)$_{10}$HEA$_{60}$ systems... It can be seen how the HCL(jef)$_{13}$-HEA$_{60}$ and HCL(jef)$_{10}$-HEA$_{60}$ networks reach these reference data after about 50–100 h, although after that they continue to increase continuously.

The behavior at short times (up to 50 h) is in good agreement with the breakage of the majority of the HCL(jef) links occurring within the first 24 h. However, the fact that equilibrium is not reached must be explained by some other concomitant degradation process. In this sense, a NaOH solution may be aggressive enough to also break the acrylic side chain esters, even though they are not *β*-activated due to the presence of amines. There are also literature data evidencing that certain acrylates similar to those used in this work can be hydrolyzed in alkaline media[31]. To confirm if this process occurs in the proposed systems, a linear homopolymer of poly-HEA was synthesized, dissolved in D_2O with a 2 wt. % NaOH, and monitored via ^1H NMR. This analysis showed changes in the spectra that are compatible with the breakdown of the acrylates (see **Figure 5.10a and 5.10b**). The broad peaks corresponding to the chain protons of polyHEA (*CH_2-CH*), initially centered at 2.4, 1.75, and 1.6 ppm, change shape and shift to broader peaks centered at 2.0 and 1.4 ppm, which is coincident with the chain displacements of polymethacrylic acid[32]. In addition, the signals of the side chain (*O-CH_2-CH_2-O* in HEA) also undergo changes compatible with hydrolysis, detecting the peaks corresponding to ethylene glycol at 3.5 ppm. Residual HEA peaks are observed centered at 4.2 and 4.0 ppms.

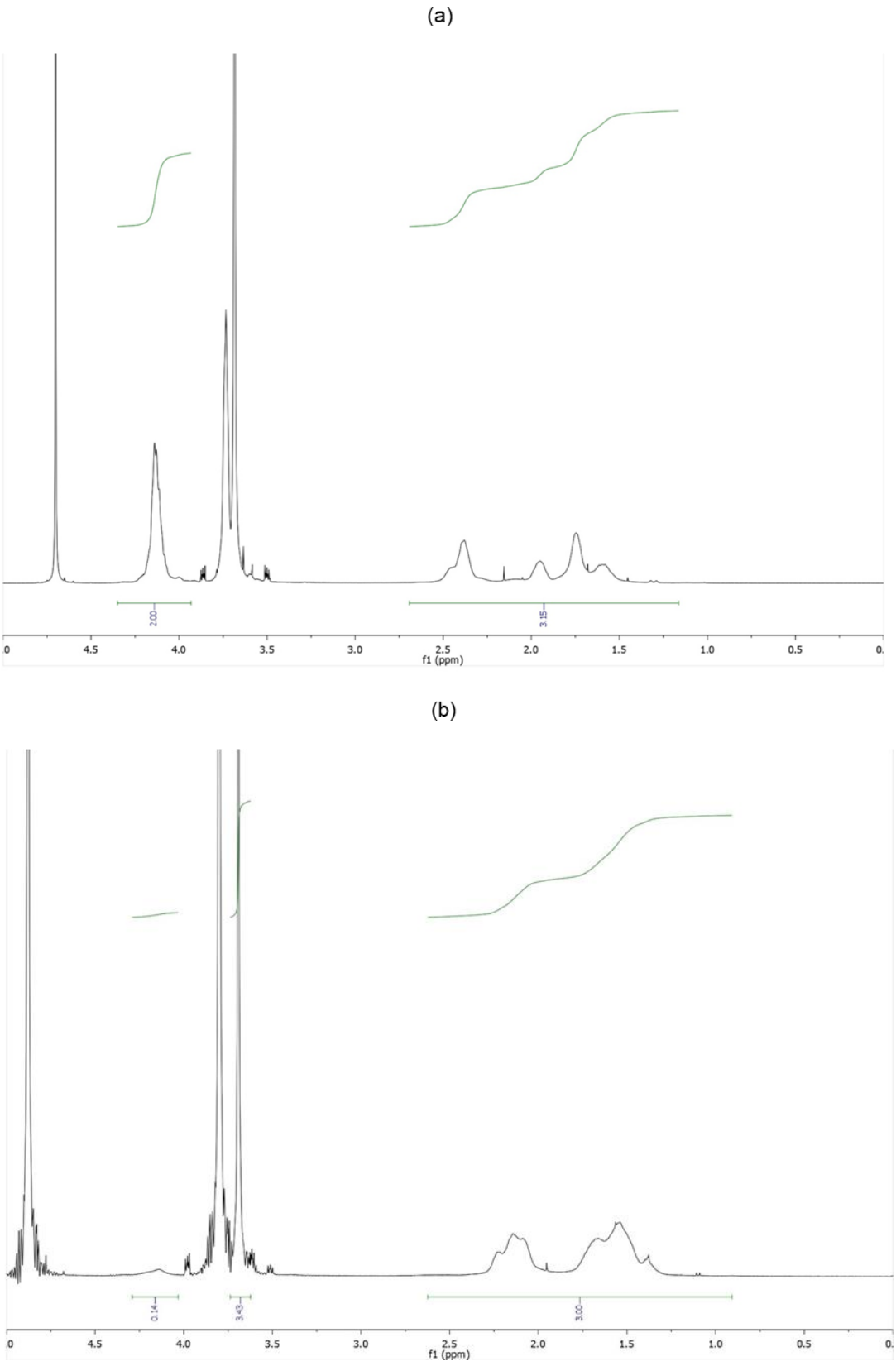

Figure 5.10. a) ^{1}H NMR spectra of polyHEA in D_2O with 2 wt. % of NaOH at time 0. b) at time 24 h.

As the objective of this work was to demonstrate that it is possible to control the transition from a type B network to a type C network, the hydrolytic process of the HCL structures was addressed using less aggressive conditions that selectively allowed for the hydrolysis of the HCL. Specifically, a pH 10 buffer medium was employed, and the swelling variation was monitored both at room temperature (RT, 20 °C) and at 60 °C to address if the temperature could play a role in the hydrolysis. For this study, the HCL(jef)$_{13}$-HEA$_{60}$ sample has been chosen because it is the sample with the greatest readjustment capacity (remember that this formulation contains the largest amount of HCL(jef), 13 wt. %). **Figure 5.11** shows the variation in swelling of this system when submerged in pH 10 buffer at RT and at 60 °C, as well as in intermediate situations where the samples were first heated at 60 °C during either 17 h or 25 h and then transferred to PBS at RT. The graph includes the data corresponding to the swelling change in an alkaline medium (2 wt. % NaOH) and in PBS as a function of the time. At pH 10 and 60 °C, a rapid increase in weight was observed until reaching a limit value close to 700% after about 70 h. The fact that an equilibrium limit value is reached, and that this value is slightly less than the swelling of the reference structure (dashed line), confirms that the pH 10 buffered medium is capable of hydrolyzing HCL(jef) but not the rest of the acrylic esters. At RT, the swelling change is much slower, which means that the rate of hydrolysis of the HCL *β*-aminoesters in the pH 10 buffer can be controlled by the temperature.

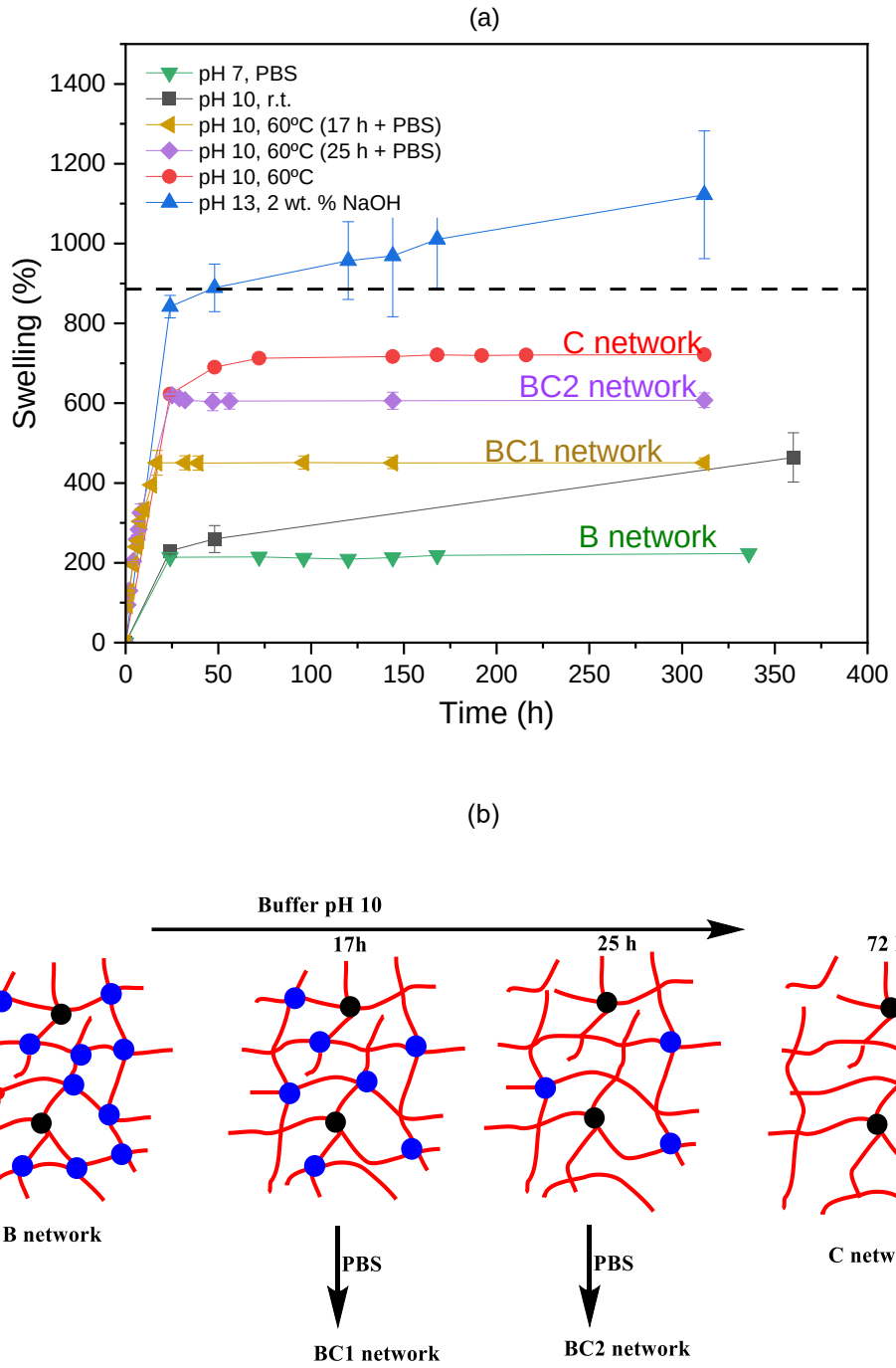

Figure 5.11. (a) Swelling of HCL(jef)$_{13}$-HEA$_{60}$ in different media or temperatures. (b) Scheme of the hydrolytic process from a B to a C network. The blue and black knots represent, respectively, the knots corresponding to HCL and PEGDMA.

Figure 5.11 shows that in PBS the equilibrium swelling value is reached after about 24 h and remains constant for weeks. This would be the swelling of the type B network. Networks with structures and swellings between network B and network C can be obtained via immersion in pH 10 for a selected time to allow

partial hydrolysis of the *β*-aminoesters, followed by the stabilization of the structure via immersion in PBS, as shown in the diagram of **Figure 5.11b**. This strategy was carried out via immersion in pH 10 for 17 and 25 h, followed by stabilization in PBS. These curves are represented in **Figure 5.11a** and show that it is possible to modulate the swelling between the two networks, B and C.

5.2.3. Proof of concept of the methodology: Preparation of 3D printed hydrogels with tunable swelling and complex structures

Once the re-adjustable behavior was thoroughly analyzed with square-shaped model parts, the dimensional readjustment in more complex pieces was addressed. Using the HCL(jef)$_{13}$-HEA$_{60}$ formulation, spheres (SP) and tubes (Tu) with the dimensions indicated in **Table 5.3** were prepared. In addition, a seahorse figure was printed to show this behavior in a piece with a more complex shape. The bottom image in **Table 5.3** shows the freshly printed seahorse and when it was swollen after immersion in PBS for 72 h. It can be observed that the initial proportions are fully maintained, which indicates that the swelling was isotropic.

Table 5.3. Data concerning spheres, tubes, and a seahorse printed from the formulation HCL(jef)$_{13}$-HEA$_{60}$.

<table>
<tr><td rowspan="8">Spheres</td><td colspan="2">Fresh printed parts, diameter (cm)</td></tr>
<tr><td>SP1: 0.50</td><td>SP2: 0.75</td></tr>
<tr><td> 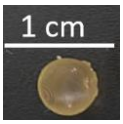
</td><td> 
</td></tr>
<tr><td colspan="2">PBS (after 48 h), swelling</td></tr>
<tr><td>SP1
140 ± 1</td><td>SP2
142 ± 2</td></tr>
<tr><td> 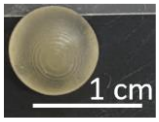
</td><td> 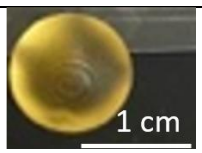
</td></tr>
<tr><td colspan="2">pH 10, 60 °C (after 372 h), swelling</td></tr>
<tr><td>SP1
853 ± 10</td><td>SP2
820 ± 73</td></tr>
</table>

<table>
<tr><td></td><td> 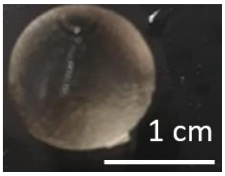
</td><td colspan="2"> 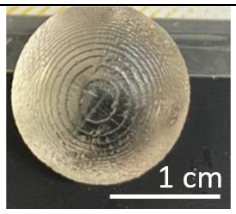
</td></tr>
<tr><td rowspan="6">Tubes</td><td colspan="3">Fresh printed parts: diameter, wall thickness, length (mm)</td></tr>
<tr><td>Tu1: 10, 0.5, 10</td><td>Tu2: 15, 0.75, 15</td><td>T3u: 20, 1, 20</td></tr>
<tr><td> 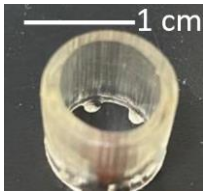
</td><td> 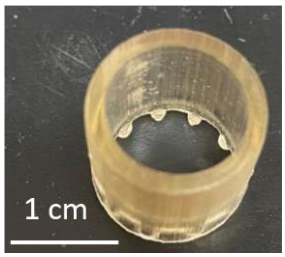
</td><td> 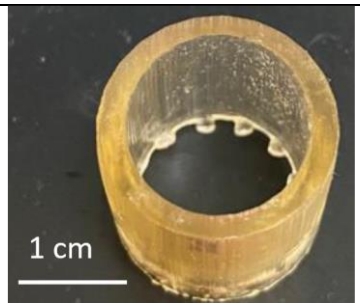
</td></tr>
<tr><td colspan="3">pH 10, 60 °C (after 144 h); swelling</td></tr>
<tr><td>Tu1
763 ± 9
 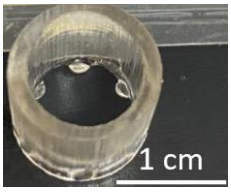
</td><td>Tu2
713 ± 15
 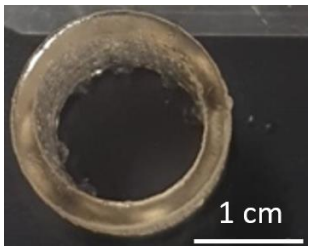
</td><td>Tu3
748 ± 48
 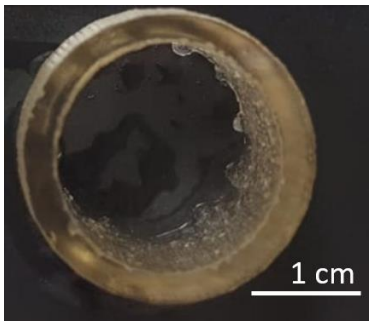
</td></tr>
<tr><td>Seahorse</td><td colspan="3"> 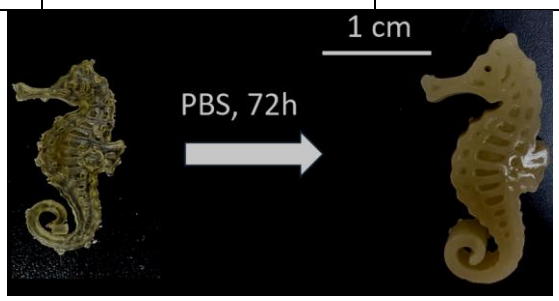
</td></tr>
</table>

Spheres SP1 and SP2 reached equilibrium swelling values after being immersed in PBS for 48 h, with values close to 150. In a basic medium, *i.e.*, pH 10 buffer, they showed a continuous increase in swelling up to approximately 300 h, with the kinetics of the larger sphere being slower than those of the smaller sphere (see **Figure 5.12a**). The tubes displayed a similar behavior (**Figure 5.12b**). It must be taken into account that these pieces, especially the spheres, have larger

dimensions than the pieces studied in **Figure 5.11**, which reached equilibrium within less than 100 h.

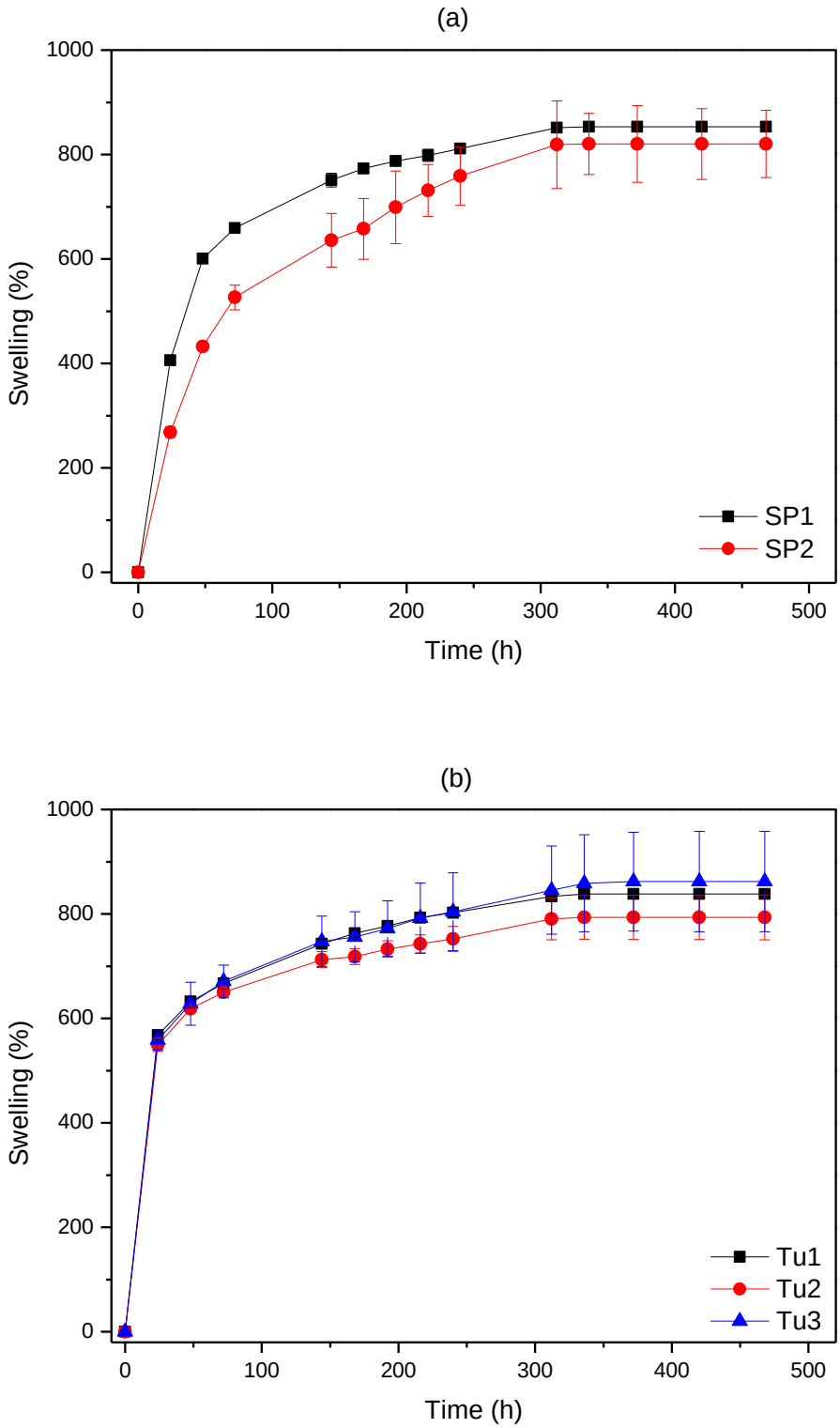

Figure 5.12. Swelling vs. time (from 1 h up to 20 days) of the spheres (a) and tubes (b) in pH 10 buffer at 60 °C.

In any case, the printed parts in **Table 5.3** show the same re-adjustability as previously described for the larger parts. In the case of the spheres, this capacity may be of interest in applications such as hydroponics and aquaponics crops [13], or in regenerative medicine to fill cavities[12], among others.

5.3. Conclusions

In this work, it has been shown that the strategy of using a mixture of stable and hydrolysable crosslinkers allows for printing pieces by VPP with different sizes and shapes, and with initial high crosslinking (PEGDMA and HCL(jef) knots) and then for transforming them into hydrogels via treatment in pH 10 buffer (with only remaining HCL(jef) knots). The swelling in water of the printed part ranges from the initial swelling (PEGDMA + HCL(jef) knots) to the swelling for total hydrolysis (only remaining PEGDMA knots are present). The intermediate swellings between these two states can be precisely controlled by adjusting the immersion time and temperature in pH 10 buffer. These target swellings have been stabilized by immersing the pieces in PBS at RT.

References

1. Nechausov, S. *et al.* Effects of ionic liquids and dual curing on vat photopolymerization process and properties of 3d-printed ionogels. *Addit Manuf* **56**, 102895 (2022).
2. Borrello, J., Nasser, P., Iatridis, J. C. & Costa, K. D. 3D printing a mechanically-tunable acrylate resin on a commercial DLP-SLA printer. *Addit Manuf* **23**, 374–380 (2018).
3. Ho, T.-C. *et al.* Hydrogels: Properties and Applications in Biomedicine. *Molecules* **27**, 2902 (2022).
4. Park, Y., Huh, K. & Kang, S.-W. Applications of Biomaterials in 3D Cell Culture and Contributions of 3D Cell Culture to Drug Development and Basic Biomedical Research. *Int J Mol Sci* **22**, 2491 (2021).
5. Jose, G., Shalumon, K. & Chen, J.-P. Natural Polymers Based Hydrogels for Cell Culture Applications. *Curr Med Chem* **27**, 2734–2776 (2020).
6. Mao, Z., Shimamoto, G. & Maeda, S. Conical frustum gel driven by the Marangoni effect for a motor without a stator. *Colloids Surf A Physicochem Eng Asp* **608**, 125561 (2021).

7. Sánchez-Correa, F., Vidaurre-Agut, C., Serrano-Aroca, Á. & Campillo-Fernández, A. J. Poly(2-hydroxyethyl acrylate) hydrogels reinforced with graphene oxide: Remarkable improvement of water diffusion and mechanical properties. *J Appl Polym Sci* **135**, 46158 (2018).
8. Wu, H., Chen, P., Yan, C., Cai, C. & Shi, Y. Four-dimensional printing of a novel acrylate-based shape memory polymer using digital light processing. *Mater Des* **171**, 107704 (2019).
9. Ni, R., Qian, B., Liu, C., Liu, X. & Qiu, J. A cross-linking strategy with moderated pre-polymerization of resin for stereolithography. *RSC Adv* **8**, 29583–29588 (2018).
10. Tai, H. *et al.* Thermoresponsive and Photocrosslinkable PEGMEMA-PPGMA-EGDMA Copolymers from a One-Step ATRP Synthesis. *Biomacromolecules* **10**, 822–828 (2009).
11. Sujan, M. I. *et al.* Bi-functional silica nanoparticles for simultaneous enhancement of mechanical strength and swelling capacity of hydrogels. *RSC Adv* **10**, 6213–6222 (2020).
12. Hong, L. T. A. *et al.* An injectable hydrogel enhances tissue repair after spinal cord injury by promoting extracellular matrix remodeling. *Nat Commun* **8**, 533 (2017).
13. Kalossaka, L. M., Sena, G., Barter, L. M. C. & Myant, C. Review: 3D printing hydrogels for the fabrication of soilless cultivation substrates. *Appl Mater Today* **24**, 101088 (2021).
14. Mitura, S., Sionkowska, A. & Jaiswal, A. Biopolymers for hydrogels in cosmetics: review. *J Mater Sci Mater Med* **31**, 50 (2020).
15. Peppas, N. A., Bures, P., Leobandung, W. & Ichikawa, H. Hydrogels in pharmaceutical formulations. *European Journal of Pharmaceutics and Biopharmaceutics* **50**, 27–46 (2000).
16. Ehrenhofer, A., Elstner, M. & Wallmersperger, T. Normalization of hydrogel swelling behavior for sensoric and actuatoric applications. *Sens Actuators B Chem* **255**, 1343–1353 (2018).
17. Liu, Y., Zhang, H., Zhang, J. & Zheng, Y. Constitutive modeling for polymer hydrogels: A new perspective and applications to anisotropic hydrogels in free swelling. *European Journal of Mechanics - A/Solids* **54**, 171–186 (2015).

18. Liz-Basteiro, P. *et al.* High resolution molds, sacrificial in aqueous media, obtained by vat photopolymerization 3D printing. *Addit Manuf* **75**, 103758 (2023).
19. Li, J. *et al.* Synthesis and properties of a low-viscosity UV-curable oligomer for three-dimensional printing. *Polymer Bulletin* **73**, 571–585 (2016).
20. Tu, J., Makarian, K., Alvarez, N. J. & Palmese, G. R. Formulation of a Model Resin System for Benchmarking Processing-Property Relationships in High-Performance Photo 3D Printing Applications. *Materials* **13**, (2020).
21. Li, Y. *et al.* Theoretical prediction and experimental validation of the digital light processing (DLP) working curve for photocurable materials. *Addit Manuf* **37**, 101716 (2021).
22. Arias-Ferreiro, G. *et al.* Printability Study of a Conductive Polyaniline/Acrylic Formulation for 3D Printing. *Polymers (Basel)* **13**, (2021).
23. Arias-Ferreiro, G., Ares-Pernas, A., Dopico-García, M. S., Lasagabáster-Latorre, A. & Abad, M.-J. Photocured conductive PANI/acrylate composites for digital light processing. Influence of HDODA crosslinker in rheological and physicochemical properties. *Eur Polym J* **136**, 109887 (2020).
24. Lee, J., Prud'homme, R. & Aksay, I. Cure depth in photopolymerization: Experiments and theory. *Journal of Materials Research - J MATER RES* **16**, 3536–3544 (2001).
25. Kowsari, K. *et al.* Photopolymer formulation to minimize feature size, surface roughness, and stair-stepping in digital light processing-based three-dimensional printing. *Addit Manuf* **24**, 627–638 (2018).
26. Garcia, C. *et al.* Smart pH-Responsive Antimicrobial Hydrogel Scaffolds Prepared by Additive Manufacturing. *ACS Appl Bio Mater* **1**, 1337–1347 (2018).
27. Zhang, Y. *et al.* High-water-content and resilient PEG-containing hydrogels with low fibrotic response. *Acta Biomater* **53**, 100–108 (2017).
28. Monleón Pradas, M. *et al.* Porous poly(2-hydroxyethyl acrylate) hydrogels. *Polymer (Guildf)* **42**, 4667–4674 (2001).
29. Preobrazhenskiy, I. I. & Putlyaev, V. I. The ability to control swelling and degradation processes of hydrogels based on a mixture of

PEGMA/PEGDA monomers. *Mendeleev Communications* **33**, 83–85 (2023).

30. Nuvoli, D. *et al.* Synthesis and characterization of poly(2-hydroxyethylacrylate)/β-cyclodextrin hydrogels obtained by frontal polymerization. *Carbohydr Polym* **150**, 166–171 (2016).
31. Talu, M. & Özgün, H. B. Alkaline hydrolysis of poly(ethyl acrylate) and styrene-ethyl acrylate copolymer. *Eur Polym J* **26**, 5–7 (1990).
32. García, D. M. *et al.* Synthesis and characterization of poly(methacrylic acid) hydrogels for metoclopramide delivery. *Eur Polym J* **40**, 1637–1643 (2004).

Part of this work has been published at Pedro Liz-Basteiro, Felipe Reviriego, Enrique Martínez-Campos, Helmut Reinecke, Carlos Elvira, Juan Rodríguez-Hernández, Alberto Gallardo, Vat Photopolymerization 3D Printing of Hydrogels with Re-Adjustable Swelling. Gels 2023, 9, 600. https://doi.org/10.3390/gels

Chapter 6. Vat photopolymerization 3D printing of VCL-based thermosensitive hydrogels for cell harvesting

For reasons of confidentiality, chapter 6 (pages 163 to 205) has been omitted.

Chapter 7. Thermosensitive hydrogels based on Poly(VCL-co-VP) loaded with carbon nanotubes for tissue engineering

7.1. Introduction

Carbon nanotubes (CNTs) are among the most extensively studied nanomaterials, renowned for their excellent electrical conductivity and appropriate mechanical properties[1]. Liquid dispersions of CNTs are emerging functional advanced materials[2] that are seen as promising candidates for applications such as biocompatible transport, drug delivery, optical limiting, optical sensors, etc[3–5]. In addition, research has shown that the modification of materials such as hydrogels with CNTs can significantly enhance their specific biofunctions[6], making them highly attractive for applications in tissue engineering. In this work, we specifically address the CNTs loading of thermosensitive hydrogels based on the vinyl-lactam VCL. As previously described, these hydrogels with a VPTT close to 34 ºC, have shown their capacity to serve as cell culture supports at 37 ºC, and to allow a non-aggressive cell detachment, even of whole monolayers, by simple temperature decrease[7–10]. CNTs loading of a hydrogel with these performances may be of interest to improve properties such as mechanical or electrical and ultimately influence cell response.

The loading of hydrogels, hydrophilic networks swollen in water, with CNTs, remains a significant challenge because CNTs exhibit poor dispersibility in aqueous medium and poor compatibility with hydrophilic structures (or highly hydrophilic when ionic hydrogels). Nevertheless, CNTs nanocomposite hydrogels have demonstrated remarkable improvements in mechanical properties and toughness[11], electrical conductivity[12], thermal stability[13], and rapid sensor response[14] compared to conventional hydrogels. Indeed, the applications of CNTs nanocomposite hydrogels span various fields of human endeavor[15].

Polymeric chains thermosensitive in aqueous media, such as those derived from VCL, are neutral and base their thermosensitivity on an appropriate amphiphilicity. Importantly, amphiphilic polymers have been found to be high dispersing agents of CNTs[16–18]. Therefore, in this chapter we hypothesize that

CNTs can be loaded on thermosensitive hydrogels through 1- dispersion of CNTs in the VCL-based amphiphilic formulation, and 2- mass polymerization. Since VCL is solid at room temperature, it is proposed in this work the use of another vinyl lactam, VP, structurally related to VCL, as a comonomer/dispersing agent. In the context of CNT dispersion, it is well known that polyVP, in addition to being highly cytocompatible[19], is an excellent non-ionic polymeric surfactant[20]. It is –although amphiphilic– slightly more hydrophilic than VCL. The use of VP therefore allows a simplified, solvent-free dispersion design, using only the polymerizable components (hydrogel chain units after polymerization), and avoiding water and/or solvents that can have a negative effect on the dispersion.

The hydrogel will therefore consist of crosslinked poly(VCL-co-VP) chains, which have been studied in the previous chapter (section 6.2.2). From this previous study, and as it will be explained later, $VCL_{85}VP_{15}$[65/35] and $VCL_{70}VP_{30}$[65/35] have been selected to disperse the CNTs and prepare the nanocomposites. However, from now on they will be labelled as $VCL_{85}VP_{15}$ and $VCL_{70}VP_{30}$ respectively, due to the complexity of the complete labels of this chapter. An optimized loaded system was evaluated using adherent endothelial and neural cell lines in order to analyse biological processes such as adhesion, proliferation, and transplant ability[21]. In addition, the conductivity properties of the hydrogel can improve cell-to-cell and cell-to-scaffold communication, and, coupled with electrical stimulation, may enable the transmission of electrical signals to electroactive tissue such as the central nervous system[22,23]. Finally, a proof-of-concept -based on the results of the previous chapter- has been developed by 3D printing by vat photopolymerization of the hydrogels loaded with CNTs.

7.2. Results and discussion

7.2.1. Dispersion and loading with CNTs

As mentioned in the introduction, the hydrogel loading procedure is based on an initial dispersion of CNTs in the VCL/VP precursor mixture (without solvent). As expected, pristine CNTs did not display an acceptable dispersibility[24–26]. Therefore, initial efforts focused on the CNT functionalization to improve their dispersibility. To this end, CNTs were treated with 4-vinylaniline and nitrite to perform the popular Tour reaction (**Figure 7.1**)[24,27–30].

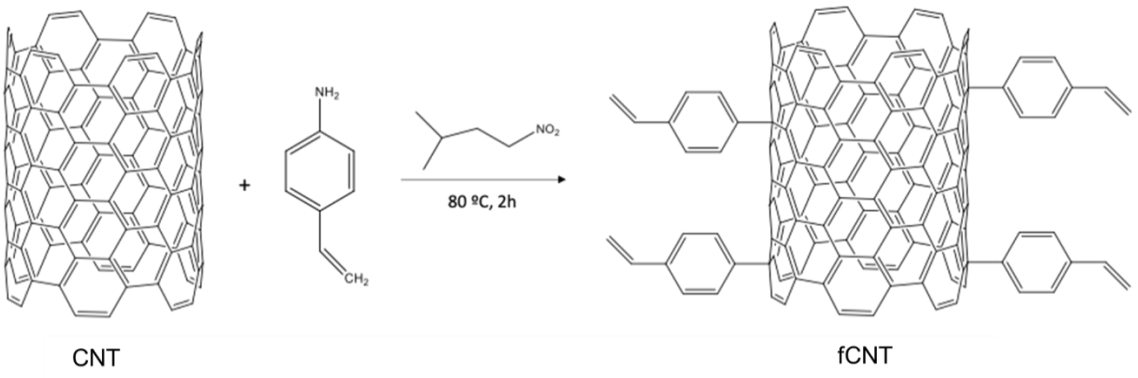

Figure 7.1. Tour reaction on CNTs with 4-vinylaniline and isoamyl nitrite.

7.2.1.1. CNT functionalization

Based on previous works[24], initial harsh conditions listed in entry 1 of **Table 7.1** were tested (as indicated in the experimental section). TGA was used to determine the functionalization degree (as wt. %); this calculation is based on the weight loss of treated CNTs at 600°C compared to pristine CNTs at the same temperature[31]. These conditions resulted in a functionalization level nearing 15 wt. % (see **Figure 7.2a**), which is relatively high (it has been labeled as HF-CNT, with HF indicating high functionalization) and it can be related to a consistent number of defects in the CNT structure, thus negatively affecting their electronic properties[32]. Therefore, the milder conditions of entries 2 and 3 were selected, which resulted respectively in wt. % functionalization corresponding to 11.6 and 4.2 wt. %, respectively. These samples have been correspondingly labeled as MF-CNT (medium functionalization) and LF-CNT (low functionalization). Therefore, the functionalization degree can be modulated by varying the reagent concentrations and the reaction time. A complete description of the three procedures can be found in the Experimental Section.

Table 7.1. Functionalization reaction conditions and characterization by Raman spectroscopy and TGA. Representative TEM images are shown at the top.

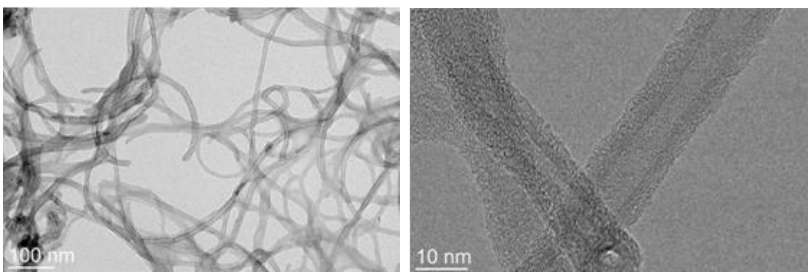

a)

Label	VA/IAN/CNTs (μL/μL/mg) [b)]	Reaction Time (h)	CNT functionalization (wt. %)	CNT functionalization (styrenic moiety mmol/g CNT)	(I_D/I_G)[c)] Raman
1. HF-CNT	180/300/15	2.0	14.2 ± 1.1	1.4 ± 0.1	1.10
2. MF-CNT	110/250/15	1.5	11.6 ± 0.6	1.1 ± 0.1	1.13
3. LF-CNT	44/200/15	1.0	4.2 ± 0.2	0.4 ± 0.0	1.37
pristine CNT	n.d.	n.d.	0	0	1.52

a) TEM images of the HF-CNT after dispersion in DMF and drying (scales 100 and 10 nm)

b) VA = 4-vinylaniline: IAN = isoamyl nitrite;

c) Ratio of Raman intensities of the D and G bands of CNTs (I_D/I_G) from Raman spectra.

Pristine, HF-CNT, MF-CNT, and LF-CNT samples have also been characterized by Raman spectroscopy, as shown in **Figure 7.2b**. The characteristic peaks corresponding to the G and D bands appear at 1590 cm^{-1} and 1350 cm^{-1} respectively[33–35]. The D band is related to the sp^3 states of carbon, and it is used as an indication of the level of disruption of the aromatic *p*-electrons system on the nanotube sidewalls[36]. The ratio of the intensities of the Raman signals associated with disordered and ordered transitions (I_D/I_G) gives valuable information regarding the effectiveness of the functionalization. The I_D/I_G value varies from 1.52 for pristine CNTs to 1.37 in functionalized LF-CNT, 1.13 in MF-CNT, and 1.10 in HF-CNT. The observed trend is the result of the introduction into the CNTs of styrenic moieties, which are composed solely of sp^2 carbon atoms that are characterized by an intense Raman signal at ~1585 cm^{-1}, thus overlapping with the D band. As the functionalization level increases, the styrenic aromatic signal at 1180 cm^{-1} becomes visible in MF-CNTs and HF-CNTs[37].

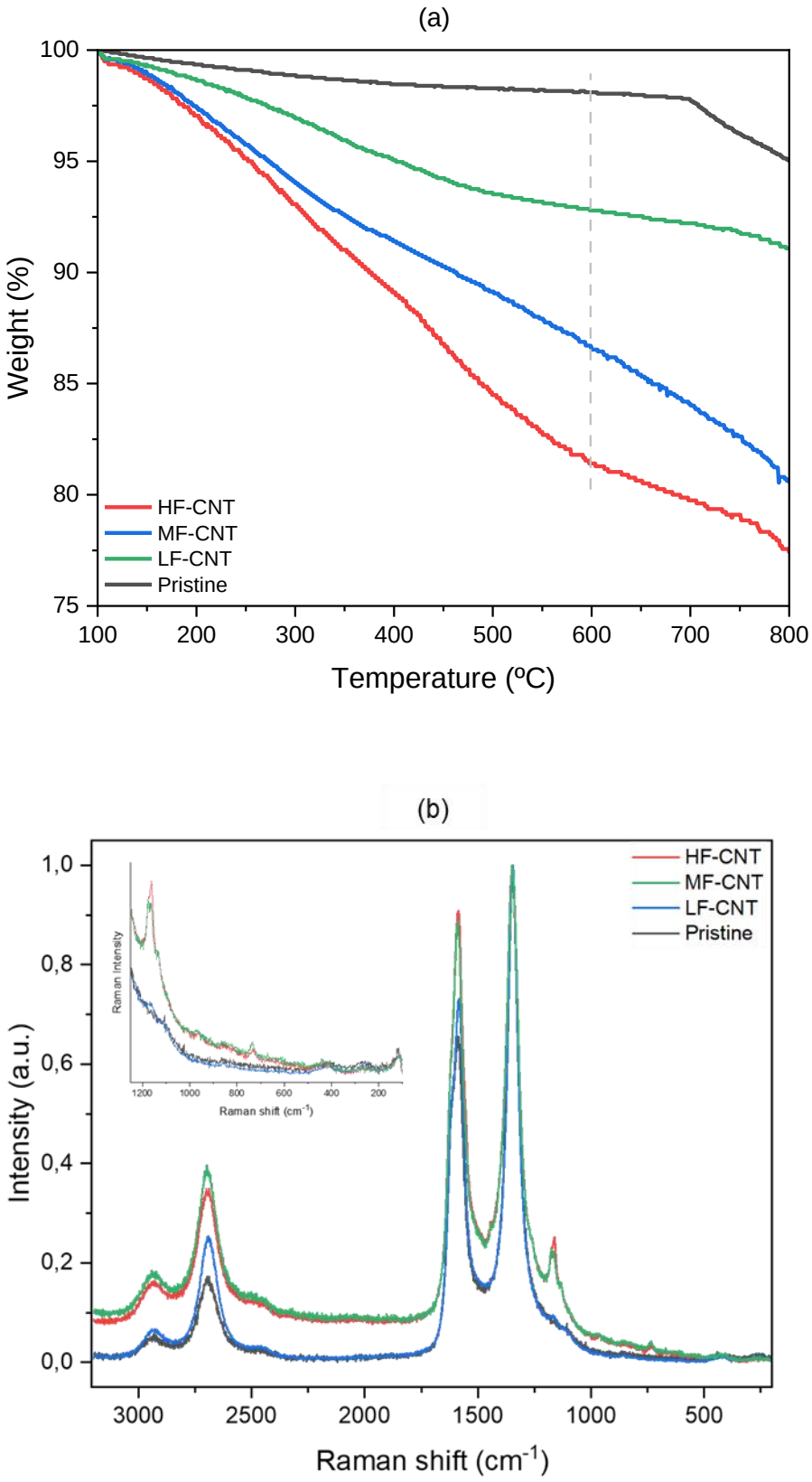

Figure 7.2. (a) Thermograms of the CNTs: pristine, LF-CNT, MF-CNT and HF-CNT. The dashed line marks the temperature of 600 ºC that was used to calculate the

functionalized level. (b) Raman spectra (532 nm excitation) of pristine CNTs and CNTs with different degrees of functionalization (i.e., LF-CNT, MF-CNT, and HF-CNT).

7.2.1.2. CNT dispersion and photocuring

Based on the previous study in section 6.2.2.1 of Chapter 6, pc-$VCL_{85}VP_{15}$ and pc-$VCL_{70}VP_{30}$, from now on $VCL_{85}VP_{15}$ and $VCL_{70}VP_{30}$ due to photocuring technology is used through this chapter and being this label shorter and simpler, have been selected as candidates for CNTs dispersion and preparation of loaded hydrogels after photocuring as for these systems rich in VCL the VPTT will be kept as close to 37°C. Some of the CNTs functionalized according to the previous section dispersed much better than the pristine CNTs in the $VCL_{85}VP_{15}$ and $VCL_{70}VP_{30}$ photocurable formulations. It is worth noting that CNTs dispersed faster in the $VCL_{70}VP_{30}$ mixture than in the $VCL_{85}VP_{15}$, so the former was the one selected for the rest of the study. This is probably due to the higher content of VP, a known surfactant unit. Therefore, we aimed to obtain $VCL_{70}VP_{30}$ loaded with functionalized CNTs.

Table 7.2 provides the general picture of the dispersibility of functionalized CNTs (*i.e.*, HF-CNT, MF-CNT, and LF-CNT) in $VCL_{70}VP_{30}$ formulation. In particular, four weight percentages were assessed, *i.e.*, 0.01, 0.1, 0.3, and 0.5 wt. %. As expected, the CNTs with the higher functionalization level (*i.e.* HF-CNT) were those that could be dispersed at CNTs wt. % till 0.3 wt. %. Nevertheless, at the lowest loading of 0.01 wt. %, also the other CNT samples (*i.e.*, LF-CNT and MF-CNT) could be dispersed.

Table 7.2. The dispersibility of the different CNTs at several wt. % is shown.

wt. % CNTs in VCL/VP	**Pristine**	**LF-CNT**	**MF-CNT**	**HF-CNT**
	Dispersibility in $VCL_{70}VP_{30}$ mixture*			
0.01	LOW	HIGH	HIGH	HIGH
0.1	LOW	MEDIUM	MEDIUM	HIGH
0.3	LOW	LOW	LOW	HIGH
0.5	LOW	LOW	LOW	LOW

* It is considered a LOW dispersion when the photocurable formulation was not a homogeneous liquid dispersion. A dispersion was considered MEDIUM when it could be photocured but the resulting hydrogel was macroscopically heterogeneous

(agglomerates were perceived even to the touch; an image is shown in Supplementary Information). A HIGH dispersion was when a macroscopically homogeneous hydrogel could be obtained after light curing.

Pristine CNTs did not disperse at any of the concentrations tested, which is not surprising considering their infamous tendency to aggregate without functionalization. Based on these results, HF-CNT were chosen for the preparation of hydrogels $VCL_{70}VP_{30}$ with different CNT content, even though a higher number of defects in the CNTs structure is to be expected with high functionalization level[38].

Hydrogels listed in **Table 7.3** were prepared by photocuring a formulation containing $VCL_{70}VP_{30}$, as described in the Experimental Section. Samples with HF-CNT content of 0.01, 0.1, and 0.3 wt. %, as well as a control without CNTs were prepared, labelled as $VCL_{70}VP_{30}CNT_X$ being X the weight percentage of CNTs per hundred of vinyl-lactam (VCL+VP=100). The different hydrogels were characterized in terms of transparency, mechanical properties, conductivity at RT; and swelling at different temperatures (to evaluate also thermosensitivity).

Table 7.3. Swelling at representative temperatures, VPTT, absorbance, mechanical properties, and conductivity values of the different loaded hydrogels. Representative images of the hydrogels are shown at the top.

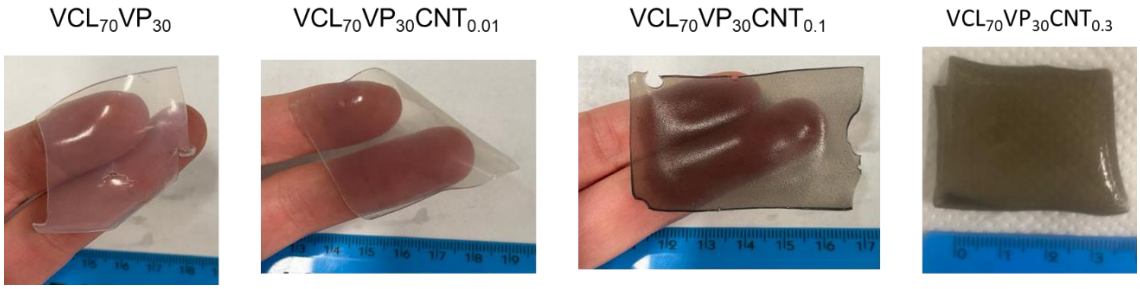

Label	Swelling % at (ºC)			VPTT (ºC)	Abs	Load (N)	ε (%)	E (MPa)	σ (S·m^{-1})
	10	37	60						
$VCL_{70}VP_{30}$	1588 ± 32	463 ± 25	140 ± 3	46	0.3 ± 0.1	12 ± 1	82 ± 2	0.6 ± 0.2	(8.6 ± 1.3)·10^{-3}
$VCL_{70}VP_{30}CNT_{0.01}$	1235 ± 71	338 ± 24	118 ± 22	43	0.2 ± 0.0	13 ± 2	72 ± 2	1.7 ± 0.4	(1.5 ± 0.3)·10^{-2}
$VCL_{70}VP_{30}CNT_{0.1}$	1199 ± 11	300 ± 26	87 ± 17	42	0.6 ± 0.0	13 ± 1	68 ± 1	2.9 ± 0.7	(2.5 ± 0.2)·10^{-2}
$VCL_{70}VP_{30}CNT_{0.3}$	1072 ± 124	291 ± 48	79 ± 17	42	1.2 ± 0.1	19 ± 2	60 ± 2	3.7 ± 0.5	(8.1 ± 1.5)·10^{-2}

*Abs = Absorbance; E = Elastic Modulus; Load = Maximum Load; ε = Elongation; σ = Electrical conductivity

Figure 7.3a shows the swelling variations of the 4 hydrogels listed in **Table 7.3** as a function of the entire temperature range. The higher the CNTs loading, the lower the swelling, especially at low temperatures, below the VPTT. This behavior can be explained by the hydrophobic contribution of the CNTs. This small hydrophobic contribution also explains the slight decrease of VPTT in the loaded systems. It is known that hydrophobic contributions shift this transition value towards lower values[39]. In any case, the thermosensitivity can be considered similar because on the one hand, the VPTT variations are very small (the shapes of the curves are similar), and, on the other hand, the swelling variations below and above the VPTT are very large in all cases.

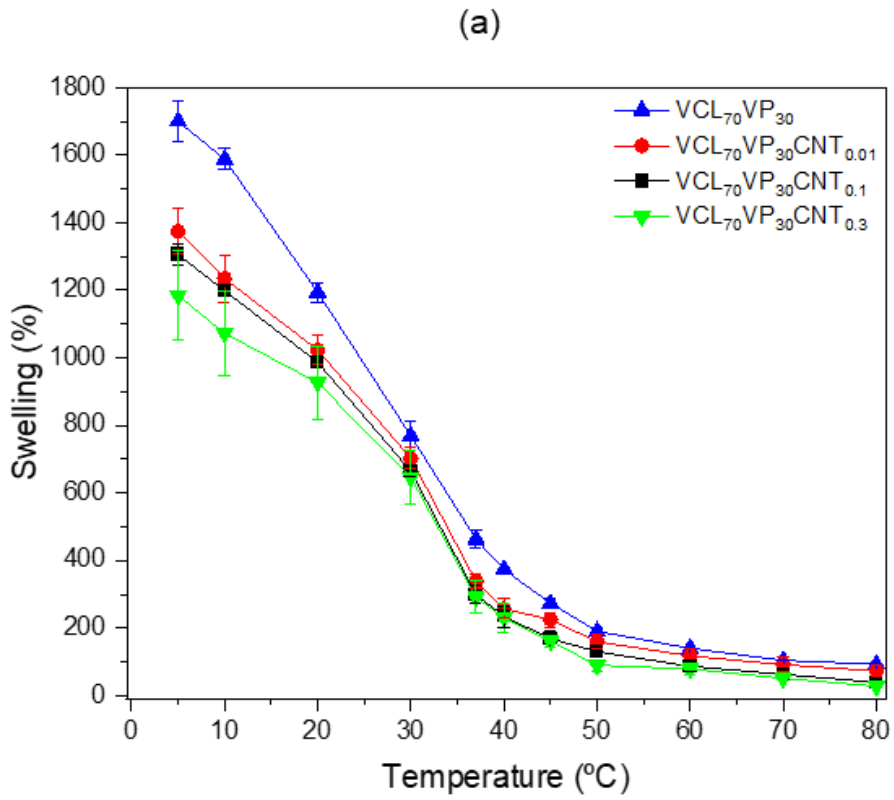

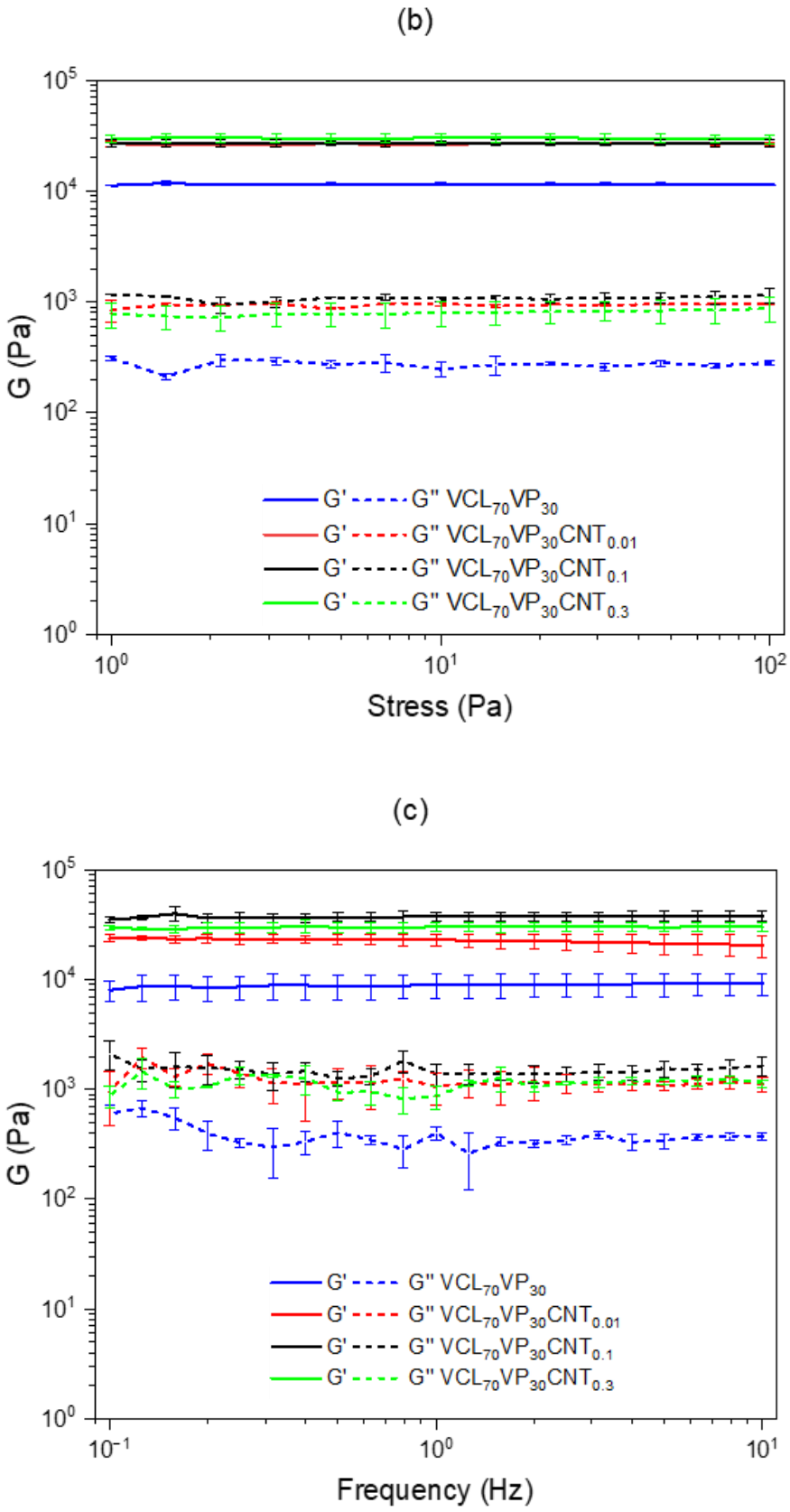

Figure 7.3. (a) Swelling (%) in PBS of the hydrogels prepared using variable amounts of HF-CNT (from 0% or control to 0.3 wt. %) as a function of temperature. Right:

Oscillatory rheology at room temperature of the loaded hydrogels obtained by photopolymerization. (b) Stress sweeps. (c) Frequency sweeps.

Regarding the mechanical properties of hydrogels, which were evaluated at 20 ºC in the hydrated state and by compression tests, an evident increase in compression modulus was observed as the HF-CNT content increased, ranging from 0.58 MPa in the control hydrogel at 20 °C (a value in the range of previously reported VCL-based hydrogels)[7] to 3.7 MPa for hydrogels with HF-CNT content of 0.3 wt. %. These values are extraordinary for this type of hydrated hydrogels. Part of the increase in modulus can be attributed to the lower water content, although swelling only decreases by 30% from $VCL_{70}VP_{30}$ to $VCL_{70}VP_{30}CNT_{0.3}$ while the modulus increases six times. Therefore, the data is indicative of a reinforcing effect of the CNT filler, in agreement with the literature[40,41]. Since the goal is to use these hydrogels for biological applications, it will be important to check if cells may be sensitive to these differences in mechanical properties.

This reinforcement effect is in agreement with the study carried out with oscillatory rheology, since stress sweeps (**Figure 7.3b**) confirmed an increase in the hydrogel elastic modulus from 11.2 ± 0.1 MPa for $VCL_{70}VP_{30}$ to 29.7 ± 2.3 MPa for $VCL_{70}VP_{30}CNT_{0.3}$. Furthermore, the linear viscoelastic region (LVR) exceeded the range of stress values tested, being indicative of high stability for all the tested samples. Frequency sweeps (**Figure 7.3c**) confirmed the stability of the hydrogels even at the highest loading level of HF-CNT, with both elastic (G′) and viscous (G″) moduli being independent of the applied frequency across the whole range tested.

The variations in the electrical conductivities of the as-prepared swollen composite hydrogels are quoted in **Table 7.3**. $VCL_{70}VP_{30}$ exhibit $8.6 \cdot 10^{-3} \pm 1.3 \cdot 10^{-3}$ $S \cdot m^{-1}$. The increasing HF-CNT content enhances the electrical conductivity by an order of magnitude reaching values from $1.5 \cdot 10^{-2} \pm 3.3 \cdot 10^{-3}$ to $8.1 \cdot 10^{-2} \pm 1.5 \cdot 10^{-2}$ $S \cdot m^{-1}$; these values corresponding to $VCL_{70}VP_{30}CNT_{0.01}$ and $VCL_{70}VP_{30}CNT_{0.3}$. As a point of interest, electrical conductivity of nerve tissues has been reported from 10^{-2} to 10^{0} $S \cdot m^{-1}$ [42–46], so that hydrogels loaded with CNTs are within or very close to the range. Above all, in accord with the results of the compression test, these results manifest the effective enhancement effect of the CNTs on the VCL-based hydrogels in both mechanical and electrical properties.

7.2.2. Biological evaluation of the hydrogels

7.2.2.1. Biological evaluation of the hydrogels with endothelial cultures

At this point, hydrogels with different wt. % of HF-CNT were evaluated as cell harvesting platforms as previously described in experimental **section 3.5.1** in **Chapter 3**. Thus, hydrogels were seeded with C166-GFP cells, and micrographs were obtained at 4 hours in order to analyze differences in early adhesion process. No evidence of a modulation of this mechanism was evidenced (**Figure 7.4a**), with a good response in all platforms. At 48 hours, endothelial monolayers were observed proliferating over hydrogels, with high-confluence areas especially in $VCL_{70}VP_{30}CNT_{0.1}$ and $VCL_{70}VP_{30}CNT_{0.3}$.

To validate these observations, double-stranded DNA was quantified in endothelial cultures proliferating over hydrogels. It can be observed in **Figure 7.4b** that CNTs content upregulated cell growing in these platforms. Especially, $VCL_{70}VP_{30}CNT_{0.1}$ samples reached a high proliferation rate, supporting the micrograph analysis shown before.

However, when hydrogels with different % of HF-CNT were used to detach endothelial monolayers by a temperature decrease as previously described, no significant amount of transplanted culture was observed in the new TCP surface. Only a few cells were observed, suggesting that cell attachment to these surfaces is stronger than in control hydrogels, as swelling behaviour was similar.

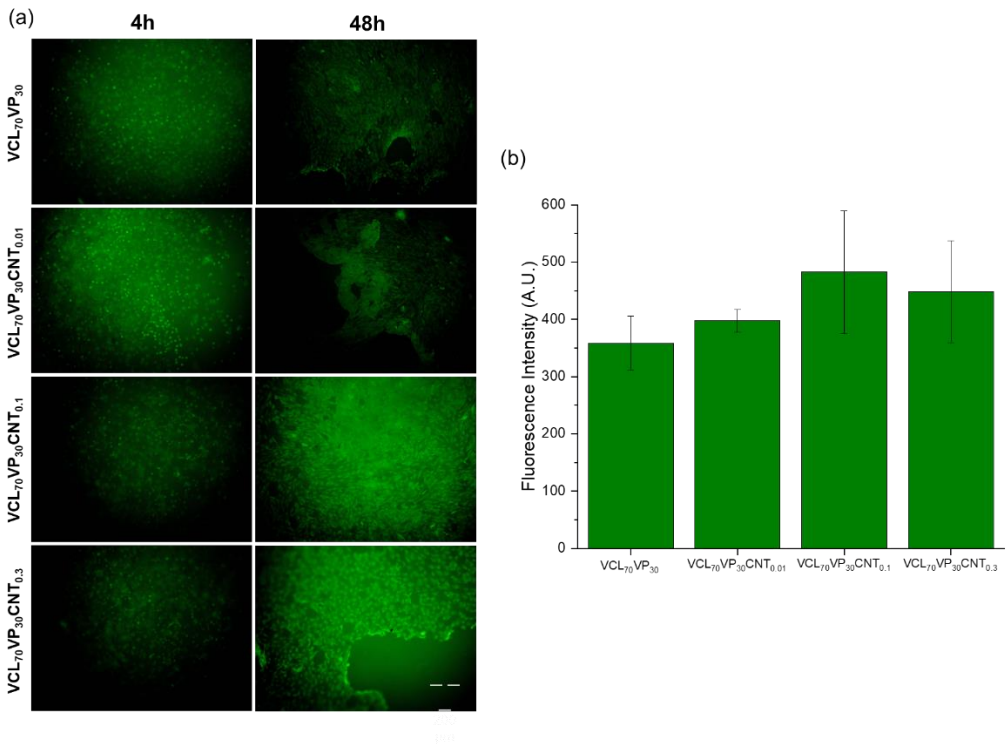

Figure 7.4. (a) Fluorescence images of C166-GFP cell cultures on the hydrogels after 4 and 48h after seeding process (scale bar: 200 μm). (b) Fluoreporter dsDNA assay on the hydrogels after 48h of the seeding process.

7.2.2.2. Biological evaluation of hydrogels with neuronal cultures

Section carried out by collaborators at "Hospital Nacional de Parapléjicos" from Toledo (Dr. Manuel Nieto-Diaz)

As HF-CNT could affect neuron adhesion, proliferation, and migration, it has been employed cultures of Neuro2a murine neuroblasts cell line seeded over hydrogel platforms with 0, 0.01, 0.1, and 0.3 wt. % CNT to evaluate their effects on neural cells. Microscopy observation of the cultures revealed that Neuro2a cells adhered well to all types of hydrogels analyzed, with no differences being observed between platforms (**Figure 7.5a-g**). Most of the cells on the hydrogels maintained a spherical shape while, when cultured directly on the plastic bottom of the well, a large part of them took a flattened shape or developed prolongations (**Figure 7.5h, i and j**). Spherical or round morphology in Neuro2a cells is associated with a loose attachment to the substrate and a high proliferative state, whereas the flattened shape is a sign of differentiation, often associated with the development of neurites[47]. Therefore, it appeared that hydrogels, including those including CNTs, limit the differentiation of Neuro2a cells in favour of a round proliferative

phenotype.

Video time-lapse (VTL) analyses of the numbers of Neuro2a cells in 5 fields per culture on the different hydrogels confirm the proliferative state of Neuro2a when cultured on the hydrogels. As shown in **Figure 7.5k**, cells proliferated at a rate comparable to that exhibited on plastic (light blue line) without showing major differences associated with the % of CNT on the hydrogel. Conversely, MTT values (**Figure 7.5l**) suggest that higher concentrations of CNT in the hydrogel may increase proliferation rate.

A final aspect revealed by the VTL analyses of the cultures over hydrogels was the lack of cell migration. While Neuro2a showed a great capacity for movement when seeded directly on plastic plates, when cultured on hydrogels hardly any cell movement was observed. Therefore, as a whole, the hydrogels, irrespectively of the CNT loading, promote a proliferative, non-differentiated, and non-migrating Neuro2a phenotype. These observations also indicate that there is no influence of CNT loading on cell response. Nevertheless, these studies are preliminary and, given the contribution of CNTs to conductivity, should be further confirmed and amplified.

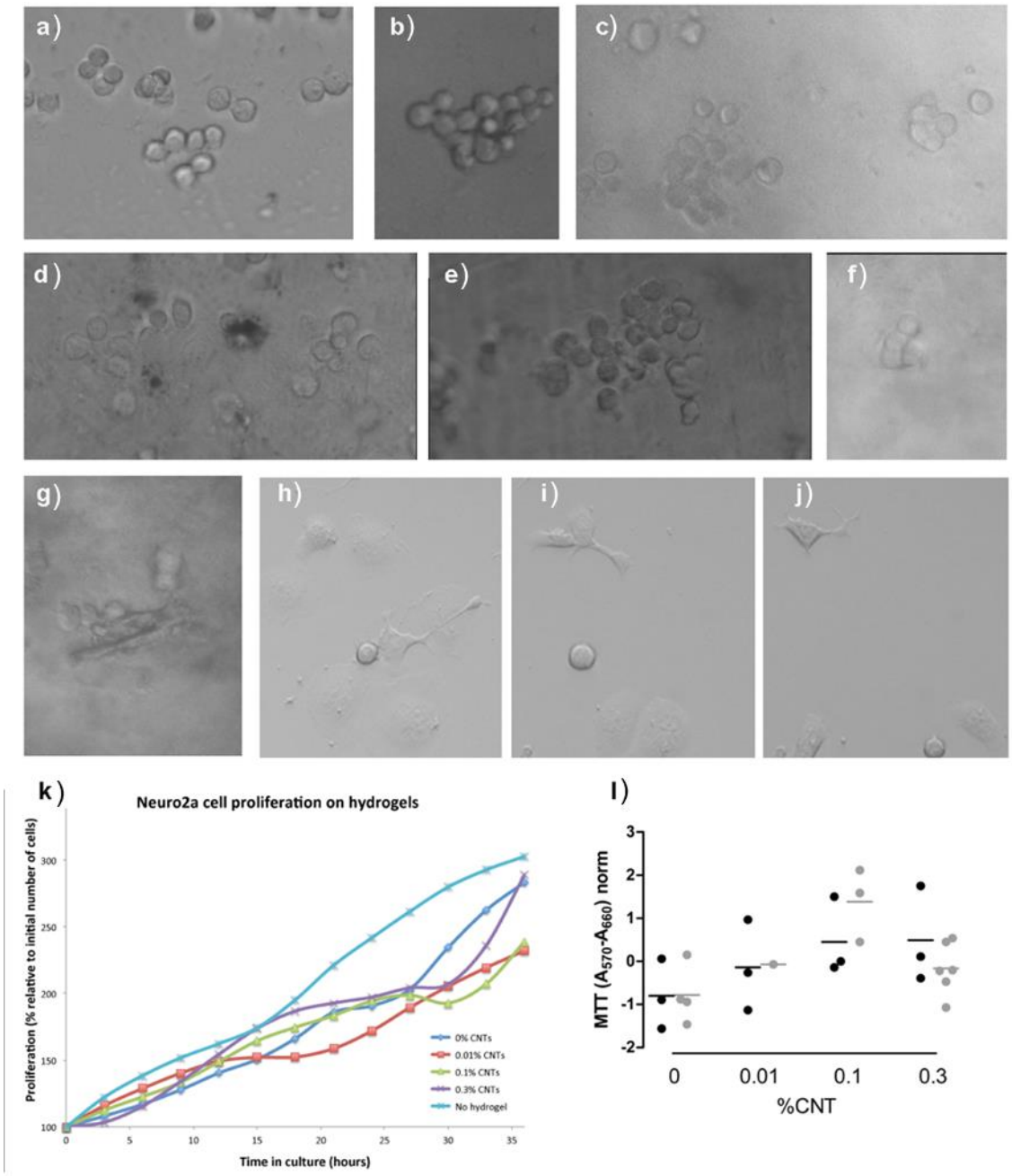

Figure 7.5. Neuro2a culture on hydrogels. a-j) Details of the cells after culture on the different hydrogels and the control (on plastic). a) $VCL_{70}VP_{30}$ after 12 hours. b) and c) $VCL_{70}VP_{30}CNT_{0.01}$ after 42 and 48 hours, respectively. d) and e) $VCL_{70}VP_{30}CNT_{0.1}$ after 36 and 48 hours respectively. f) and g) $VCL_{70}VP_{30}CNT_{0.3}$ at 24 and 27 hours. h), i), and j) Culture on plastic at 48, 24, and 0 hours after sowing. Except for the control images that were taken in the same field, all images correspond to different wells or fields. k). Proliferation on the different hydrogels measured as the number of cells in a field every 3 hours (for a total of 36 hours). Values are expressed as percentage relative to sowing

time. l) MTT values after 48 hours of culture on the hydrogels. Values were standardized to make values comparable among the two independent experiments.

7.2.3. 3D Printing by vat photopolymerization

For reasons of confidentiality, this section (pages 221 to 224) has been omitted.

7.3. Conclusions

The functionalization of CNTs was effectively achieved, enabling their homogeneous impregnation into the copolymer matrix, leading to high dispersibility in the matrix until 0.3 wt. %. The incorporation of high-functionalization CNTs significantly improved the mechanical and conductive properties of the hydrogels. Importantly, cell adhesion and proliferation were positively correlated with the increasing percentage of HF-CNT in the hydrogel composition, indicating their potential in supporting cellular activities. Furthermore, the hydrogels were compatible with alternative cell lines, including Neuro2a neural cell line, showing promising results in terms of cellular integration and functionality. The ability to successfully print these optimized CNT-loaded hydrogels using LCD 3D printing technology underscores the practical applicability and versatility of these advanced biomaterials. This result is promising for future applications, in particular in the field of the 3D printing of thermosensitive hydrogels loaded with CNTs for biological applications. In addition, the successful printability of these resins indicates their potential usefulness in the creation of intricate and highly detailed structures, which is essential for biological applications such as neural tissue. This opens up new opportunities for the development of advanced biomedical devices and materials with the ability to print complex shapes at high resolution. These findings collectively highlight the potential of VCL-VP copolymer-based hydrogels, reinforced with functionalized CNTs, as robust platforms for a wide range of biomedical applications, including tissue engineering and regenerative medicine.

References

1. Li, X. *et al.* A PNIPAAm-based thermosensitive hydrogel containing SWCNTs for stem cell transplantation in myocardial repair. *Biomaterials* **35**, 5679–5688 (2014).

2. Strokov, I., Abramchuk, S. & Makhaeva, E. Salt and pH effect on thermoresponsive behavior of multiwalled carbon nanotube (MWCNT)/poly(N-vinylcaprolactam) dispersion. *Colloid Polym Sci* **297**, (2019).

3. De Volder, M. F. L., Tawfick, S. H., Baughman, R. H. & Hart, A. J. Carbon Nanotubes: Present and Future Commercial Applications. *Science (1979)* **339**, 535–539 (2013).

4. Tasis, D., Tagmatarchis, N., Bianco, A. & Prato, M. Chemistry of Carbon Nanotubes. *Chem Rev* **106**, 1105–1136 (2006).

5. Sahoo, N. G., Rana, S., Cho, J. W., Li, L. & Chan, S. H. Polymer nanocomposites based on functionalized carbon nanotubes. *Prog Polym Sci* **35**, 837–867 (2010).

6. Shin, S. *et al.* Carbon-Nanotube-Embedded Hydrogel Sheets for Engineering Cardiac Constructs and Bioactuators. *ACS Nano* **7**, (2013).

7. García-Sobrino, R. *et al.* Cell harvesting on robust smart thermosensitive pseudo-double networks prepared by one-step procedure. *Eur Polym J* **209**, 112925 (2024).

8. García-Sobrino, R. *et al.* Fabrication of 3D cylindrical thermosensitive hydrogels as supports for cell culture and detachment of tubular cell sheets. *Biomaterials advances* **144**, 213210 (2022).

9. García-Sobrino, R. *et al.* Hydrogels with dual sensitivity to temperature and pH in physiologically relevant ranges as supports for versatile controlled cell detachment. *Biomaterials Advances* **159**, 213826 (2024).

10. Martínez-Campos, E. *et al.* Thermosensitive hydrogel platforms with modulated ionic load for optimal cell sheet harvesting. *Eur Polym J* **103**, (2018).

11. Liu, Z., Lu, A., Yang, Z. & Luo, Y. Enhanced swelling and mechanical properties of P(AM-co-SMA) semi-IPN composite hydrogels by impregnation with PANI and MWNTs-COOH. *Macromol Res* **21**, 376–384 (2013).

12. MacDonald, R. A., Voge, C. M., Kariolis, M. & Stegemann, J. P. Carbon nanotubes increase the electrical conductivity of fibroblast-seeded collagen hydrogels. *Acta Biomater* **4**, 1583–1592 (2008).

13. Sui, K., Gao, S., Wu, W. & Xia, Y. Injectable supramolecular hybrid hydrogels formed by MWNT-grafted-poly(ethylene glycol) and α-cyclodextrin. *J Polym Sci A Polym Chem* **48**, 3145–3151 (2010).

14. Shin, S. R. *et al.* Aligned Carbon Nanotube–Based Flexible Gel Substrates for Engineering Biohybrid Tissue Actuators. *Adv Funct Mater* **25**, 4486–4495 (2015).

15. Adewunmi, A., Ismail, S. & Sultan, A. Carbon Nanotubes (CNTs) Nanocomposite Hydrogels Developed for Various Applications: A Critical Review. *J Inorg Organomet Polym Mater* **26**, (2016).

16. Zhang, J. & Wang, A. pH- and thermo-responsive dispersion of single-walled carbon nanotubes modified with poly(N-isopropylacrylamide-co-acrylic acid). *J Colloid Interface Sci* **334**, 212–216 (2009).

17. Soll, S., Antonietti, M. & Yuan, J. Double Stimuli-Responsive Copolymer Stabilizers for Multiwalled Carbon Nanotubes. *ACS Macro Lett* **1 1**, 84–87 (2012).

18. Li, Z., Tang, M., Bai, W. & Bai, R. Preparation of Hydrophilic Encapsulated Carbon Nanotubes with Polymer Brushes and Its Application in Composite Hydrogels. *Langmuir* **33**, (2017).

19. Alencar de Queiroz, A. A., Gallardo, A. & San Román, J. Vinylpyrrolidone–N,N′-dimethylacrylamide water-soluble copolymers: synthesis, physical–chemical properties and proteic interactions. *Biomaterials* **21**, 1631–1643 (2000).

20. Aranaz, I., Reinecke, H., Elvira, C. & Gallardo, A. Compositionally-tunable surface nanostructuration of microspheres obtained from a self-stabilizing copolymerization of methylmethacrylate and vinylpyrrolidone. *Polymer (Guildf)* **52**, 2991–2997 (2011).

21. Guvendiren, M., Perepelyuk, M., Wells, R. G. & Burdick, J. A. Hydrogels with differential and patterned mechanics to study stiffness-mediated myofibroblastic differentiation of hepatic stellate cells. *J Mech Behav Biomed Mater* **38**, 198–208 (2014).

22. Gao, C., Song, S., Lv, Y., Huang, J. & Zhang, Z. Recent Development of Conductive Hydrogels for Tissue Engineering: Review and Perspective. *Macromol Biosci* **22**, 2200051 (2022).

23. Qin, C. *et al.* Advances in Conductive Hydrogel for Spinal Cord Injury Repair and Regeneration. *Int J Nanomedicine* **18**, 7305–7333 (2023).

24. Costa, P. *et al.* Effect of carbon nanotube type and functionalization on the electrical, thermal, mechanical and electromechanical properties of carbon nanotube/styrene–butadiene–styrene composites for large strain sensor applications. *Compos B Eng* **61**, 136–146 (2014).

25. Lorenz, H. *et al.* Advanced elastomer nano-composites based on CNT-hybrid filler systems. *Compos Sci Technol* **69**, 2135–2143 (2009).

26. Das, A. *et al.* Modified and unmodified multiwalled carbon nanotubes in high performance solution-styrene-butadiene and butadiene rubber blends. *Polymer (Guildf)* **49**, 5276–5283 (2008).

27. Bahr, J. L. & Tour, J. M. Covalent chemistry of single-wall carbon nanotubes. *J Mater Chem* **12**, 1952–1958 (2002).

28. Price, B. K. & Tour, J. M. Functionalization of Single-Walled Carbon Nanotubes “On Water”. *J Am Chem Soc* **128**, 12899–12904 (2006).

29. Bahr, J. & Tour, J. Highly Functionalized Carbon Nanotubes Using in Situ Generated Diazonium Compounds. *Chemistry of Materials - CHEM MATER* **13**, (2001).

30. Dyke, C. & Tour, J. Solvent-Free Functionalization of Carbon Nanotubes. *J Am Chem Soc* **125**, 1156–1157 (2003).

31. Marchesan, S., Kostarelos, K., Bianco, A. & Prato, M. The winding road for carbon nanotubes in nanomedicine. *Materials Today* **18**, 12–19 (2015).

32. Bosi, S. *et al.* Carbon based substrates for interfacing neurons: Comparing pristine with functionalized carbon nanotubes effects on cultured neuronal networks. *Carbon N Y* **97**, 87–91 (2016).

33. Tomova, A. *et al.* Functionalization and Characterization of MWCNT Produced by Different Methods. *Acta Phys Pol A* **129**, 405–408 (2016).

34. Costa, S., Borowiak-Palen, E., Kruszynska, M., Bachmatiuk, A. & Kalenczuk, R. Characterization of carbon nanotubes by Raman spectroscopy. *Materials Science- Poland* **26**, (2008).

35. Nayak, R. R., Lee, K. Y., Shanmugharaj, A. M. & Ryu, S. H. Synthesis and characterization of styrene grafted carbon nanotube and its polystyrene nanocomposite. *Eur Polym J* **43**, 4916–4923 (2007).

36. Tian, R. *et al.* An efficient route to functionalize singe-walled carbon nanotubes using alcohols. *Appl Surf Sci* **255**, 3294–3299 (2008).

37. Noda, L. K. & Sala, O. A resonance Raman investigation on the interaction of styrene and 4-methyl styrene oligomers on sulphated titanium oxide. *Spectrochim Acta A Mol Biomol Spectrosc* **56**, 145–155 (2000).

38. Marchesan, S., Melchionna, M. & Prato, M. Wire Up on Carbon Nanostructures! How To Play a Winning Game. *ACS Nano* **9**, 9441–9450 (2015).

39. Aguilar, M. R., Elvira, C., Gallardo, A., Vazquez, B. & Román, J. Smart Polymers and Their Applications as Biomaterials. *Topics in Tissue Engineering* **3**, (2007).

40. Bratovcic, A. Nanocomposite Hydrogels Reinforced by Carbon Nanotubes. *Int J Eng Res Appl* **10**, 30–41 (2020).

41. Rozhin, P., Kralj, S., Soula, B., Marchesan, S. & Flahaut, E. Hydrogels from a Self-Assembling Tripeptide and Carbon Nanotubes (CNTs): Comparison between Single-Walled and Double-Walled CNTs. *Nanomaterials* **13**, (2023).

42. Liu, X. *et al.* Functionalized carbon nanotube and graphene oxide embedded electric conductive hydrogel synergistically stimulates nerve cell differentiation. *ACS Appl Mater Interfaces* **9**, (2017).

43. Tasaki, I. A NEW MEASUREMENT OF ACTION CURRENTS DEVELOPED BY SINGLE NODES OF RANVIER. *J Neurophysiol* **27**, 1199–1206 (1964).

44. Ranck, J. B. & BeMent, S. L. The specific impedance of the dorsal columns of cat: An anisotropic medium. *Exp Neurol* **11**, 451–463 (1965).

45. Roth, B. The Electrical Conductivity of Tissues. in (2000). doi:10.1201/9781420049510.ch10.

46. McCann, H., Pisano, G. & Beltrachini, L. Variation in Reported Human Head Tissue Electrical Conductivity Values. *Brain Topogr* **32**, (2019).

47. Tremblay, R. *et al.* Differentiation of N2a cells into dopamine neurons. (2008).

48. Arias-Ferreiro, G., Ares-Pernas, A., Dopico-García, M. S., Lasagabáster-Latorre, A. & Abad, M.-J. Photocured conductive PANI/acrylate composites for digital light processing. Influence of HDODA crosslinker in rheological and physicochemical properties. *Eur Polym J* **136**, 109887 (2020).

49. Lee, Y.-H., Lee, J.-B., Maeng, W.-Y., Koh, Y.-H. & Kim, H.-E. Photocurable ceramic slurry using solid camphor as novel diluent for conventional digital light processing (DLP) process. *J Eur Ceram Soc* **39**, 4358–4365 (2019).

50. Arboleda-Clemente, L., Ares-Pernas, A., García, X., Dopico, S. & Abad, M. J. Influence of polyamide ratio on the CNT dispersion in polyamide 66/6 blends by dilution of PA66 or PA6-MWCNT masterbatches. *Synth Met* **221**, 134–141 (2016).

51. Paleo, A. J., Sencadas, V., van Hattum, F. W. J., Lanceros-Méndez, S. & Ares, A. Carbon nanofiber type and content dependence of the physical properties of carbon nanofiber reinforced polypropylene composites. *Polym Eng Sci* **54**, 117–128 (2014).

52. García-Fonte, X., Ares-Pernas, A., Cerecedo, C., Valcárcel, V. & Abad, M. J. Influence of phase morphology on the rheology and thermal conductivity of HDPE/PA6 immiscible blends with alumina whiskers. *Polym Test* **71**, 56–64 (2018).

53. Liz-Basteiro, P. *et al.* High resolution molds, sacrificial in aqueous media, obtained by vat photopolymerization 3D printing. *Addit Manuf* **75**, 103758 (2023).

54. Ligon, S., Liska, R., Stampfl, J., Gurr, M. & Mülhaupt, R. Polymers for 3D Printing and Customized Additive Manufacturing. *Chem Rev* **117**, (2017).

55. Voet, V. *et al.* Biobased Acrylate Photocurable Resin Formulation for Stereolithography 3D Printing. *ACS Omega* **3**, 1403–1408 (2018).

56. Arias-Ferreiro, G. *et al.* Printability Study of a Conductive Polyaniline/Acrylic Formulation for 3D Printing. *Polymers (Basel)* **13**, (2021).

57. Li, Y. *et al.* Theoretical prediction and experimental validation of the digital light processing (DLP) working curve for photocurable materials. *Addit Manuf* **37**, 101716 (2021).

58. Liz-Basteiro, P. *et al.* Vat Photopolymerization 3D Printing of Hydrogels with Re-Adjustable Swelling. *Gels* **9**, (2023).

Chapter 8. Overview and final conclusions

The diagram in **Figure 8.1** illustrates the process developed during the thesis, which involves all the steps in the preparation and use of materials used in this PhD, starting from the synthesis of the photopolymerizable resins and the fabrication (in this case by AM) to the evaluation of their potential applications, herein focusing on the biomedical area. The different steps are interconnected and thus a control in each of the steps allow us to produce versatile materials and explore a wide myriad of possible innovations in the use of networks such as hydrogels.

The starting point of this thesis is based on a novel strategy for the synthesis of networks and their possible applications have been presented. The strategy proposed is based on the chemical design of a novel class of crosslinking agents that can be hydrolyzed in basic aqueous media.

In order to validate the concept, this thesis started by designing and fabricating photocrosslinked parts by 3D printing through vat photopolymerization using exclusively the novel crosslinking agents in their preparation. As expected, the parts fabricated could be dissolved in basic water, allowing them to be used in applications such as high-resolution molds. These initial experiments allowed us to establish the basis for other preparations in particular focusing on obtaining readjustable hydrogels that, as is thoroughly depicted in the thesis, exhibit potential for different biorelated applications. The idea of using hydrolysable crosslinkers was successfully adopted in combination with permanent crosslinkers to prepare tailor-made hydrogel networks with both variable chemistry and swelling capacity by introducing different hydrophilic monomers and also with the ratio between permanent and hydrolysable crosslinkers among others. This property facilitates their use as implantable devices, such as surgical fillers. To the best of our knowledge, this approach offers unprecedented unique opportunities since the chemical composition is directly defined by the feed composition but also the final degree of swelling can be finely tuned by the partial hydrolysis of the network.

Provided the basis for the preparation of hydrogel networks based on different (meth)acrylate monomers, it resulted in interest to explore other monomers.

Inspired by the ongoing work within the group we introduced an additional challenge attempting to prepare VCL-based thermosensitive hydrogels by vat photopolymerization. For this purpose, we started from an original formulation of photosensitive resins previously developed in our group (now part of the iFABCell technology) that in view of the impossibility of being directly printed was redesigned and optimized to be employed in VPP 3D printing. For that purpose, in addition to the use of hydrolysable crosslinkers in the photosensitive resin, as has been depicted above, we made an intensive effort to find also other strategies including the use of a solvent, or the addition of another vinyl-lactam, which allowed the resin to be liquid (thus solubilizing VCL, solid at room temperature) and stable at room temperature. All these three alternatives were explored and successfully employed for the preparation of thermoresponsive hydrogels although we found that the final properties of the hydrogel clearly are, at least to some extent, related to the approach followed for the preparation.

In the last part of this thesis, it was attempted to go one step beyond and it was decided to investigate the incorporation of both active compounds as well as nanometer-size additives within the networks for two different purposes. On the one hand, Icariin is an extensively employed biomolecule for stimulating cell growth, differentiation of chondrocytes as well as differentiation of embryonic stem cells towards cardiomyocytes, depending on the biological niche. Thus, its incorporation within the hydrogels enable us to induce the formation and harvest of differentiated cell monolayers.

On the other hand, the hydrogels were also loaded with carbon nanotubes (CNTs). Herein, the objective was both to simultaneously improve their mechanical and confer to the material electrical conductivity. Based on collaborations with the HNP in Toledo, this composite was evaluated for its potential interest in the development of conductive hydrogel supports for neuronal cell culture. The hydrogels designed for these two applications, although they are in the initial steps, exhibited a huge potential and preliminary testing concluded that they have been successfully employed as supports for non-aggressive detachment of cell monolayers by temperature change, in the case of endothelial cells and, in the case of, those containing CNTs have been shown to permit neuronal cell culture.

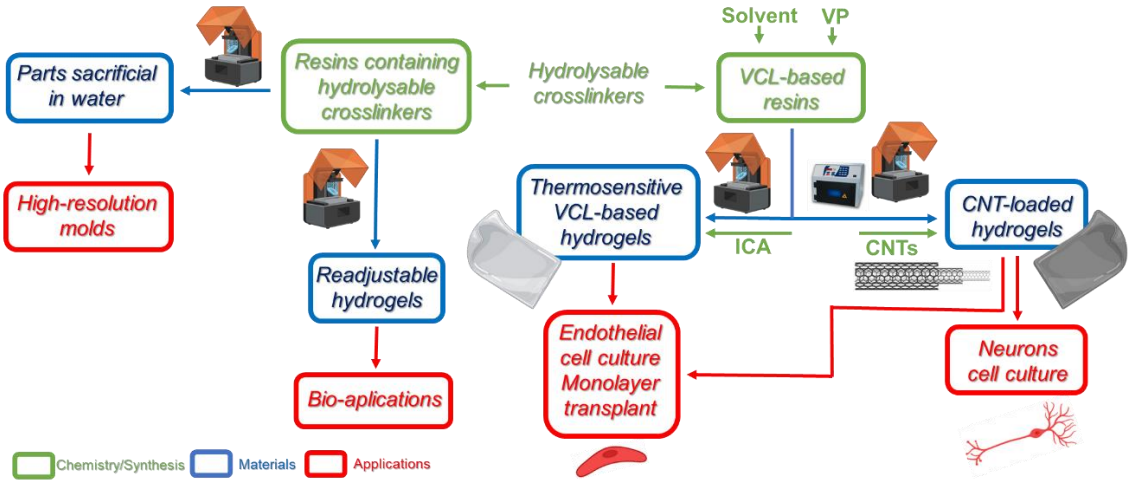

Figure 8.1. Scheme of the development of the thesis.

At this stage, I would like to highlight and summarize the most relevant achievements obtained in my PhD thesis:

1. A scalable method, developing a one-step strategy for the preparation of hydrolysable crosslinkers, has been established for producing printable formulations with hydrolysable crosslinkers. The 3D printing of these resins via VPP consistently results in sacrificial parts that dissolve in basic water, confirming the hypothesis that sacrificial networks can be created with hydrolysable crosslinkers. The flexibility in adjusting the formulation components has allowed tuning the printed parts' properties, such as young modulus, fracture stress, and elasticity, with thermal resistance ranging from 180-240 ºC.

2. Furthermore, the materials developed including exclusively hydrolysable crosslinkers were successfully employed for the fabrication of sacrificial molds. The applicability of these molds in different thermal and chemical environments has been demonstrated by three different proofs-of-concept where these molds were successfully employed in the preparation of 3D parts based on thermoplastics, bi-component silicone systems, or VCL-based thermosensitive hydrogels liquid formulations. The potential of these materials to be employed as molds relies both on the high resolution obtained as well as the fully customizable design of the mold that could be easily removed in basic aqueous solutions.

3. It has been demonstrated that combining stable and hydrolysable crosslinkers enables the 3D printing of pieces via VPP varying sizes and shapes. Initially, the parts exhibit high crosslinking and therefore only a limited swelling (PEGDMA and HCL(jef) knots), which can be transformed into hydrogels (*i.e.*, highly swollen materials) by treatment in a pH 10 buffer, leaving only PEGDMA knots. The swelling behavior of the printed part can be precisely controlled, ranging from initial swelling to the final swelling after total hydrolysis of HCL(jef), depending on the immersion time, the pH of the aqueous solution, and the solution temperature. Stabilization of the target swelling was achieved by immersing the pieces in PBS at room temperature. These optimized hydrogels could be utilized in applications such as surgical filling for regenerative medicine.
4. In this thesis, it has been shown that thermosensitive hydrogels based on VCL can be successfully 3D printed via VPP using different strategies. A key discovery is that the EGDMA/DVI crosslinker ratio directly influences layer printing, with ratios of 65/35 or higher improving interlayer adhesion and yielding stronger hydrogel structures.
5. The three strategies explored to 3D print VCL-based hydrogels—using a liquid solvent, a hydrolysable crosslinker, and an additional liquid vinyl-lactam—allowed to fabricate of VCL-based hydrogel through VPP. The first strategy, which incorporates a solvent, shows that NMP offers the best balance between printability and mechanical strength. The second strategy, involving a hydrolysable crosslinker, allows faster printing and results in hydrogels similar to those produced by traditional photocuring methods after a week of hydrolysis. The third strategy, which includes an additional hydrophilic vinyl-lactam, enables modulation of the VPTT, swelling, and mechanical properties.
6. Moreover, 3D printed VCL-based hydrogels exhibited cell detachment properties upon lowering the temperature, as shown by evaluating a selected material. Therefore, it has been shown that they can be used in cell sheet engineering.
7. 3D printing of hydrogels loaded with ICA has been accomplished, enabling controlled and temperature-dependent drug release. Therefore, this

achievement opens up significant opportunities in the field of direct printing of drug-loaded hydrogels with high-resolution and complex structures, enabling controlled drug release at different temperatures.

8. Functionalization of CNTs enabled their uniform dispersion in a VCL/VP formulation and in the corresponding up to 0.3 wt. %, significantly enhancing the mechanical and conductive properties of the hydrogels. HF-CNT content of 0.3 wt. % improved cell adhesion and proliferation, showing potential for these hydrogels to support cell response activities. These CNT-loaded hydrogels demonstrated compatibility with cell lines like Neuro2a, indicating promising results for cell viability and functionality.

   Additionally, the successful 3D printing of these loaded hydrogels highlights their potential for creating intricate, high-resolution structures, particularly for neural tissue applications. This development paves the way for advanced biomedical devices and materials, especially in tissue engineering and regenerative medicine as cell sheet engineering.

The results obtained and summarized above demonstrated on the one hand the feasibility of developing photoprintable functional materials based on (met)acrylates suitable for obtaining partially or totally sacrificial networks, if applicable, hydrogels. On the other hand, it has been demonstrated the feasibility of printing by vat photopolymerization hydrogels based on a vinyl-lactam such as VCL; worth mentioning that this objective has been achieved by means of 3 different strategies. Finally, VCL-based thermosensitive hydrogels loaded with Icariin as well as functionalized CNTs have been developed that allow the modulation of the properties and provide either bioactivity or conductivity, while maintaining the properties of cell detachment and its printability. Although these last two parts of the work have been accomplished partially, these promising results settle the basis for further related investigations.

Scientific Contributions

Publication of the Thesis results:

Patents (2)

❖ *Patent in PCT phase (WO2024003429A1).* ***Title****: "Entrecruzantes hidrolizables y productos derivados de ellos".* ***Priority number****: ES202230575A, 27 de junio de 2022.* ***Owners****: Consejo Superior Investigaciones Científicas (CSIC).* ***Authors***: **P. Liz-Basteiro,** R. Sanz-Horta, F. Reviriego, E. Martínez-Campos, H. Reinecke, C. Elvira, A. Gallardo, J. Rodríguez-Hernández.

❖ *Technology being assessed for patentability*. ***Title:*** "Impresión 3D de hidrogeles derivados de vinil-lactamas mediante fotopolimerización". ***Owners***: *Consejo Superior Investigaciones Científicas (CSIC).* ***Authors****:* **P. Liz-Basteiro**, C. Elvira, A. García-Crespo, H. Reinecke, J. Rodríguez-Hernández, E. Martínez, A. Gallardo.

Published papers (3)

❖ **P. Liz-Basteiro,** R. Sanz-Horta, F. Reviriego, E. Martínez-Campos, H. Reinecke, C. Elvira, J. Rodríguez-Hernández, A. Gallardo. High resolution molds, sacrificial in aqueous media, obtained by vat photopolymerization 3D printing. **Additive Manufacturing**, 75 (2023), 103758. DOI: https://doi.org/10.1016/j.addma.2023.103758

❖ **P. Liz-Basteiro**, F. Reviriego, E. Martínez-Campos, H. Reinecke, C. Elvira, J. Rodríguez-Hernández, A. Gallardo. Vat Photopolymerization 3D Printing of Hydrogels with Re-Adjustable Swelling. **Gels**, (2023), 9(8):600. DOI: https://doi.org/10.3390/gels9080600

❖ R. García-Sobrino, C. García, **P. Liz-Basteiro**, H. Reinecke, C. Elvira, J. Rodríguez-Hernández, E. Martínez-Campos, A. Gallardo. Cell harvesting on robust smart thermosensitive pseudo-double networks prepared by one-step procedure. **European Polymer Journal**, (2024), 209, 112925. DOI: https://doi.org/10.1016/j.eurpolymj.2024.112925

In preparation (2)

P. Liz-Basteiro, G. Arias-Ferreiro, D. Marin, E. Martínez-Campos, H. Reinecke, C. Elvira, J. Rodríguez-Hernández, M. Nieto-Diaz, D. Reigada, R. M. Maza, S. Marchesan, A. Gallardo. Thermosensitive hydrogels based on Poly(VCL-co-VP) loaded with carbon nanotubes for tissue engineering. *Status: Under review by international collaborators*

P. Liz-Basteiro, A. García-Crespo, S. Márquez, P. Franco, E. Martínez-Campos, H. Reinecke, C. Elvira, J. Rodríguez-Hernandez, A. Gallardo. Vat photopolymerization 3D printing of VCL-based thermosensitive hydrogels for cell harvesting**.** *Status: writing results and discussion*

Conferences presentations:

❖ **2021.** Modulation of the thermal sensitivity of vinylcaprolactam-based copolymer hydrogels. 5th Young Polymer Scientists Seminar (SEJIPOL 2020-2021), Madrid (Spain). (*Oral communication*)

❖ **2022.** Digital light processing 3D printing of sacrificial molds and hydrogels. 6th Young Polymer Scientists Seminar (SEJIPOL 2022), Madrid (Spain). (*Oral communication*)

❖ **2022.** Modulation of the thermal sensitivity of vinylcaprolactam-based copolymer hydrogels. XVI Reunión del Grupo Especializado de Polímeros (RSEQ/RSEF) - SLAP 2022 (GEP-SLAP 2022), San Sebastián (Spain). (*Oral communication and poster*)

❖ **2022.** Impresión 3D por estereolitografía de moldes sacrificables e hidrogeles. Congreso Nacional de Materiales (CNMAT 2022), Ciudad Real (Spain). (*Oral communication*)

❖ **2022.** Hidrogeles sensibles a temperatura y pH. Ajuste de la respuesta a los estímulos. VI Simposio Anual en Química Avanzada, Madrid (Spain). (*Oral communication*)

❖ **2023.** Characterization and corrosion resistance of Mg-Zn-Ca alloys for biomedical applications. XI Congreso de Jóvenes Investigadores de Polímeros (JIP 2023), Alicante (Spain). (*Oral communication*)

❖ **2024.** Impresión 3D mediante Digital Light Processing (DLP) de hidrogeles termosensibles basados en vinil-lactamas. Congreso Nacional de Materiales (CNMAT 2024), Málaga (Spain). (*Oral communication*)

❖ **2024.** High Resolution Molds, Sacrificial In Aqueous Media, Obtained By Vat Photopolymerization 3D Printing. XVII Reunión del Grupo Especializado de Polímeros (RSEQ/RSEF) - (GEP 2024), Madrid (Spain). (*Oral communication*)